Linking ADSL and GRK4 to ciliopathies of the nervous system and the kidney

Dissertation

zur Erlangung des Grades eines

Doktors der Naturwissenschaften

der Mathematisch-Naturwissenschaftlichen Fakultät

und

der Medizinischen Fakultät

der Eberhard-Karls-Universität Tübingen

vorgelegt

von

Julian Gerhards

aus Dernbach (Westerwald), Deutschland

2023

Tag der mündlichen Prüfung: 12.05.2023

Dekan der Math.-Nat. Fakultät: Prof. Dr. Thilo Stehle

Dekan der Medizinischen Fakultät: Prof. Dr. Bernd Pichler

1. Berichterstatter: Prof. Dr. Melanie Philipp

2. Berichterstatter: Dr. Jens Lüders

Prüfungskommission: Prof. Dr. Melanie Philipp

Prof. Dr. Ludger Schöls

Dr. Jens Lüders

Prof. Dr. Stefan Liebau

Erklärung / Declaration:

Ich erkläre, dass ich die zur Promotion eingereichte Arbeit mit dem Titel:

Linking ADSL and GRK4 to ciliopathies of the nervous system and the kidney

selbständig verfasst, nur die angegebenen Quellen und Hilfsmittel benutzt und wörtlich oder inhaltlich übernommene Stellen als solche gekennzeichnet habe. Ich versichere an Eides statt, dass diese Angaben wahr sind und dass ich nichts verschwiegen habe. Mir ist bekannt, dass die falsche Abgabe einer Versicherung an Eides statt mit Freiheitsstrafe bis zu drei Jahren oder mit Geldstrafe bestraft wird.

I hereby declare that I have produced the work entitled

Linking ADSL and GRK4 to ciliopathies of the nervous system and the kidney

submitted for the award of a doctorate, on my own (without external help), have used only the sources and aids indicated and have marked passages included from other works, whether verbatim or in content, as such. I swear upon oath that these statements are true and that I have not concealed anything. I am aware that making a false declaration under oath is punishable by a term of imprisonment of up to three years or by a fine.

Tübingen, den 15.05.2023 Julian Gerhards

Datum / Date Unterschrift /Signature

Statement of contributions according to § 9 (2):

Sophia Aicher did part of the expression pattern of *adsl*. She performed WMISH and took pictures (5.1).

Prof. Melanie Philipp generated the mutant fishline Grk4 1.2. Additionally, she did the whole cloning for the ΔRH version of GRK4 (3.1, 5.11, 5.17).

Dr. Lars D. Maerz performed the expression pattern of *grk4* and took pictures of the embryos. Moreover, he did rescue experiments of Grk4 depleted zebrafish embryos with RNA encoding zebrafish WT Grk4 or one of the patient variants. He counted cyst formation in the glomeruli and measured cilia length of these embryos (5.8, 5.15).

Oliver Wenzke did initial experiments in HEK cells and assessed cell size and mTOR signaling. He also generated a stable HEK GRK4 knock-out cell line (5.18).

Conny Donow, Monika Häußler, Dr. Lars D. Maerz, Elke Zabinsky and Prof. Melanie Philipp cloned following plasmids: pCRII-zfAdsl, pCRII-zfAngptl3, pCRII-zfGrk4 5'UTR, pCRII-zfSouthpaw, pCS2+-zfGrk4, pCS2+-zfGrk4 K216M/K217M, pCS2+-zfGrk4 UTRORF, pCS2+Flag-hGRK4 α, pCS2+Flag-hGRK4 β, pCS2+Flag-hGRK4 γ, pCS2+Flag-hGRK4 δ, pCS2+Flag-hGRK4 R65L, pCS2+Flag-hGRK4 A142V and pCS2+Flag-hGRK4 K216M/K217M, pCS2+Flag-hGRK4 ΔRH and pCS2+-zfGrk4 ΔRH (3.10).

For the ADSL part of this thesis: I performed all zebrafish injections, live phenotype analysis, as well as all WMISH for the assessment of the LR asymmetry defects. Furthermore, I did all AB stainings, counted neuronal cells numbers and did the measurements of cilia length. Additionally, I made all cartilage stainings and analyzed them.

For the GRK4 part of this thesis: I performed most of the zebrafish injections, live phenotype analysis, cyst countings and AB stainings. All treatments of zebrafish embryos or cells were done by myself. Furthermore, I made all qPCR experiments and measured cell size, cilia length and the dilatation of the pronephric duct, unless indicated otherwise.

Part of the results of the chapter 5.1 - 5.7 are already published:

Dutto I, Gerhards J, Herrera A, Souckova O, Škopová V, Smak JA, Junza A, Yanes O, Boeckx C, Burkhalter MD, Zikánová M, Pons S, Philipp M, Lüders J, Stracker TH. Pathway-specific effects of ADSL deficiency on neurodevelopment. Elife. 2022 Feb 8;11:e70518. doi: 10.7554/eLife.70518. PMID: 35133277; PMCID: PMC8871376

The GRK4 study has just been accepted by JASN:

Gerhards J, Maerz LD, Matthees ESF, Donow C, Moepps B, Premont RT, Burkhalter MD, Hoffmann C, Philipp M. Kinase activity is not required for GRK4 restraining mTOR signaling during cilia and kidney development. JASN

Table Index

Figure Index

List of Abbreviations

	Abbreviation	Word
A	A	Atrium
	abs	absolute
	ACE	Angiotensin-Converting Enzyme
	actub	Acetylated α-Tubulin
	ADPKD	Autosomal Dominant Polycystic Kidney Disease
	ADSL	Adenylosuccinate Lyase
	ADSL-D	Adenylosuccinate Lyase Deficiency
	Agt	Angiotensinogen
	Ang I	Angiotensin I
	Ang II	Angiotensin II
	angptl3	*Angiopoietin-like 3*
	anti-DIG	Anti-Dioxigenin Alkaline Phosphatase
	ARPKD	Autosomal Recessive Polycystic Kidney Disease
	as	antisense
	ATG MO	Translation Blocking MO
	ATR	Ataxia Telangiectasia and RAD3-related
B	BB	Basal Body
	BCIP	5-Bromo-4-Chlor-3-Indolylphosphate
	BLAST	Basic Local Alignment Search Tool
	bp	Base Pair
	BSA	Bovine Serum Albumin
C	$CaCl_2$	Calcium Chloride
	CAS	Chemical Abstracts Service
	cDNA	Complementary DNA

	cm	Centimeter
	cmlc2	*cardiac myosin light chain 2*
	CTRL	Control
	CTRL MO	Standard Control MO
	CV	Ciliary vesicle
D	D	D-Loop
	Da	Dalton
	DAP	Distal Appendage
	DAPI	4,6-Diamidin-2-Phenylindol
	DFC	Dorsal Forerunner Cell
	DHH	Desert Hedgehog
	DMSO	Dimethyl Sulfoxide
	DNA	Deoxyribonucleic Acid
	DNase	Deoxyribonuclease
	DNPS	*De Novo* Purine Synthesis
	dNTP	Deoxyribose Nucleoside Triphosphate
E	EB	Elution Buffer
	E. coli	*Escherichia coli*
	EDTA	Ethylenediaminetetraacetic acid
	EK	Ekkwill
	EtOH	Ethanol
F	FBS	Fetal Bovine Serum
	FCS	Fetal Calf Serum
	fw	Forward
G	g	Gram
	GLI	Glioma-associated Oncogen
H	h	Hours

	h	Human
	HCl	Hydrochloric Acid
	HEPES	N-(2-Hydroxyethyl)piperazine-N'-(2-ethanesulfonic acid)
	HH	Hedgehog
	H_2O	Water
	HiFi	High-Fidelity
	hpf	Hours Post Fertilization
I	IDT	Integrated DNA Technologies
	IF	Immunofluorescence
	IFT	Intraflagellar Transport
	IHH	Indian Hedgehog
K	k	Kilo
	kb	Kilo Base Pair
	KCl	Potassium Chloride
	KD	Knock Down
	KiDe	Kinase-Dead
	KH_2PO_4	Potassium Dihydrogen Phosphate
	KO	Knock Out
	KOH	Potassium Hydroxide
	KV	Kupffer's Vesicle
L	L	L-Loop
	l	Litre
	LB	Lysogeny Broth
	LB agar	Lennox LB Agar
	LOF	Loss-of-Function
	LOPAC®	Library of Pharmacologically Active Compounds
	LR	Left-Right

	LRO	Left-Right Organizer
M	M	Molar
	mA	Milliampere
	MC	Mother Centriole
	MeOH	Methanol
	mg	Milligram
	$MgCl_2$	Magnesium Chloride
	$MgSO_4$	Magnesium Sulfate
	min	Minute
	ml	Millilitre
	mM	Millimolar
	MO	Morpholino Oligonucleotide
	mRNA	Messenger Ribonucleic Acid
	mTOR	Mechanistic Target of Rapamycin
	mTORC1	mTOR Complex 1
	mTORC2	mTOR Complex 2
N	NaCl	Sodium Chloride
	$NaHCO_3$	Sodium Hydrogen Carbonate
	Na_2HPO_4	Disodium Hydrogen Phosphate
	NaOH	Sodium Hydroxide
	NBT/BCIP	Nitro Blue Tetrazolium/5-Bromo-4-Chloro-3-Indolyl Phosphate
	ndr1	*nodal-related 1*
	ndr2	*nodal-related 2*
	ng	Nanogram
	NGS	Normal Goat Serum
	NHE3	Sodium/Hydrogen Exchanger Isoform 3
	NI	Non-Injected

	NLS	Nuclear Localization Sequence
	nm	Nanometer
	nM	Nanomolar
	ns	Not Significant
O	o/n	Over Night
	ORF	Open Reading Frame
P	p	P Value
	p	Pico
	PBDT	PBST + DMSO
	PBS	Phosphate Buffered Saline
	PBST	PBS + Tween®20
	PC1	Polycystin 1
	PC2	Polycystin 2
	PCR	Polymerase Chain Reaction
	PCV	Preciliary Vesicle
	Pen/Strep	Penicillin/Streptomycin
	PFA	Paraformaldehyde
	pH	Acidity/Basicity Scale
	PKCζ	Protein Kinase C Zeta
	PKD	Polycystic Kidney Disease
	PKHD1	Polycystic Kidney and Hepatic Disease 1
	PM	Primary Microcephaly
	PTCH1	Patched 1
	PTU	1-Phenyl-2-Thiourea
Q	qPCR	Quantitative PCR
R	RAS	Renin-Angiotensin-System
	rev	Reverse

	RNA	Ribonucleic Acid
	RNase	Ribonuclease
	RPAP3	RNA Polymerase II Associated Protein 3
	rpm	Rounds Per Minute
	RT	Room Temperature
S	S1	Biosafety Level 1
	SDAP	Subdistal Appendage
	SD	Standard Deviation
	SDHA	Succinate Dehydrogenase Complex Flavoprotein Subunit A
	SDS	Sodium dodecyl sulfate
	sec	Second
	SEM	Standard Deviation of the Mean
	SHH	Sonic Hedgehog
	SM	Secondary Microcephaly
	SMO	Smoothened
	S.O.C.	Super Optimal Broth Medium with Added Glucose
	spaw	*southpaw*
	splMO	Splice Site Blocking MO
	SS	Somite Stage
	SSC	Saline Sodium Citrate
	SUFU	Suppressor of Fused Homolog
T	TAC	Theses Advisory Committee
	TAE	Tris-Acetate-EDTA
	Taq	Thermophilus Aquaticus
	tb	Tailbud
	TBS	Tris Buffered Saline
	TBST	TBS + Tween®20

	TM	Transmembrane
	tRNA	transfer RNA
U	U	Enzyme Unit
	UP	Universal Probe
	UTR	Untranslated Region
V	V	Ventricle
	V	Volt
W	WB	Western Blot
	WMISH	Whole Mount In Situ Hybridization
	w/o	Without
	wt	Wild Type
	WTU	Water Treatment Unit
Z	zf	Zebrafish

1 Abstract

Cilia are highly conserved antennae-like structures that are involved in many developmental processes and signaling. Malformations of cilia are often associated with clinical phenotypes like microcephaly, infertility, edema formation, congenital heart defects or renal abnormalities (1). These diseases are known as ciliopathies. In the last years, the number of genes that cause ciliopathies increased. For potential treatment of ciliopathies, it is important to better understand cilia function and signaling. This work identified two novel regulators of cilium biogenesis, namely Adenylosuccinate lyase (ADSL) and G protein-coupled receptor kinase 4 (GRK4).

Genetic variants of ADSL predispose to a condition termed ADSL deficiency (ADSLD). Patients suffering from ADSLD show a broad spectrum of clinical phenotypes, reaching from psychomotor delay, mental retardation or microcephaly to hyperactivity. We found that several of these phenotypes are associated to dysfunctional cilia. Molecularly, the accumulation of the toxic intermediate SAICAr affects cilia structure and function. Beside this we also found that enhanced DNA damage after loss of Adsl came from the lack of nucleosides and not from the accumulation of SAICAr . Taken together, these results showed that we have pathway-specific phenotypes of ADSLD. Further research is important for a better understanding of the complex pathology of ADSLD.

Furthermore, we discovered GRK4 also as a new regulator of kidney development ciliogenesis. Up to date, genetic variants of GRK4, that are found in patients suffering from high blood pressure, are often associated with a hyperactivity towards dopamine receptors. Here we showed that GRK4 extends its function, independently of its kinase activity. We postulate that GRK4 regulates mechanistic target of rapamycin (mTOR) signaling. Affecting mTOR led to a related phenotype like the GRK4 depletion, namely cilia elongation and dysfunctional kidneys in the zebrafish embryos. We were able to reproduce our results in human and murine cells. Interestingly, we found that the genetic variants of GRK4 failed to rescue any of the observed phenotypes. Further studies are important to identify potential interaction partners of GRK4 and how GRK4 influences mTOR signaling.

2 Introduction

2.1 Cilia architecture

Cilia are highly conserved antenna-like structures. They play important roles during embryogenesis, development and homeostasis. Depending on their inner architecture, one differentiates between motile and immotile/primary cilia. Motile cilia are able to beat and transport extracellular fluids along a tissue like for example the cerebrospinal fluid in the brain ventricles or mucus in the respiratory airways (2,3). In comparison, primary cilia are not able to move and have chemo- or mechanosensory properties (4). Cilia are, depending on their function, between 1–10 µm long and have a diameter of around 250–300 nm (5,6). The inner structure, termed as axoneme, consists of 9 microtubule doublets of an A and B tubule. Primary cilia have a so-called 9+0 architecture, which means that they lack a central microtubule pair which is crucial for cilia motility (Figure 1A). Most motile cilia, on the other hand, possess a central microtubule doublet, that is surrounded by a central sheath. Such 9+2 motile cilia have an inner and outer dynein arm, which is connected to the microtubule doublet. Each of these microtubule doublets is linked to its neighbors by nexin links. Additionally, the nine microtubules are connected to the central sheath by radial spokes (Figure 1B). A special form of motile cilia are the nodal cilia. They also have the inner and outer dynein arms and nexin links, but lack the central microtubule pair with its central sheath (9+0 composition) (Figure 1C).

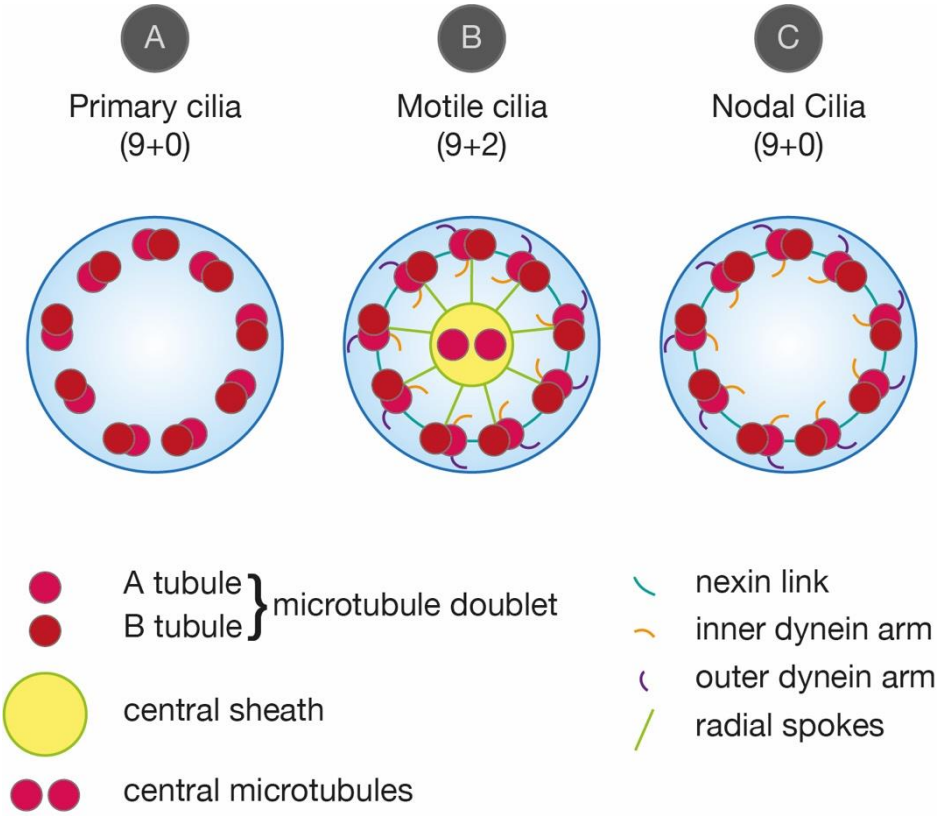

Figure 1: Cilia architectures

Cilia consist of nine microtubule doublets composed of an A and B tubule. A: Primary cilia show a so called 9+0 microtubule composition. B: Motile cilia have a 9+2 composition. Their nine microtubule doublets have an inner and outer dynein arm and are connected to their neighbors by nexin links. Moreover, they exhibit radial spokes to the central sheath, where a central microtubule pair is located. C: Nodal cilia are a specialized form of motile cilia. They lack the central microtubules (9+0 composition).

2.2 Cilia assembly

The axoneme elongates directly from a mature mother centriole (MC). Centrioles are highly conserved structures which in contrast to cilia consist of nine microtubule triplets forming a cartwheel (7). Each mature MC has a varying number of subdistal appendages (SDAPs) and nine distal appendages (DAPs) that are located at the distal end of the MC (8). One of the first steps during ciliogenesis is the docking of preciliary vesicles (PCVs) to the DAPs (9),(10) (Figure 2 1). These PCVs are transported by Dynein and multiple other factors to the pericentrosomal area of microtubules. Here they fuse with the DAPs (10) and form the ciliary vesicle (CV) (11) (Figure 2 2). This CV contains factors like RAB8 and ARL13b (12–14), which are important for the maturation of the MC to the basal body (BB) (15,16). These factors promote the outgrowth of the ciliary membrane. Parallel with the docking and

fusion of the CV, cilia elongation is initiated by other DAP proteins. One major role plays the centriolar coiled-coil protein of 110 kDa (CP110). CP110 can be found directly at the distal end of the BB. It stops the microtubule from growing by acting like a cap on top of the centriole. Removing CP110 initiates ciliogenesis (17–19). Simultaneously, the intraflagellar transport (IFT) complex assembles at the DAPs and the two motor proteins Kinesin-2 and cytoplasmic Dynein-2 are recruited (20,21). The next step is the formation of the ciliary transition zone (TZ) (Figure 2 4). This TZ is important for protein transition in and out of the cilium. Due to its complex protein network, malfunction of the TZ is often associated with ciliopathies like Joubert or Meckel syndrome (21). Within the TZ small Y-shaped linkers connect each microtubule doublet to the ciliary membrane (22). By the elongation of the microtubules, the ciliary sheath fuses with the plasma membrane. One important step during this process is the formation of the ciliary pockets. They serve as a domain for endocytosis and docking of the Intraflagellar Transport (IFT) machineries (5). The two motor proteins Kinesin-2 and Dynein-2 form the IFT machinery together with the IFT complex A and B and some accessory proteins like the BBSome. The IFT complexes act as an adapter between the two motor proteins and their cargo proteins. Complex A interacts with Dynein-2, whereas complex B is linked to Kinesin-2. Kinesin-2 is important for the transport of proteins from the ciliary base to the tip (Figure 2 5). This process is called the anterograde transport and plays a crucial role in cilia assembly and maintenance. In contrast, Dynein-2 transports cargo proteins from the ciliary tip back to the base, which is called the retrograde IFT (21,23,24) (Figure 2 6). Complex A and B are always linked to each other, even if they are not directly needed for the transport of the opposite direction. Dissociation of these two complexes can lead to defective ciliary transport mechanisms (25), which is one of many faces of ciliopathies.

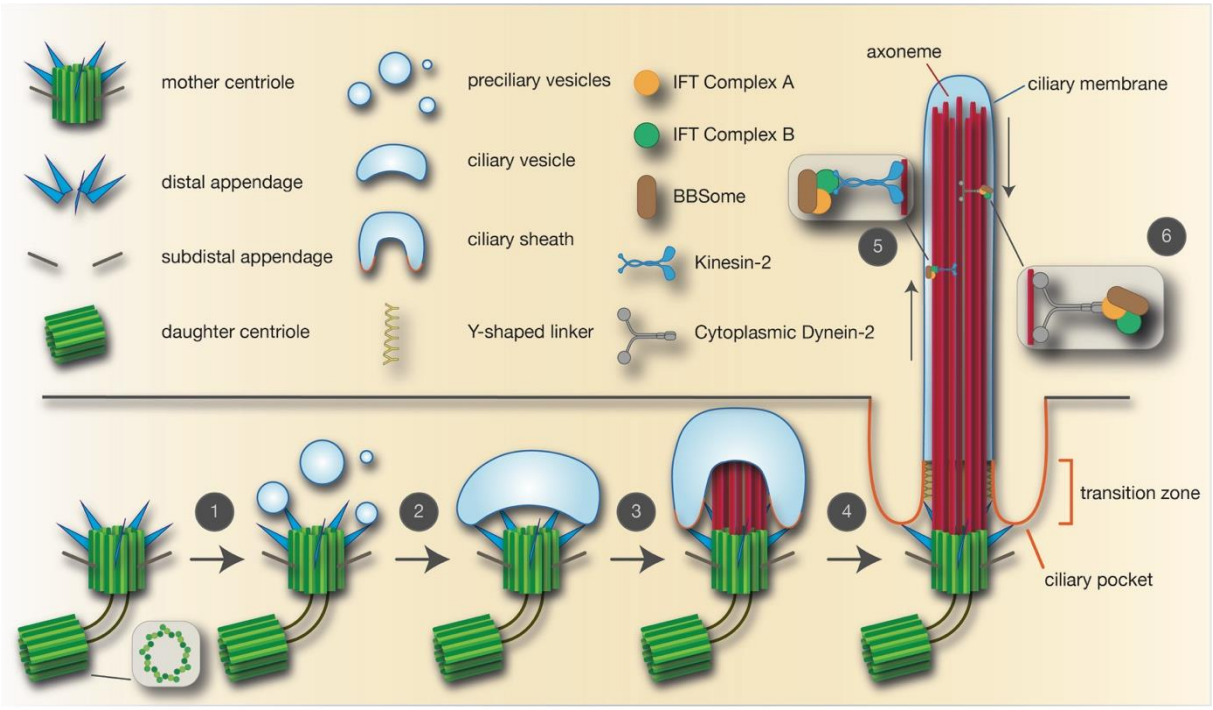

Figure 2: Cilia assembly

One of the first steps during ciliogenesis is the docking of preciliary vesicles to the distal appendages of a mother centriole (1). By fusing together, they build the ciliary vesicle, which contains multiple proteins, important for the maturation of the mother centriole to the basal body and ciliogenesis (2). Removing CP110 (not shown in this figure) initiates the elongation of the microtubule doublets (3). Shortly after this the transition zone forms, which plays an important role in transition of proteins in and out of the cilium (4). The intraflagellar transport (IFT) complex B and its motorprotein Kinesin-2 are responsible for the transport of cargo proteins from the ciliary base to the tip (5, anterograde transport). The transport of proteins from the ciliary tip back to the base (retrograde transport) is mediated by the IFT complex A with its motorprotein Dynein-2 (6). The microtubule doublets elongate after the IFT machineries transport ciliary proteins. By fusion of the ciliary sheath with the plasma membrane, the cilium is exposed to the outside of the cell (4). There, motile cilia can create fluid flows or primary, non-motile cilia, can sense external signals. Figure adapted from (21).

2.3 Ciliopathies

Cilia can be found on almost every cell of vertebrates. This makes them to an important factor as cilia are associated to many diseases (1,26–29). Mutations in genes encoding cilia assembly, maintenance or signaling proteins can lead to malformed or dysfunctional cilia (1). These cilia-associated disorders are also called ciliopathies. As cilia can be found on almost every cell, the spectrum of clinical phenotypes varies greatly and the number of conditions newly linked to cilia dysfunction remains growing (1). One example for a typical cilia-related phenotype is the heterotaxia syndrome. A symmetry breakage during early embryogenesis leads to the development of the so called left-right (LR) body axis, which is defined by the asymmetric positioning of the inner organs. This “normal” placement of the

inner organs is called *situs solitus* (Figure 3). If the inner organs are completely mirrored there is no clinical impact. (30). This arrangement is called *situs inversus totalis* (Figure 3). In case only one or a few organs are affected in their form or position the clinical relevance increases, and one speaks of heterotaxia (31).

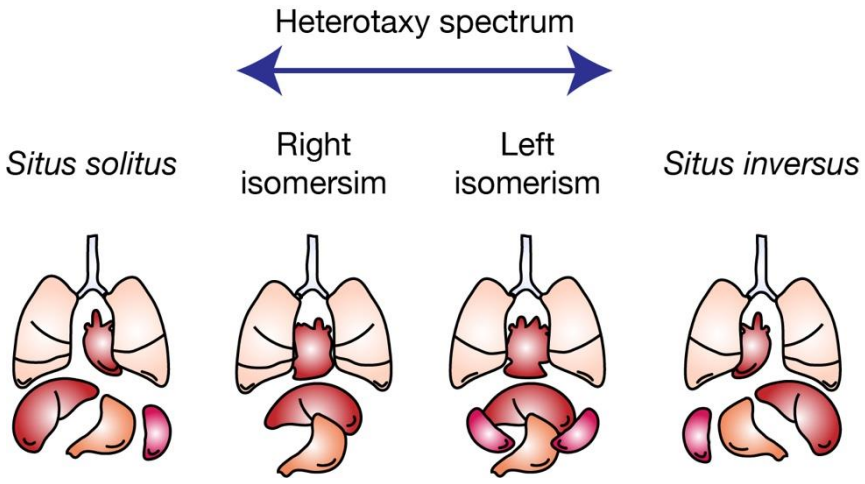

Figure 3: LR asymmetry and heterotaxy

Cartoon of the position of human inner organs reflecting *situs solitus*, heterotaxy and *situs inversus*. *Situs solitus* is considered to be the normal LR asymmetry in human bodies. The right lung is trilobed, whereas the left lung is bilobed. The liver is located on the right side, the spleen and stomach on the left side. *Situs inversus* is the completely mirrored image of *situs solitus*. Heterotaxy spectrum: right isomerism, with a doubled trilobed lung and a clustering of stomach and liver in the middle of the body. The spleen is absent. Left isomerism shows a double dilobed lung with multiple spleens and a clustering of the stomach and liver in the middle.

Responsible for the symmetry breakage is a LR organizer (LRO), termed Node in mice or Kupffer's Vesicle (KV) in zebrafish (32–35). During gastrulation dorsal forerunner cells (DFCs) cluster at the tailbud region of the developing zebrafish embryo where they form a fluid filled sphere, the KV (33,36,37). Motile cilia inside of the KV create a counterclockwise fluid flow (33,38) leading to the activation of the Nodal cascade only on the left side (30,36), which consist of the Tgf-β factor *nodal/southpaw* and *lefty2* and the homeobox transcription factor *pitx2* (36,39,40). This asymmetric gene induction initiates the LR asymmetry of the inner organs (Figure 4). Therefore, malformed or malfunctional cilia in the KV may cause the heterotaxia syndrome by an incorrect LR asymmetry.

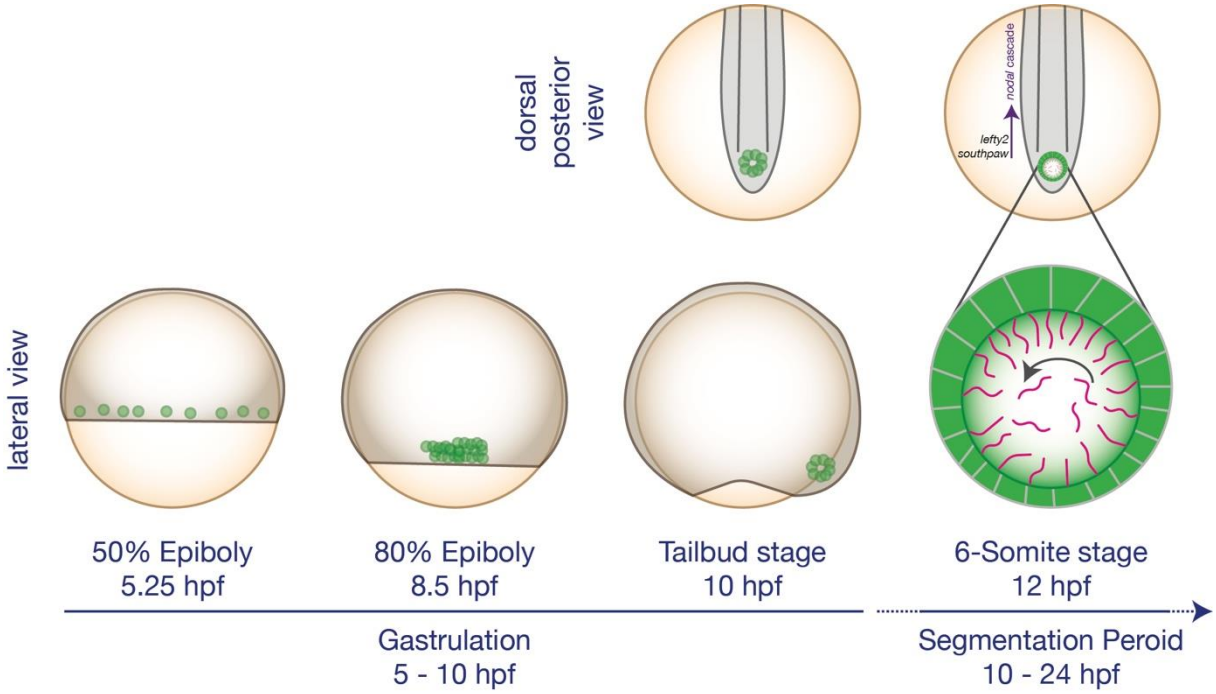

Figure 4: Formation of the Kupffer's vesicle in zebrafish embryos

During gastrulation dorsal forerunner cells (green dots) start to migrate and cluster at the base of the extending tailbud. From tailbud stage on these cells form a fluid-filled vesicle, called Kupffer's vesicle (KV). Motile cilia inside the KV create a counterclockwise fluid flow, which triggers the nodal cascade on left side of the embryo and genes like *lefty2* or *southpaw* get activated. This nodal cascade determines the LR asymmetry in the developing embryo.

Another prominent example for a ciliopathy is polycystic kidney disease (PKD) (1,27,28). PKD can occur in at least two different forms: autosomal dominant (ADPKD) or autosomal recessive (ARPKD). The autosomal dominant form of PKD is the most prevalent variant and restricted to adults. One major reason for ADPKD is a mutation in the genes encoding for the ion channels Polycystin1 (PC1) and Polycystin 2 (PC2) (1,27,28). Mutations in these genes lead to cyst formation in the kidney, mainly in the distal part of the nephron and the collecting duct (27). Also, hypertension has been described as a clinical phenotype of ADPKD (41). In contrast, patients suffering from ARPKD show a more severe clinical phenotype with an early onset during childhood or perinatally (42). Mutations in the gene namely polycystic kidney and hepatic disease 1 (*PKHD1*) are mostly responsible for ARPKD (42,43).

In addition to laterality determination and PKD, cilia also play an important role in neurodevelopment, as they are found on neuronal progenitor cells and on differentiated

neurons (44), where they are necessary for promoting the Hedgehog (HH) pathway (26,29). HH signaling is initiated by binding of one of the ligands Desert (DHH), Indian (IHH) or Sonic (SHH) to its receptor. For example, forebrain development depends on proper SHH signaling via primary cilia signaling (44,45). In the absence of the ligand SHH, the membrane receptor Patched 1 (PTCH1) is located to the cilium. It constitutively prevents the translocation of the G protein-coupled receptor Smoothened (SMO) into the cilium. Another G protein-coupled receptor, called GPR161, also locates to the cilium. GPR161 triggers a signaling cascade, which ultimately leads to the activation of Protein kinase A (PKA). PKA in turn activates a cascade which modifies the zinc finger proteins glioma-associated oncogene (GLI) 2 and GLI3. The modified forms of GLI2 and GLI3 translocate to the nucleus where they act as a transcriptional repressor (GLIR). In contrast, GLI1 acts as a transcriptional activator that is constitutively active and its expression is increased upon SHH activation. Furthermore, the GLI transcription factors also traffic to the ciliary tip in a complex with a protein called suppressor of fused homolog (SUFU). The interaction with SUFU leads to inactivation of the GLI transcription factors in the absence of SHH signaling (46) (Figure 5A)

After ligand binding, PTCH1 leaves the cilium and SMO then translocates into the cilium which in turn leads to the removal of GPR161. This prevents the activity of GPR161 towards PKA and the modifications of GLI2 and GLI3 to transcriptional repressors (47). The GLI transcription factors accumulate at the ciliary tip and dissociate from SUFU. These activated forms of GLI (GLIA) now translocate to the nucleus where they activate the transcription for several genes that are involved in development (Figure 5B). Alterations in cilia-mediated SHH signaling through impaired cilia may lead to a disturbed activation of SHH target genes and ultimately to malformations of the forebrain as shown in ADSLD (48).

Another example of a cilia defect resulting in aberrant neural development is a null mutation *alien* (*aln*) in the gene *tetratricopeptide repeat domain 21B (Ttc21b)* (49). This gene encodes for a protein called IFT139, which is located to the axoneme of the cilium and involved in the retrograde IFT. *Ift139*$^{aln/aln}$ mutants have defective cilia leading to

neurodevelopment defects like dorsal-ventral patterning defects or the loss of dorsal cortex (49,50).

To summarize, cilia are crucial for correct brain development, since changes in cilia structure or signaling can affect progenitor cell fate specifications, neuronal migration or neurogenesis (49,51,52). During neuronal development, cilia are found on progenitor cells and on differentiated neurons (44), where they are necessary for promoting SHH signaling.

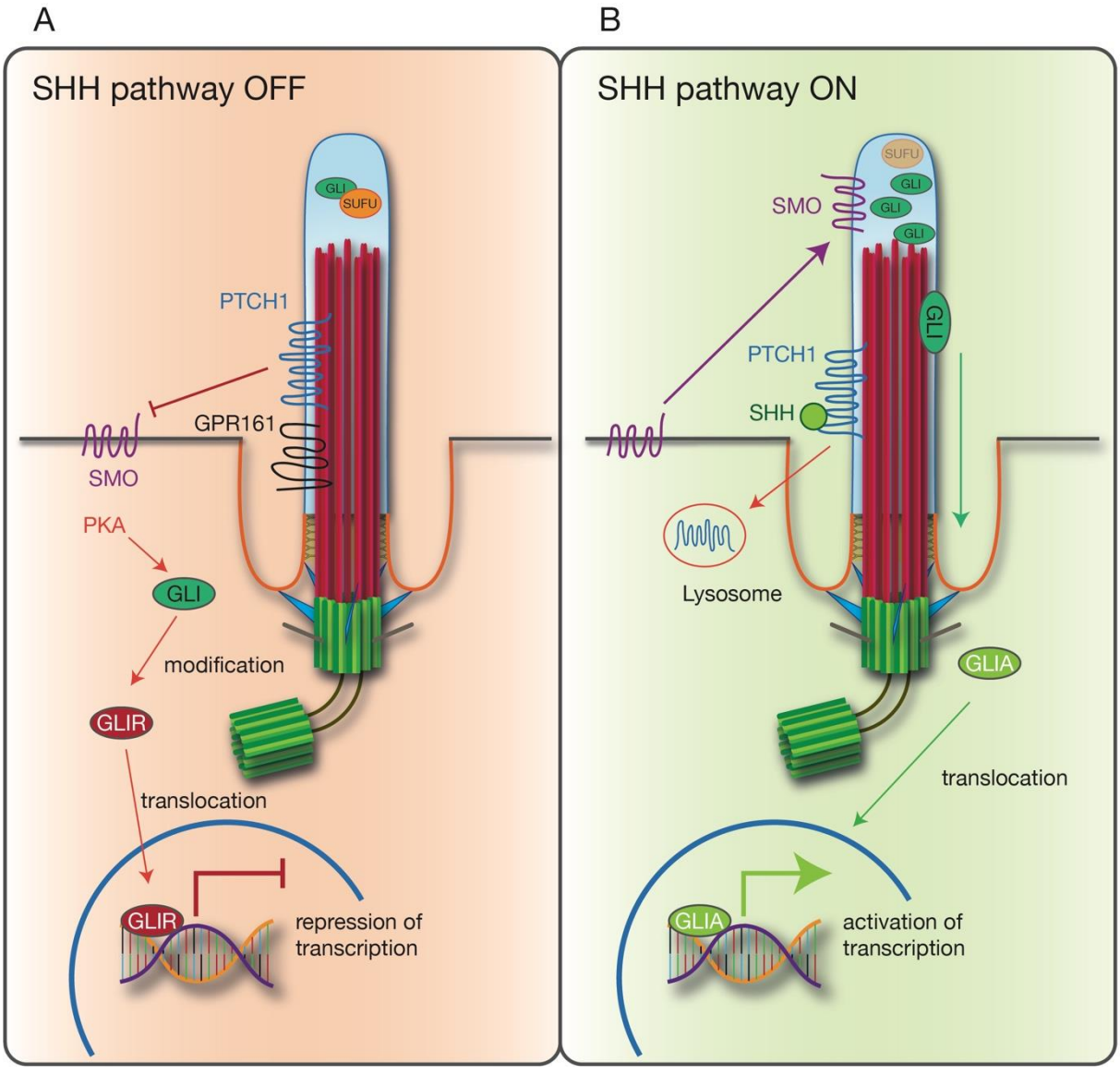

Figure 5: SHH signaling pathway

Cartoon of SHH signaling activation in the primary cilium (adapted from Andreu-Cervera et al. 2021 (44). **A**: When the SHH pathway is off, PTCH1 inhibits SMO. GLI transcription factors are located in the ciliary tip and bound to SUFU, which inhibits them. GLI factors are also degraded by a signaling cascade of GPR161 and PKA and translocate to the nucleus, where they act as a repressor (GLIR) for the transcription of target genes. **B**: Upon ligand binding, PTCH1 leaves the cilium and SMO translocates to the ciliary tip.

The GLI transcription factors dissociate from SUFU and translocate to the nucleus, where they act as activator (GLIA) of target genes.

2.4 Adenylosuccinate Lyase Deficiency

ADSL is a protein that participates in the *de novo* synthesis pathway of purines (DNPS) (48). It consists of a coiled coil domain, a low complexity region and the lyase domain at the C-Terminus. Two genetic variants of ADSL, namely *R426H* and *V429A,* are associated with a disease called ADSLD (Figure 6).

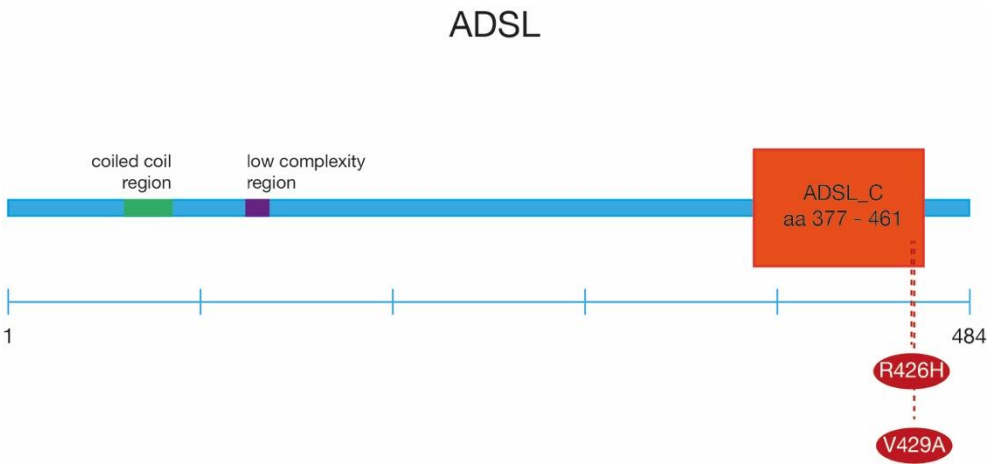

Figure 6: Protein structure of the human ADSL

The human *ADSL* gene encodes for a 484 amino acid (aa) protein. It consists of a coiled coil domain in the N-terminal region at position aa 59 to 83 and a low complexity region from aa 120 to aa 132. The Adenylosuccinate lyase C-terminus (ADSL_C) is from aa 377-461. Two genetic variants in the C-terminus are directly associated with ADSLD, namely *R426H* and *V429A.*

ADSL catalyzes two steps in the DNPS: first, the conversion of aminoimidazolosuccinicarboxamideribotide (SAICAR) to aminoimidazolocarboxamideribotide (AICAR) (Figure 7 11) and second in the purine salvage pathway the conversion of adenylosuccinate (S-AMP) to adenosin-5'-monophosphate (AMP) (Figure 7 15).

The first step in the tetrahydrofolate (THF) cycle is the reaction from folate to dihydrogenfolate (DHF) via the dihydrofolatereductase (DHFR). (Figure 7 1). DHF is then converted to THF, again by the DHFR (Figure 7, 2). Worth mentioning is, that Methotrexate (MTX) acts as an inhibitor for DHFR. After three other reaction steps, the

end product of the THF cycle, called 10-formyl-THF (or 10-CHO-THF), will be used in the following DNPS (Figure 7 3).

In the DNPS the steps 4-13 are catalyzed by 6 different enzymes. A trifunctional enzyme (visualized in blue dots), two bifunctional (visualized in green and purple dots) and three monofunctional (visualized in light red dots). After the transformation of D-ribose-5-phosphat to α-5-phospho-D-ribosyl-1-pyrophosphate via ribose-phosphate pyrophosphokinase (PRPS), phosphoribosyl pyrophosphate amidotransferase (PPAT) catalyzes the step 4. The next two steps (5 and 6, but also step 8) are catalyzed by the trifunctional enzyme glycinamide ribonucleotide synthetase-glycinamide ribonucleotide transformylase-aminoimidazole ribonucleotide synthetase (GARS-GART-AIRS). The seventh steps is catalyzed by the formylglycinamidine ribonucleotide synthase (FGAMS). The first bifunctional enzyme in this pathway, namely aminoimidazole ribonucleotide carboxylase-aminoribosyl aminoimidazole succinocarboxamide ribonucleotide synthetase (AIRC-SAICARS), takes part in the steps 9 and 10. Then, ADSL catalyzes the eleventh step. The last two steps (12 and 13) of the DNPS are catalyzed by another bifunctional enzyme called aminoimidazolecarboxamide ribonucleotide formyltransferase – inosine monophosphate (IMP) cyclohydrolase (AICARFT-IMPCH or ATIC). It is important to say, that for the reaction 6 and 12, the cell requires 10-CHO-THF, which comes from the above mentioned THF cycle.

The end product of the DNPS, IMP, will then be transformed in the following purine salvage pathway. IMP can be converted to xantosine-5'-monophosphate or it is converted to S-AMP via adenylosuccinate synthase (ADSS). S-AMP will then be transformed to AMP, which is catalyzed by ADSL. Two important end products of this purine salvage pathway are adenine and guanine, both necessary for life (53).

ADSLD represents an autosomal recessive disease that was first described by Jaeken and van den Berghe in 1984 (54). They found elevated levels of two toxic intermediates, called SAICAr (the dephosphorylated form of SAICAR) and S-Ado (the dephosphorylated form of S-AMP), in body fluids, especially in the cerebrospinal fluid (CSF), as well as in the blood and the urine of 3 juvenile patients. The patients suffered from severe psychomotor delays

and autism (54). Of note, it seems that the concentration and ratio between SAICAr and S-Ado is one of the major features contributing to the severity of the clinical phenotypes of ADSLD, as this leads SAICAr-dependently to more severe symptoms (48,55). Based on this observation, several studies support the hypothesis that the accumulation of these toxic intermediates is determining the clinical phenotypes, rather than the disturbed DNPS (48,56,57).

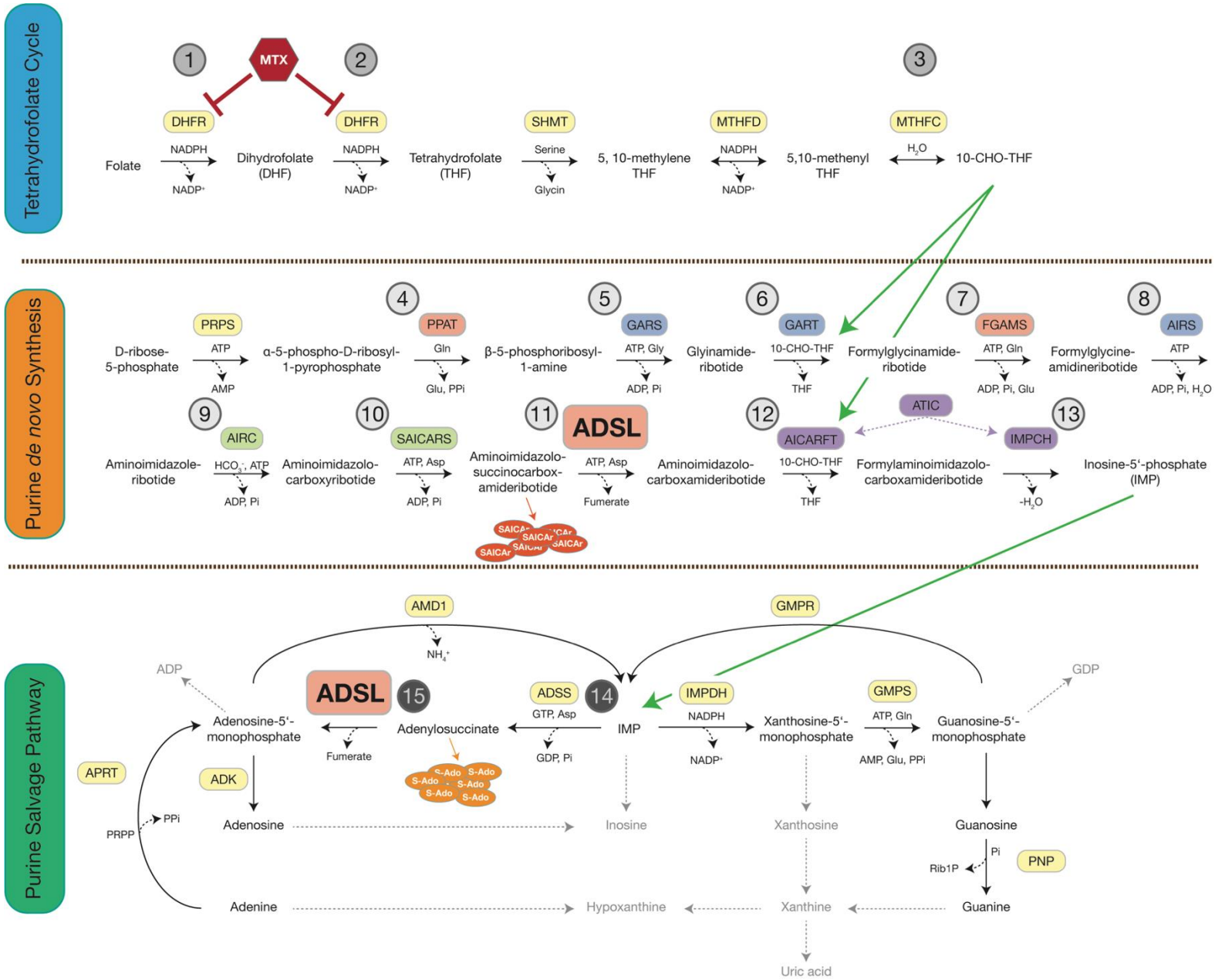

Figure 7: ADSL and the de novo purine synthesis pathway

For abbreviations of enzymes, product names and reaction steps see text of 2.4.

Light red bubbles show three monofunctional enzymes in the DNPS.

Purple and green bubbles show two bifunctional enzymes in the DNPS.

Blue bubbles show a trifunctional enzyme in the DNPS.

Accumulation of toxic intermediates during step 11 and 15 if ADSL does not function properly.

Adapted from Dutto et al. 2022 (48).

2.5 G protein-coupled receptor signaling

G protein-coupled receptors (GPCR) are the largest family of receptors and regulate numerous biological processes. Upon stimulation by an extracellular signal GPCRs act as signal transducer and translate the signal into an intracellular response. GPCRs can be divided in 5 subfamilies: rhodopsin-like, secretin-like, metabotropic, adhesion and frizzled receptors (58). Their structure is composed of 7-transmembrane (TM) α-helices, three extracellular and three intracellular loops. The N-terminus reaches in the extracellular space, while the C-terminus is intracellular (59) (Figure 8). Different ligands, like proteins, ions or other chemicals, can bind to the GPCR (60). Binding of the ligand leads to a conformational change of the GPCRs, which in turn leads to an intracellularly activation of a heterotrimeric G protein. This G protein complex is composed of a Gα, and Gβγ subunit. When inactive, the subunits form an heterotrimer with Gα bound to GDP (61–63). Upon ligand binding, the conformational change of the GPCRs results in the dissociation of GDP from the Gα subunit. Gα then rapidly binds GTP as it has a very short lifetime in the unbound state. This is a rate-limiting step in G-protein activation (61,64). Binding of GTP to Gα leads to the dissociation of the Gβγ dimer from the Gα subunit. The monomeric Gα subunit as well as the Gβγ subunit are able to trigger downstream signaling cascades like the recruiting of G protein-coupled receptor kinases (GRKs) at the membrane by the Gβγ subunit (60).

GRKs and a second protein family called Arrestins also can interact with the activated form of a GPCR (65). GRKs and Arrestins are involved in GPCR desensitization, internalization and recycling of GPCRs (66). Thereby, they are key players in the regulation of GPCR signaling. To date there have been seven different GRKs identified in humans. These seven GRKs are divided in three big families: GRK1 and GRK7 belong to the opsin family, whereas GRK2 and GRK3 create the β-adrenergic receptor family. The GRK4 family consists of GRK4, GRK5 and GRK6 (67). While GRK2,3,5 and 6 are ubiquitously expressed, GRK1 and 7 are restricted to rod and cone cells. For GRK4 it has been shown that it is expressed in the testis, the kidney and the cerebellum (68,69). Unpublished data of the Phillip lab showed that GRK4 is also expressed in the heart, the liver, spleen and in muscles of mice.

After recruiting of GRK to GPCRs by Gβγ, the GRKs phosphorylate a serine/threonine residue of the C-terminal region of the GPCR. This leads to binding of Arrestin. Arrestins can be divided into two subfamilies: the visual Arrestins, consisting of Arrestin 1 or rod Arrestin with Arrestin 4 or also called cone Arrestin, and in sensory Arrestins, consisting of Arrestin 2 or β-Arrestin 1 and Arrestin 3, which is also called β-Arrestin 2 (64,70–72). The binding of Arrestin to the phosphorylated residues of the GPCR inhibits further coupling of another G protein. The signaling cascade stops and the GPCR is desensitized (73). Desensitized GPCRs will be internalized and degraded or recycled (60) (Figure 8).

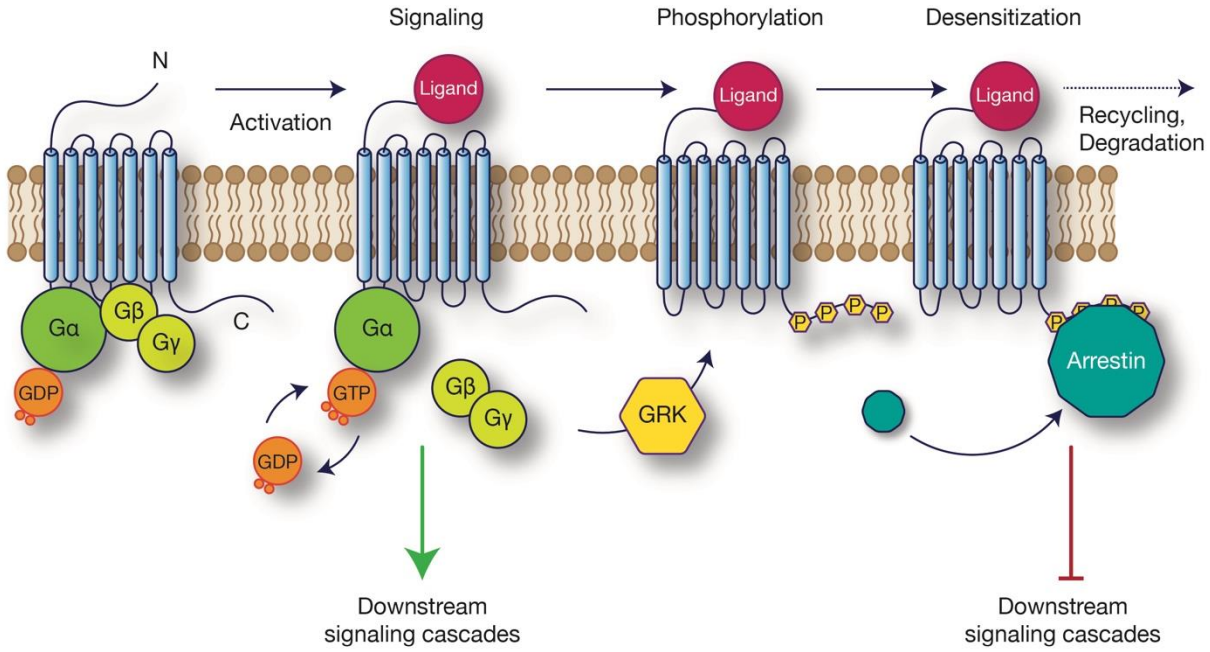

Figure 8: The GPCR signaling cascade

The 7-TM GPCR has an inactive G protein complex consisting of a Gα,β and γ subunit bound at the intracellular region. The Gα subunit is coupled to GDP. Upon ligand binding at the N-terminus in the extracellular region, the GPCR undergoes conformational changes which leads to an exchange from GDP to GTP at the Gα subunit and the dissociation of Gα from the Gβ,γ dimer. Both subunit complexes activate downstream signaling cascades like the recruitment of GRKs at the membrane. GRKs phosphorylate serine/threonine residues of the C-terminus of a GPCR. Arrestins are able to recognize them and bind there. This process is also called GPCR desensitization as it stops the G-protein mediated signaling. The arrestin-bound GPCR will then be internalized and degraded or recycled.

2.6 G protein-coupled receptor kinase 4 in associated hypertension

The kidney as a ciliated organ is important to regulate blood pressure and fluid balance (1). The renin-angiotensin-system (RAS) is a key player that controls these processes through sodium uptake (74). If sodium is needed in our body, the RAS is activated by extracellular

stimuli. Thereby, Renin cleaves a 10 amino acid peptide from the N-terminus of Angiotensinogen (Agt) leading to Angiotensin 1 (Ang I). Ang I is then subsequently cleaved by the Angiotensin-converting enzyme (ACE) in Angiotensin II (Ang II) which is the major effector peptide generated by the RAS (74–76). Ang II activates the Angiotensin II type 1 receptor (AT1) which in turn stimulates the expression and activation of the Sodium/Hydrogen (Na^+/H^+) exchanger isoform 3 (NHE3) at the brush border of the proximal tubule (77,78). For sodium release, the Na^+/K^+ ATPase is also activated by the AT1 (79).

The antagonist to the RAS is the dopaminergic system (DA). The Dopamine receptors belong to the family of GPCRs and are divided into two subfamilies: the D1-like receptors, consisting of D1 and D5, and the D2-like receptors, consisting of D2, D3 and D4. One differentiates between D1-like and D2-like receptors based on their G protein subtype coupling (67). Both subfamilies of the dopamine receptors are expressed in different regions of the mammalian kidney. So are the D1, D5 and D3 receptors expressed in the proximal tubule while the D1, D5, D3 and D4 receptors are expressed in the collecting duct (80). After ligand binding, the G protein dissociates from its GPCR. The released G protein mediates a signaling cascade that regulates the homeostasis by decreasing the salt concentration and water reabsorption. This process is regulated by an inhibitory effect on the expression and activity of NHE3 and the Na^+/K^+ ATPase (81). Besides this function, Dopamine is also required to inhibit the expression of AT1 (67). In conclusion, activated Dopamine receptors trigger the excretion of sodium in the urine which is called natriuresis.

To protect the receptor from overstimulation, GRKs phosphorylate serine/threonine residues of the GPCR. Phosphorylation of GPCR leads to the binding of Arrestin, which prevents the reassociation of the G protein complex to the receptor. The GPCR gets desensitized and degraded or recycled and the G protein mediated signaling cascade stops, leading to increased reabsorption of sodium into the blood. Due to osmosis reasons the reabsorption of water also increases and by that the blood pressure (80).

These two reciprocal systems precisely control sodium homeostasis and thereby blood pressure (74,81). Therefore, alterations in this sensible system can lead to clinical

phenotypes like high blood pressure that affects about two third of adults older than 65 that suffer from hypertension. Of note, high blood pressure is considered as a clinical symptom, whereas hypertension is a health disorder. A reason for hypertension is attributed to a functional change of the dopamine receptor by GRK4 (82).

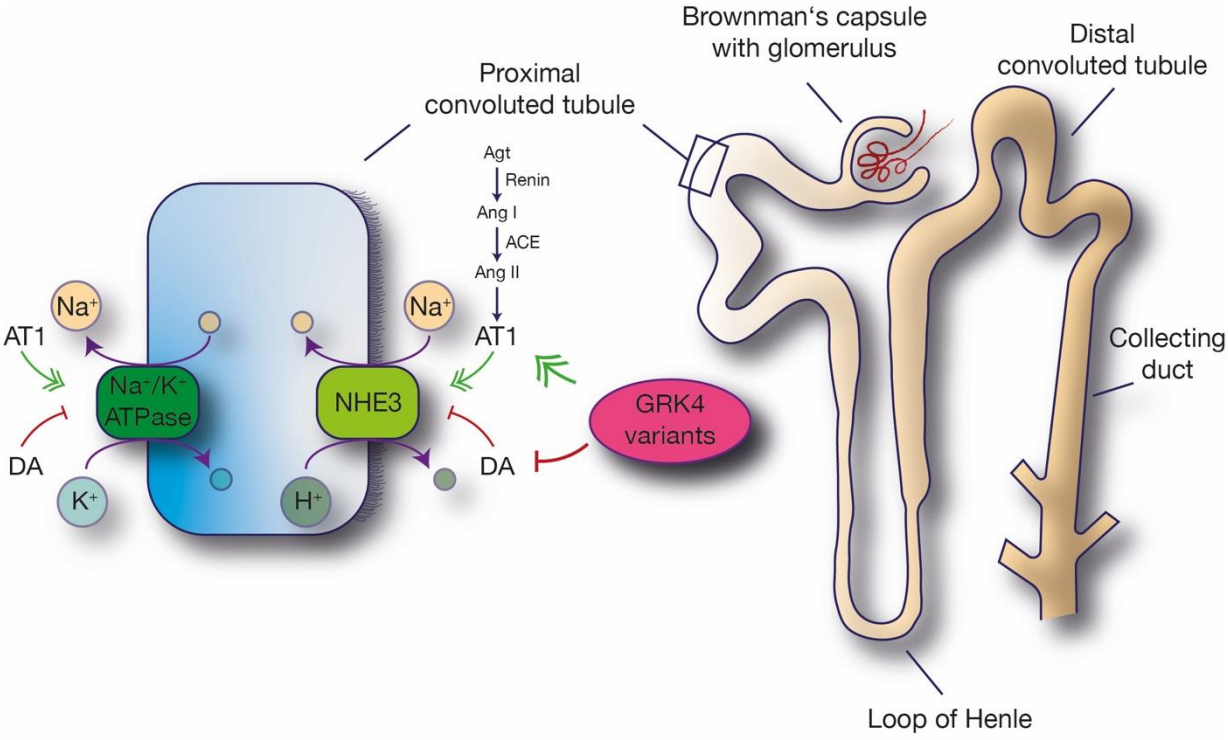

Figure 9: The interplay of the RAS and DA controls sodium balance in the proximal convoluted tubule

The renin-angiotensin-system (RAS) regulates the reuptake of sodium in our blood. Renin cleaves Angiotensinogen (Agt) in Angiotensin I (Ang I). The Angiotensin-converting enzyme (ACE) cleaves Ang I in Ang II, which in turns activates AT1 that stimulates the expression and activity of the Sodium/Hydrogen (Na^+/H^+) exchanger isoform 3 (NHE3). AT1 also activates the Na^+/K^+ ATPase that transports sodium out of the cells into the blood and with that water due to osmosis reasons. The Dopaminergic system (DA) acts as counter to the RAS. Increased dopamine levels inhibit the activity of NHE3 and Na^+/K^+ ATPase. Genetic variants of GRK4 have been found to stimulate the RAS and inhibit the DA.

GRK4 has been identified as the kinase responsible for the phosphorylation of Dopamine receptors in the proximal tubule. *GRK4* encodes for four different isoforms in humans: α (which is the full-length version of GRK4) β, γ and δ, which are a little shorter than the full-length version (Figure 10). The importance of each isoform is still unclear and needs further evaluation. GRK4 has two important protein domains: The G-protein signaling (RGS) homology (RH) domain is important for protein-protein interactions, while the kinase domain is required for the phosphorylation of serine/threonine residues.

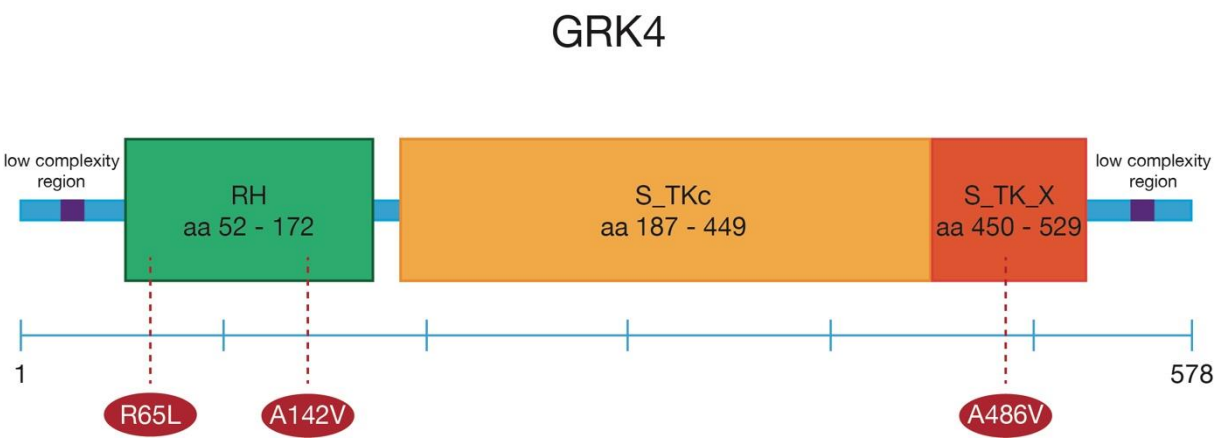

Figure 10: Structure of the human GRK4

Human GRK4 is a 578 aa protein. This version is called the α or full length version of GRK4. There are also three shorter isoforms of GRK4, namely β γ and δ. The β-isoform is 564 aa long, γ-isoform 532 aa and δ-isoform is the shortest with 500 aa. Two low complexity regions can be found from aa 18-31 and from 551-562. From aa 52-172 GRK4 has a G-protein signaling (RGS) homology (RH) domain. From aa 187-449 we can see the Serine/Threonine protein kinase, catalytic domain (S_TKc). From aa 450-529 GRK4 has the extension to the Serine/Threonine-type protein kinase (S_TK_X). Two genetic variants of GRK4, *R65L* and *A142V* are located in the RH domain. The genetic variant *A486V* is located in the extension of the kinase domain. All of them are known to be hyperactive towards phosphorylation of dopamine receptors (83).

Genetic variants of GRK4 are associated with hypertension (82). Patients suffer from an increased GRK4 activity and impaired dopamine receptor function in renal proximal tubule cells (80). This leads to loss of natriuresis and in turn increases blood pressure. Of note, it has been shown that GRK4 variants are able to increase the activity and expression of AT1 receptors which increase sodium level and water reabsorption (67) (Figure 9).

Besides the function of GRKs in phosphorylating GPCRs, it has also been demonstrated that they are important during different processes like ciliogenesis. Especially for GRK5 is has been shown, that it localizes to cilia where it controls cilia function and cilia structure (84).

2.7 Aim of this work

Ciliopathies have a very broad spectrum of clinical phenotypes, reaching from congenital heart defects to hearing loss or infertility, but also renal anomalies or mental disability (1). Therefore, cilia, or more precisely, regulators of cilia function and/or cilia structure, are highly interesting targets for potential drug treatments. The major goal of this study is to investigate ADSL and GRK4 as two new regulators of cilium biology.

To address this, I have performed loss-of-function (LOF) experiments to strengthen the hypothesis that the accumulation of the toxic intermediates SAICAr and S-Ado mainly affects ciliogenesis and by that the pathology of ADSLD. I also analyzed phenotypes that come from the lack of nucleosides. Additionally, I evaluated the genetic variants of ADSL that are associated with ADSLD using my ADSL LOF model.

I also investigated the role of GRK4 during kidney development. LOF studies in human fibroblasts, murine kidney cells and zebrafish embryos were performed to show that GRK4 regulates ciliogenesis independently of its kinase activity. Furthermore, I analyzed a downstream pathway that is affected after GRK4 LOF.

3 Materials

3.1 *Danio rerio* strains

Table 1: *Danio rerio* strains used for this study

Danio rerio strain	ZFIN or transgenic ID
AB wild type (AB)	ZDB-GENO-960809-7
Ekkwill wild type (EK)	ZDB-GENO-990520-2
Tg(cmlc2:GFP) (cmlc2-GFP)	ZDB-TGCONSTRCT-140716-2
Wt1b-GFP (kind gift of Christoph Englert (85))	ZDB-ALT-071127-1 (86)
Grk4 1.2	Generated by Prof. Melanie Philipp

3.2 *Danio rerio* Media and Supplements

Table 2: Media and supplements for zebrafish maintenance and breeding

Medium/Supplement	Composition/Manufacturer	Application
1x E3	100 ml 50x E3 stock 5 l H_2O 2-3 drops 1 % methylene blue	Zebrafish embryo experiments and culturing
50x E3	29.2 g NaCl 1.26 g KCl 4.86 g $CaCl_2 \cdot 2H_2O$ 8.14 g $MgCl_2 \cdot 6H_2O$ 1800 ml H_2O 0.1 M NaOH to adjust pH to 7.2	Stocksolution for 1x E3

Egg Water	0.3 g Instant Ocean® 0.75 g $CaSO_4$ 0.036 mg $NaHCO_3$ 2-3 drops 1 % methylene blue H_2O to 1 l	Zebrafish embryo culturing
Embryo Medium	5 ml Hank's solution 1 0.5 ml Hank's solution 2 5 ml Hank's solution 4 5 ml Hank's solution 5 5 ml Hank's solution 6 (freshly made) 479.5 ml H_2O adjust pH to 7.2	Zebrafish treatment, preparation of Methylcellulose and injection plate
Hank's Solution 1	8 g NaCl 0.4 g KCl 100 ml H_2O	Embryo medium
Hank's Solution 2	0.358 g Na_2HPO_4 0.6 g KH_2PO_4 100 ml H_2O	Embryo medium
Hank's Solution 4	0.72 g $CaCl_2$ 50 ml H_2O	Embryo medium
Hank's Solution 5	1.23 g $MgSO_4 \cdot H_2O$ 50 ml H_2O	Embryo medium
Hank's Solution 6	0.35 g $NaHCO_3$ 10 ml H_2O	Embryo medium
Instant Ocean®	Instant Ocean® Sea Salt (Spectrum Brands, Inc., USA)	Zebrafish maintenance
Zebrafish dry food	Zebrafeed 200-400 (Sparos, Portugal)	Zebrafish feeding

Zebrafish live food	Great Salt Lake Artemia Cysts (Aqua Schwarz GmbH, Germany)	Zebrafish feeding

3.3 Morpholino antisense oligonucleotides (MO)

All MOs were purchased from GeneTools, LLC (USA).

Table 3: MOs used for zebrafish embryo injections

MO	Sequence
Adsl ATG MO	5'- TCCCTCCATGCCTGCAGCGGTTAAA
Adsl splMO	5'- CCAACTGTGGGAGAGAGCGACTGTA
Grk4 ATG MO	5'- GTCAGAAGAAAGATCCCATGCAGTC
Grk4 CTRL MO	5'- GTGACAACAAACATCCCATCCAGTC
Standard CTRL MO (CTRL MO)	5'- CCTCTTACCTCAGTTACAATTTATA

3.4 Cell lines

Table 4: Cell lines used during this study

Cell Line	Manufacturer
Human Retinal Pigment Epithelial Cells (RPE1)	Kind gift of Stracker Lab (87)
Human Embryonic Kidney 293 cells (HEK)	American Type Culture Collection (ATCC) (USA)
Human hTERT Immortalized 1BR3 Wild-Type Fibroblasts (1BR3)	Genome Damage and Stability Centre, University of Sussex (United Kingdom)
Mouse Inner Medullary Collecting Duct Cells (IMCD3)	Kind gift of Sören Lienkamp (Freiburg, Germany)

3.5 Media and Supplements for Cell Culture

Table 5: Media and Supplements used for cell culture

Media/Supplement	Manufacturer	Application
Phosphate Buffered Saline (PBS)	Sigma-Aldrich Inc. (USA), Cat.# D8537	RPE1, hTERT 1BR3, IMCD3 and HEK culturing
Fetal Bovine Serum, qualified, heat inactivated	Life Technologies Limited (USA), Cat.# 10500-064	RPE1, hTERT 1BR3, IMCD3 and HEK culturing
Opti-MEM™, Reduced Serum Medium, no phenol red	Life Technologies Limited (USA), Cat.# 11058-021	Transfection of RPE1, hTERT 1BR3, IMCD3 and HEK
Penicillin-Streptomycin (Pen/Strep)	Life Technologies Corporation (USA), Cat.# 15140-122	RPE1, hTERT 1BR3, IMCD3 and HEK culturing
Trypan Blue Staining	Life Technologies (USA), Cat.# T10282	for cell counting with Countess™ Automated Cell Counter
Trypsin EDTA (1x)	Life Technologies Limited (USA), Cat.# 25300-054	RPE1, hTERT 1BR3, IMCD3 and HEK detaching
Dulbecco's Modified Eagle's Medium – high glucose (DMEM)	Sigma-Aldrich Inc. (USA), Cat.# D6429	HEK culturing
Dulbecco's Modified Eagle Medium:Nutrient Mixture F-12 (1:1) (1x) (DMEM/F-12)	Life Technologies Limited (United Kingdom), Cat.# 11320-074	RPE1 and IMCD3 culture
Minimum Essential Medium (MEM) α	Life Technologies Limited (United Kingdom), Cat.# 22571-020	hTERT 1BR3 culturing
Matrigel® Matrix, Basement Membrane, Growth Factor reduced	Corning Inc. (USA), Cat.# 354230	3D matrix for growing spheroids

3.6 siRNA for cell culture

Table 6: siRNAs used for this study

siRNA	concentration	Manufacturer	Application
ON-TARGET plus Mouse Grk4 siRNA SMARTpool	20 µM in H_2O ad. inj.	Dharmacon Inc. (USA), Cat.# L-040342-02-0010	Knockdown of GRK4 in IMCD3
ON-TARGET plus Human Grk4 siRNA SMARTpool	20 µM in H_2O ad. inj.	Dharmacon Inc. (USA), Cat.# L-004625-00-0005	Knockdown of GRK4 in 1BR3
FlexiTube siRNA AllStars Negative Control	20 µM in H_2O ad. inj.	QIAGEN® (Germany), Cat.# SI03650318	Negative control in RNAi experiments

3.7 Bacteria strain

Table 7: Bacteria used for this study

Bacteria strain	Manufacturer	Application
One Shot™ TOP10 Chemically Competent *E. coli*	Invitrogen (USA)	Cloning

3.8 Bacteria Media and Supplements

Table 8: Media and Supplements for bacteria

Medium/Supplement	Composition/Manufacturer	Application
Super Optimal Broth medium with added glucose (S.O.C. medium)	Invitrogen (USA)	Transformation of bacteria
Lysogeny broth (LB) plates	32 mg Lennox L Agar 1 l distilled H_2O	Bacteria culture

	100 µg/ml ampicillin or kanamycin (after autoclaving)	
Lennox L Agar	Invitrogen (USA)	LB plate preparation
Lennox L Broth Base	Invitrogen (USA)	LB Broth Base medium
Ampicillin	AppliChem (Germany)	Bacteria culture
Kanamycin	AppliChem (Germany)	Bacteria culture

3.9 Vectors

Table 9: Vectors used for cloning reactions

Vector	Resistance	Manufacturer	Application
pCS2+	Ampicillin	Philipp Lab	Cloning

3.10 Plasmids

Table 10: Plasmids used in this study

Name	Insert	cloned with
pCRII-zfAdsl	921bp fragment of zfAdsl	
pCRII-zfAngptl3	1010bp fragment of Angiopoietin like3 for WMISH	
pGEMT-zfCmlc2	Partial cDNA of zfCmlc2	Kind gift of D. Yelon
pCRII-zfLefty1	zfLefty1	Kind gift of J. Yost
pCRII-zfGrk4 5'UTR	637bp fragment of zGRK4	
pCRII-zfSouthpaw	952 bp fragment of zfSouthpaw	
pCS2+-Flag-zfAdsl MO mut	Flag-tagged zfAdsl for rescue injections	EcoRI/XhoI

pCS2+-hADSL	ORF of hADSL	ClaI/StuI
pCS2+-hADSL R426H	ORF of hADSL R426H	ClaI/StuI
pCS2+-hADSL V429A	ORF of hADSL V426A	ClaI/StuI
pCS2+-zfGrk4	ORF of zfGrk4	ClaI/StuI
pCS2+-zfGrk4 K216M/K217M	Kinase dead (KiDe) version of zfGrk4	ClaI/StuI
pCS2+zfGrk4 c580_585del	construct resembling Grk4 mutant 1.2	ClaI/StuI
pCS2+-zfGrk4 UTRORF	part of 5'-UTR + ORF of zfGrk4 for MO test	ClaI/StuI
pCS2+-zfGrk4 ΔRH	Construct resembling the hGRK4 ΔRH with the respective amino acids of zebrafish Grk4	ClaI/StuI
pCS2+Flag-hGRK4 α	Flag-tagged hGRK4 α version (=full length variant)	ClaI/StuI
pCS2+Flag-hGRK4 β	Flag-tagged hGRK4 β version	ClaI/StuI
pCS2+Flag-hGRK4 γ	Flag-tagged hGRK4 γ version	ClaI/StuI
pCS2+Flag-hGRK4 δ	Flag-tagged hGRK4 δ version	ClaI/StuI
pCS2+Flag-hGRK4 R65L	Flag-tagged hGRK4 R65L	ClaI/StuI
pCS2+Flag-hGRK4 A142V	Flag-tagged hGRK4 A142V	ClaI/StuI
pCS2+Flag-hGRK4 K216M/K217M	Flag-tagged KiDe version of hGRK4	ClaI/StuI
pCS2+Flag-hGRK4 ΔRH	Flag-tagged human GRK4 deleted of aa39-180	ClaI/StuI
pCS2+-zfGrk4 ΔRH	construct resembling the hGRK4 ΔRH with the respective amino acids of zebrafish Grk4	ClaI/StuI

A great thank to Conny Donow, Monika Häußler, Dr. Lars D. Maerz, Elke Zabinsky and Prof. Melanie Philipp for cloning following plasmids: pCRII-zfAdsl, pCRII-zfAngptl3, pCRII-zfGrk4 5'UTR, pCRII-zfSouthpaw, pCS2+-zfGrk4, pCS2+-zfGrk4 K216M/K217M,

pCS2+-zfGrk4 UTRORF, pCS2+Flag-hGRK4 α, pCS2+Flag-hGRK4 β, pCS2+Flag-hGRK4 γ, pCS2+Flag-hGRK4 δ, pCS2+Flag-hGRK4 R65L, pCS2+Flag-hGRK4 A142V, pCS2+Flag-hGRK4 K216M/K217M, pCS2+Flag-hGRK4 ΔRH and pCS2+Flag-zfGRK4 ΔRH.

3.11 Primers

Table 11: Primers used for genotyping, PCR and qPCR with UP and cloning

Name	Sequence 5' →3'	UP
zfAdsl WMISH fw 921 bp	5'-GAT GCT CAG GTA AGC GAG ATG	
zfAdsl WMISH rev 921 bp	5'-ATA GAC CAC CAG GCC TTC AGT	
HA-hADSL Fw ClaI	5'- ACG TAT CGA TAT GTA CCC ATA CGA TGT TCC AGA TTA CGC TGC GGC TGG AGG CGA TCA T	
hADSL Rev StuI	5'- ACG TAG GCC TCT ACA GAC ATA ATT CTG CTT TCA CC	
SP6 (for sequencing)	5'- ATT TAG GTG ACA CTA TAG	
T7 (for sequencing)	5'- TAA TCA CTG TAC AGG GGA AAG TC	
zfGrk4 CRISPR WT Fw	5'- TGG GAT TTA CGG TGC ATT GTT ATT AGT GAA	
zfGrk4 CRISPR mut Fw	5'- CAT TAC AGG GTA TTG GGC ATT T	
zfGrk4 CRISPR combo Rev	5'- ACC ACT GAT AAC GCC CAT TCA ATC AAA TG	
zfGRK4 Fw ClaI	5'- ACG TAT CGA TAT GGA GAT TGA GAA TAT CGT GGC C	
zfGRK4 Rev StuI	5'- ACG TAG GCC TAG CCC CTC CCC CTC TGA G	
zfGrk4 c 580_585del Fw	5' ACA GGG TAT TGG GCG GAT TTG GTG AGG T	
zfGrk4 c 580_585del Rev	5'- ACC TCA CCA AAT CCG CCC AAT ACC CTG T	

hGRK4 fw.	5'- GAG GCA CAT TGA ATT CTT GGA	59
hGRK4 rev.	5'- CAC AAT CAC TTC GGT CCT CA	59
zfgrk4 fw.	5'- GAC CGG CGA GTT TGT GAG	79
zfgrk4 rev.	5'- AGC GCT CCT TTG GAT CTT TAC	79

3.12 In Situ probes

Table 12: List of in situ probes used in this study

Detected Gene	Linearized with	Transcribed with	Source
adsl	NotI	SP6	S. Aicher
angptl3	NotI	SP6	M. Philipp
cmlc2	NotI	T7	D. Yelon
grk4	EcoRV	SP6	M. Häußler
lefty1	MIuI	T7	J. Yost
southpaw	NotI	SP6	M. Philipp

3.13 Enzymes and Proteins

Table 13: Enzymes and proteins used for this study

Enzyme/Protein	Supplier
Bovine Serum Albumin Fraction V	Roche (Switzerland)
DNase I recombinant, RNase-free	Roche (Switzerland)
Proteinase K	Roche (Switzerland)
Q5® High-Fidelity DNA Polymerase	New England BioLabs® Inc. (USA)
***Taq* DNA Polymerase**	New England BioLabs® Inc. (USA)
Universal Pierce-Nuclease	Thermo Fisher Scientific (USA)

3.14 Restriction Enzymes

Since December 15, 2021 the CutSmart® Buffer (Cat.# B7204) and NEBuffer™ x were replaced by rCutSmart™ Buffer (Cat.# B6004S) and NEBuffer™ set (r1.1,r2.1, r3.1) (all New England BioLabs® Inc.)

Table 14: Restriction enzymes used for this study

Enzyme	Buffer	Supplier
ClaI	rCutSmart™ Buffer	New England BioLabs® Inc. (USA)
EcoRI	NEBuffer™ r2.1	New England BioLabs® Inc. (USA)
EcoRV	NEBuffer™ r3.1	New England BioLabs® Inc. (USA)
NotI	NEBuffer™ r3.1	New England BioLabs® Inc. (USA)
StuI	rCutSmart™ Buffer	New England BioLabs® Inc. (USA)
XhoI	NEBuffer™ r2.1 NEBuffer™ r3.1 rCutSmart™ Buffer	New England BioLabs® Inc. (USA)

3.15 Antibodies

Table 15: List of antibodies used during this study

Antibody	Species	Dilution	Supplier with Clone or Cat.#
Alexa Fluor™ 488 F(ab')2 fragment of goat anti-mouse IgG	Goat	1:1000	Invitrogen (USA)
Alexa Fluor™ Plus 488 donkey anti-Rabbit IgG	Donkey	1:1000	Invitrogen (USA)

Alexa Fluor™ Plus 555 donkey anti-mouse IgG	Donkey	1:1000	Invitrogen (USA)
Alexa Fluor™ 568 donkey anti-rabbit IgG	Donkey	1:1000	Invitrogen (USA)
Alexa Fluor™ Plus 647 donkey anti-rabbit IgG	Donkey	1:5000	Invitrogen (USA)
Alexa Fluor™ Plus 800 donkey anti-mouse IgG	Donkey	1:5000	Invitrogen (USA)
Anti-acetylated α tubulin	Mouse	1:500-1:1000	Sigma-Aldrich. Inc. (USA) clone 6-11B-1
Anti-ADSL	Rabbit	1:200	Atlas Antibodies (Sweden), HPA000525
Anti-Digoxigenin alkaline phosphatase (Anti-DIG)	Sheep	1:5000	Roche (Switzerland)
Anti DRD1-rabbit Polyclonal	Rabbit	1:1000	Proteintech® (United Kingdom), Cat.# 17934-1-AP
Anti DRD5-rabbit Polyclonal	Rabbit	1:1000	Proteintech® (United Kingdom), Cat.# 20310-1-AP
Anti-ELAVL3/4	Rabbit	1:1000	GeneTex, Inc. (USA), Cat.# GTX128365
Anti-Flag (DYKDDDK Tag Antibody (Binds to same epitope as Sigma's Anti-Flag® M2 Antibody))	Rabbit	1:1000	Cell Signaling Technology®, Cat.# 2368S
Anti-γH2AX	Rabbit	1:400	GeneTex, Inc. (USA), Cat.# GTX127342
Anti-γ tubulin	Rabbit	1:1000	Sigma-Aldrich, Inc. (Germany), Cat.# T5192
Anti-GAPDH	Mouse	1:500	Acris (USA), Cat.# ACR001P

Anti-PKCζ	Rabbit	1:500	Santa Cruz (USA), Cat.# sc-216
Anti-SOX2	Rabbit	1:1000	Abcam (United Kingdom), Cat.# ab97959
Anti-ZO-1	Rabbit	1:1000	Proteintech® (United Kingdom), Cat.# 21773-1-AP

3.16 Drugs

Table 16: List of drugs used for zebrafish and cell manipulation

Drug	Dissolved in	Working concentration	Application	Manufacturer
EmbryoMax® Nucleosides (100x)	H_2O	1x	Zebrafish treatment	Merck KGaA (Germany), Cat.# ES-008-D
Fenoldopam	DMSO	10 µM	Zebrafish and cell treatment	LOPAC®1280 Sigma-Aldrich (Germany), Cat.# LO1280
Methotrexate hydrate (MTX)	DMSO	100 µM	Zebrafish treatment	Cayman Chemicals (USA), CAS# 133073-73-1
Rapamycin	DMSO	30 nM	Cell treatment	LC Laboratories (USA), Cat.# R-5000
Rapamycin	DMSO	500 nM	Zebrafish treatment	LC Laboratories (USA), Cat.# R-5000
SCH 39166 (hydrobromide)	DMSO	1 µM	Cell treatment	Cayman Chemicals (USA), CAS# 1227675-51-5

3.17 Kits

Table 17: Kits used during this study

Kit	Application	Supplier
Amaxa™ Cell Line Nucleofector™ Kit R	Nucleofection of cells	Lonza Group AG (Switzerland)
AmpliCap-Max™ T7 High Yield Message Maker Kit	Generation of capped RNA	CellScript™ (USA), Cat.# C-ACM04037
DIG RNA Labeling Mix	Generation of in situ probes	Roche (Switzerland), Cat.# 11277073910
Lipofectamine® 3000 Transfection Kit	Transfection of cells	Invitrogen (USA), Cat.# L3000-008
Lipofectamine® RNAiMax Transfection Reagent	Transfection of cells	Invitrogen (USA), Cat.# 13778-150
Luna Universal qPCR Master Mix	qPCR	New England BioLabs® Inc. (USA)
mMESSAGE mMACHINE™ SP6 Kit	Generation of capped RNA	Invitrogen (USA), Cat.# AM1340
Monarch® DNA Gel Extraction Kit	Purification of DNA	New England BioLabs® Inc. (USA)
ProtoScript® II First Strand cDNA Synthesis Kit	Generation of cDNA	New England BioLabs® Inc. (USA)
QIAGEN® Plasmid *Plus* Midi Kit	Midiprep	QIAGEN® (Germany), Cat.# 12941
Quick-RNA™ Microprep Kit	RNA isolation	Zymo Research (USA), Cat.# 1051
TOPO™ TA Cloning™ Kit, Dual Promoter, with pCR™II-TOPO™ Vector and One Shot™ TOP10F' Chemically Competent *E. coli*	Cloning	Invitrogen (USA), Cat.# K465040

USB® Ligate-IT™ Rapid Ligation Kit	Ligation for cloning	Affymetrix, Inc. USB (USA), Product numbers: 78400/78401

3.18 Buffers and Solutions

Table 18: Recipes of buffers and solutions used for experiments, if not mentioned in the text.

Buffer/Solution	Composition	Application
4 % Paraformaldehyde (PFA)	2 g PFA 75 µl 1 M NaOH 5 ml 10x PBS H_2O to 50 ml	Fixation of embryos and cells
20x Tricaine	400 mg Tricaine 97.9 ml H_2O 2.1 ml 1 M Tris pH=9 adjust pH to 7	Live phenotype and cyst analysis
10x Phosphate Buffered Saline (PBS)	80 g NaCl 2 g KCl 14.4 g Na_2HPO_4 2 g KH_2PO_4 H_2O to 1 l adjust pH to 7.4 after autoclaving	General Buffer
1x PBS	1 ml 10x PBS 49 ml H_2O	Immunofluorescence (IF) wash buffer
1x PBS plus 0.1 % Tween®20 (1x PBST)	1 ml 10x PBS 0.5 ml 10 % Tween®20 48.5 ml H_2O	WMISH and IF
1x PBST plus 1 % Dimethyl sulfoxide (DMSO) (1x PBDT)	49.5 ml PBST 0.5 ml DMSO	IF

20x Saline Sodium Citrate (SSC)	175 g NaCl 88.3 g Tri-sodiumcitrate·2H_2O H_2O to 1 l adjust pH to 7.2	WMISH
500x Nitro blue tetrazolium/5-bromo-4-chloro-3-indolyl phosphate (NBT/BCIP)	Roche (Switzerland)	WMISH
Ponceau S staining solution	0.2 % Ponceau S 3 % Trichloroacetic acid H_2O	Western Blot (WB)
SDS Lysis Buffer	1 % SDS 1x Phosphatase Inhibitor 1x Complete Mini EDTA free Protease Inhibitor Cocktail tablets, 10 % 1M Tris pH 6.8	WB and BCA assay for protein content
10x Tris-Buffered Saline (TBS)	6.05 g Tris-HCl 8.76 g NaCl H_2O to 1 l adjust pH to 7.4	WB
1x TBS	1 ml 10x TBS 49 ml H_2O	WB
1x TBS plus 0.1 % Tween®20 (TBST)	1 ml 10x TBS 0.5 ml 10 % Tween®20 48.5 ml H_2O	WB
Transblot Buffer	3.03 g Tris 11.5 g Glycine 100 ml MeOH add H_2O to 1 l	WB

Western Wash	50 mM Tris pH 7.4 150 mM NaCl 0.2 % BSA 0.2 % NP-40	WB
10x Standard *Taq* Buffer	New England BioLabs® Inc. (USA)	PCR
5x Q5® Reaction Buffer	New England BioLabs® Inc. (USA)	PCR
Deoxynucleotide (dNTP) Solution Mix	New England BioLabs® Inc. (USA)	PCR
P1 Buffer	50 mM Tris·Cl 10 mM EDTA 100 µg/ml RNase A H_2O adjust pH to 8	Mini and Midiprep
P2 Buffer	200 mM NaOH 1 % SDS H_2O	Mini and Midiprep
P3 Buffer	1 M Potassium acetate H_2O adjust pH to 5.5	Miniprep
Permeabilization Buffer	7 mg/ml gelatin from cold water fish skin 0.5 % Triton X-100 PBS	IF of IMCD3 spheroids

3.19 Chemicals and Reagents

Table 19: List of chemicals and reagents used during this study

Chemical/Reagent	Supplier
100 bp DNA Ladder	New England BioLabs® Inc. (USA)
1 kb DNA Ladder	New England BioLabs® Inc. (USA)
2-Log DNA Ladder	New England BioLabs® Inc. (USA)
Acetone	Neolab (Germany)
Alcian Blue 8 GX	Merck KGaA (Germany)
Ammonium Acetate	Merck KGaA (Germany)
Aqua ad injectabilia (ad. inj.)	Braun (Germany)
Aqua Resist	VWR International GmbH (Germany)
β-Mercaptoethanol	AppliChem (Germany)
Bicinchoninic Acid Solution (BCA)	Sigma-Aldrich Inc. (USA)
Bolt™ 4-12 % Bis-Tris Plus	Invitrogen (USA)
Bolt™ MES SDS Running Buffer (20x)	Invitrogen (USA)
5-bromo-4-chloro-3-indolyl-β-D-galactopyranoside (X-Gal)	Sigma-Aldrich Inc. (USA)
Bromphenol Blue	Merck KGaA (Germany)
Calcium Chloride ($CaCl_2$)	Sigma-Aldrich Inc. (USA)
Chloroform	Merck KGaA (Germany)
Citric Acid	Merck KGaA (Germany)
Complete Mini EDTA-free Protease Inhibitor Cocktail Tablets	Roche (Switzerland)
Copper (II) Sulfate Solution	Sigma-Aldrich Inc. (USA)
Deoxynucleoside Triphosphates (dNTPs)	New England BioLabs® Inc. (USA)
Disodium Hydrogen Phosphate (Na_2HPO_4)	Merck KGaA (Germany)

Dimethyl Sulfoxide (DMSO)	Carl Roth GmbH & Co. KG (Germany)
Ethanol Absolute (EtOH)	Sigma-Aldrich Inc. (USA)
Ethylenediaminetetraacetic acid (EDTA)	AppliChem GmbH (Germany)
Formamide	AppliChem GmbH (Germany)
Gelatin from Cold Water Fish Skin	Sigma-Aldrich Inc. (USA)
Glycerol anhydrous p.A.	AppliChem GmbH (Germany)
Glycine, Electrophoresis Grade	MP Biomedicals (USA)
Heparin	AppliChem GmbH (Germany)
Hydrogen Peroxide 30 %	Otto Fischar GmbH & Co. KG (Germany)
Immersol™ 518F	Carl Zeiss Sports Optics GmbH
Isopropanol	Honeywell International Inc. (Germany)
Levamisol-HCl	Sigma-Aldrich Inc. (USA)
Magnesium Chloride ($MgCl_2$)	Merck KGaA (Germany)
Magnesium Chloride Hexahydrate ($MgCl_2 \cdot 6H_2O$)	Sigma-Aldrich Inc. (USA)
Magnesium Sulfate ($MgSO_4 \cdot H_2O$)	Merck KGaA (Germany)
Methanol (MeOH)	Honeywell International Inc. (Germany)
Methylcellulose	Sigma-Aldrich Inc. (USA)
Methylene Blue	Sigma-Aldrich Inc. (USA)
Midori Green Advance DNA Stain	Nippon Genetics Europe GmbH (Germany)
500x Nitro Blue Tetrazolium/5-Bromo-4-Chloro-3-Indolyl Phosphate	Roche (Switzerland)
Nonfat Dried Milk Powder	AppliChem GmbH (Germany)
Normal Goat Serum	Vector Laboratories (USA)
NP-40 (IGEPAL® CA-630)	Sigma-Aldrich Inc. (USA)

Odyssey® Blocking Buffer (TBS)	LI-COR Biosciences (USA)
Paraformaldehyde (PFA)	Sigma-Aldrich Inc. (USA)
Phenol:Chloroform:Isoamylalcohol 25:24:1	AppliChem GmbH (Germany)
5x Phenolred	Sigma-Aldrich Inc. (USA)
1-Phenyl-2-Thiourea (PTU)	Sigma-Aldrich Inc. (USA)
Ponceau S	Sigma-Aldrich Inc. (USA)
Potassium Acetate (CH_3CO_2K)	Merck KGaA (Germany)
Potassium Chloride (KCl)	Merck KGaA (Germany)
Potassium Dihydrogen Phosphate (KH_2PO_4)	Merck KGaA (Germany)
Potassium Hydroxide (KOH)	Merck KGaA (Germany)
Precision Plus Protein™ Kaleidoscope™ Standard	Bio-Rad Laboratories Inc. (USA)
Ribonucleic Acid from Torula Yeast Type VI	Sigma-Aldrich Inc. (USA)
Sodium Acetate ($C_2H_3NaO_2$)	Honeywell International Inc. (Germany)
Sodium Chloride (NaCl)	Merck KGaA (Germany)
Sodium Dodecyl Sulfate (SDS)	Carl Roth GmbH & Co. KG (Germany)
Sodium Hydrogen Carbonate ($NaHCO_3$)	AppliChem GmbH (Germany)
Sodium Hydroxide (NaOH)	Merck KGaA (Germany)
13 % Sodium Hypochlorite (NaOCl)	Bernd Kraft GmbH (Germany)
Tricaine	Sigma-Aldrich Inc. (USA)
Trichloroacetic acid	Sigma-Aldrich Inc. (USA)
Tris	AppliChem GmbH (Germany)
Trisodiumcitrate·$2H_2O$	Merck KGaA (Germany)

Triton™ X-100	Sigma-Aldrich Inc. (USA)
Tween® 20	Sigma-Aldrich Inc. (USA)
Type G Immersion Liquid	Leica Microsystems GmbH (Germany)
UltraPure™ Agarose	Invitrogen (USA)
Universal ProbeLibrary Set, Human Probe #1-#90	Roche (Switzerland)
Vectashield® Hard Set™ Mounting Medium with DAPI H-1500	Vector Laboratories (USA)
Vectashield® Mounting Medium for Fluorescence H-1000	Vector Laboratories (USA)
Vectashield® Mounting Medium for Fluorescence with DAPI H-1200	Vector Laboratories (USA)

3.20 Software

Table 20: Different softwares used for this study

Software	Version	Developer
4Peaks	1.8	Nucleobytes B.V. (Netherlands)
Adobe Acrobat DC	22.0	Adobe Inc. (USA)
Adobe Creative Cloud	5.6.5.58	Adobe Inc. (USA)
Adobe Illustrator	26.2.1	Adobe Inc. (USA)
Adobe Photoshop	23.3	Adobe Inc. (USA)
EndNote	20.4	Clarivate (United Kingdom)
FIJI	2.0.0-rc-69/1.52p	Johannes Schindelin, Ignacio Arganda-Carreras, Albert Cardona, Mark Longair, Benjamin Schmid and others

GraphPad Prism	8.4.3 (471)	GraphPad Software Inc. (USA)
Leica Application Suite X	3.7.23245.3	Leica Microsystems GmbH (Germany)
LightCycler® 480 Software	1.5.1.62	Roche (Switzerland)
Mendeley Cite	1.45.0	Mendeley (United Kingdom)
Microsoft Excel	16.59 (22031300)	Microsoft Corporation (USA)
Microsoft PowerPoint	16.59 (22031300)	Microsoft Corporation (USA)
Microsoft Word	16.59 (22031300)	Microsoft Corporation (USA)

3.21 Disposable Materials

Table 21: List of disposable materials used during this study

Material	Manufacturer
10 µl graduated TipOne Filter Tip, Natural (sterile)	Starlab International GmbH (Germany)
20 µl Filter Tips, graduated, racked, PP, natural, sterile, 96 tips/rack	Greiner Bio-One GmbH (Germany)
300 µl Filter Tips, graduated, racked, PP, natural, sterile, 96 tips/rack	Greiner Bio-One GmbH (Germany)
1250 µl Filter Tips, graduated, racked, PP, natural, sterile, 96 tips/rack	Greiner Bio-One GmbH (Germany)
10 µl XL Pipette Tips, Graduated, Refill, PP, Natural, non-sterile	Greiner Bio-One GmbH (Germany)
200 µl Bevelled TipOne® Tip, Yellow, Refills (non-sterile)	Starlab International GmbH (Germany)

1,250 µl XL graduated TipOne® Tip, Natural, Racks (non-sterile)	Starlab International GmbH (Germany)
Adhesive clear qPCR Seals, Sheets, 140x77 mm, Peelable	Biozym Scientific GmbH (Germany)
Aluminum Foil	Cofresco Frischhalteprodukte GmbH & Co. KG (Germany)
Borosilicate Glass Capillaries	World Precision Instruments, Inc. (USA)
Cell Spreader	Biologix Group Limited (Canada)
Colour coded Inserts, mixed	Sarstedt AG & Co. KG (Germany)
Countess™ Cell Counting Chamber Slides	Invitrogen (USA)
Cover Glass 24x50 mm Thickness No. 1.5	VWR International (USA)
CryoPure Tube, 1.6 ml	Sarstedt AG & Co. KG (Germany)
Cuvettes Polystyrene 10x4x45 mm	Sarstedt AG & Co. KG (Germany)
Dow Corning® High Vacuum Silicone Grease	Sigma-Aldrich Inc. (USA)
Eppendorf Combitips® advanced 10 ml	Eppendorf SE (Germany)
Essence 2 in 1 Base + Top Coat	Cosnova GmbH (Germany)
Filtropur V50 0.2 Vacuum Filter	Sarstedt AG & Co. KG (Germany)
Kimtech® Science Precision Wipes	Kimberly-Clark Corporation (USA)
Lens Paper for Valuable Optics	Motic® (Hong Kong)
Microtube Tough-Spots®	Diversified Biotech, Inc. (USA)
Microtube Tough-Tags®	Diversified Biotech, Inc. (USA)
Nitrocellulose/Filter Paper Sandwiches 0.2 µm	Bio-Rad Laboratories Inc. (USA)
Nunc™ Lab-Tek™ II Chambered Coverglass	Thermo Fisher Scientific (USA)
Pasteur Capillary Pipettes short size 150 mm	WU Mainz (Germany)

PCR Plastics, Tube Strips with Single Flat Caps	Nippon Genetics Europe GmbH (Germany)
PCR 96-well TW-MT plate, white	Biozym Scientific GmbH (Germany)
Pipette, 5 ml, Graduated 1/10 ml, sterile	Greiner Bio-One GmbH (Germany)
Pipette, 10 ml Graduated 1/10 ml, sterile	Greiner Bio-One GmbH (Germany)
Pipette, 25 ml, Graduated 2/10 ml, sterile	Greiner Bio-One GmbH (Germany)
Sempercare® edition IC M	Semperit AG (Austria)
Single-frosted slides	VWR International (USA)
Sponge Pad Xcell II™ Blotting	Invitrogen (USA)
TC Dish 100, Standard	Sarstedt AG & Co. KG (Germany)
TC-Plate 6 Well, Standard F	Sarstedt AG & Co. KG (Germany)
TC-Plate 12 Well, Standard F	Sarstedt AG & Co. KG (Germany)
TC-Plate 24 Well, Standard F	Sarstedt AG & Co. KG (Germany)
TimeTape® Labeling Tape	TimeMed Labeling Systems, Inc. (USA)
Tork Extra Soft Facial Tissue Premium	Tork (Germany)
Transfer Pipette 3.5 ml	Sarstedt AG & Co. KG (Germany)
Tube 13 ml, 100x16 mm PP	Sarstedt AG & Co. KG (Germany)

3.22 Instruments

Table 22: List of Instruments used for this study

Instrument	Manufacturer
AxioCam MRc	Carl Zeiss Sports Optics GmbH
Axio Imager M1	Carl Zeiss Sports Optics GmbH
Bolt™ Mini Gel Tank	Thermo Fisher Scientific (USA)
Calibration Check Microprocessor pH Meter HI 221	Hanna Instruments (USA)

Centrifuge 5415D	Eppendorf SE (Germany)
Centrifuge 5430	Eppendorf SE (Germany)
Centrifuge 5810R	Eppendorf SE (Germany)
C-MAG MS7 Magnetic Stirrer	IKA-Werke GmbH & Co. KG (Germany)
Compact Shaker KS 15	Edmund Bühler GmbH (Germany)
Confocal Microscope Platform STELLARIS 5	Leica Microsystems GmbH (Germany)
Consort EV231Power Supply	Merck KGaA (Germany)
Countess™ II Automated Cell Counter	Invitrogen (USA)
Daewoo Microwave	Winiadaewoo Electronics America Inc. (USA)
Digital Monochrome Printer P95DE	Mistubishi Electric (Japan)
Digital Rockers Thermo Scientific™	Thermo Fisher Scientific (USA)
Dumostar®-Biology 11295-10 Foreceps	FST Dumont (Switzerland)
Easypet® 3	Eppendorf SE (Germany)
Eplax Vero Power 231 Power Supply	Eplax GmbH (Germany)
Eppendorf Research® Plus 0.5 – 10 µl	Eppendorf SE (Germany)
Eppendorf Research® Plus 2 – 20 µl	Eppendorf SE (Germany)
Eppendorf Research® Plus 10 – 100 µl	Eppendorf SE (Germany)
Eppendorf Research® Plus 20 – 200 µl	Eppendorf SE (Germany)
Eppendorf Research® Plus 100 – 1000 µl	Eppendorf SE (Germany)
Eppendorf Xplorer® 5 - 100 µl	Eppendorf SE (Germany)
External Light Source for Fluorescence Excitation Leica EL6000	Leica Microsystems GmbH (Germany)
FastGene Blue/Green LED FlashLight	Nippon Genetics Europe GmbH (Germany)

FastGene Mini Centrifuge	Nippon Genetics Europe GmbH (Germany)
FemtoJet®	Eppendorf SE (Germany)
FemtoJet® 4i	Eppendorf SE (Germany)
Freezer -20 °C	Liebherr (Germany)
Fridge 4 °C	Liebherr (Germany)
Fujitsu LCD Display B24-8 TS Pro	Fujitsu Limited (Japan)
Heraeus Biofuge 13 Centrifuge	Heraeus (Germany)
HXP 120 C	Leistungselektronik Jena GmbH (Germany)
iBright™ FL1500	Invitrogen (USA)
Incubator Hood TH 15	Edmund Bühler GmbH (Germany)
Leica DFC9000 GT Microscope Camera	Leica Microsystems GmbH (Germany)
Leica DMi8 S	Leica Microsystems GmbH (Germany)
Leica M125C Microscope	Leica Microsystems GmbH (Germany)
Leica M205 FCA Microscope	Leica Microsystems GmbH (Germany)
Leica MC 190 HD Microscope Camera	Leica Microsystems GmbH (Germany)
Leica S9i Microscope	Leica Microsystems GmbH (Germany)
Memmert U40 Oven	Memmert GmbH & Co. KG (Germany)
Micro Centrifuge 110 VAC	Carl Roth GmbH & Co. KG (Germany)
Mini Blot Module	Invitrogen (USA)
MN-15119061 Joystick Micromanipulator	Narishige Group (Japan)
Multipette® M4 1 µl – 10 ml	Eppendorf SE (Germany)
Multipette® plus	Eppendorf SE (Germany)
Nanodrop One^{C}	Thermo Fisher Scientific (USA)
Nucleofector® 2b Device	Lonza Group AG (Switzerland)

Oko-Touch	Okolab srl (Italy)
Olympus CKX41 Inverted Cell Culture Microscope	Olympus Corporation (Japan)
Owl™ D2 Wide-Gel Electrophoresis System	Thermo Fisher Scientific
P-1000 Flaming/Brown Micropipette Puller	Sutter Instrument (USA)
PerfectBlue™ Power Supply	VWR International (USA)
PG 8583	Miele & Cie. KG (Germany)
pH Electrode HI 1131	Hanna Instruments (USA)
PHEONIX Instrument Laboratory centrifuge CD-0412-50	Phoenix Instrument GmbH (Germany)
Pipetman M P20M	Gilson Inc. (USA)
PowerEase™ Touch 120 W Power Supply	Invitrogen (USA)
qPCR LightCycler® 480	Roche (Switzerland)
Repeater® plus	Eppendorf SE (Germany)
RI-150 Refrigerated Incubator	Thermo Fisher Scientific (USA)
RiOs™ Essential 16 Water Purification System	Merck KGaA (Germany)
Rocker 2D Digital Shaker	IKA-Werke GmbH & Co. KG (Germany)
Sanyo Ultra-Low Temperature Freezer -86 °C MDF-594	Sanyo Electric Co., Ltd., (Japan)
Sartorius A120S Analytical Balance	Sartorius AG (Germany)
Sartorius CP622 Toploading Balance	Sartorius AG (Germany)
Scanlaf Mars 1200	LaboGene (Denmark)
SimpliAmp™ Thermal Cycler	Thermo Fisher Scientific (USA)
SmartTouch™ Control Unit	Leica Microsystems GmbH (Germany)

Synergy® Water Purification System	Merck KGaA (Germany)
TCS SP5	Leica Microsystems GmbH (Germany)
Tecniplast Tritone Automatic Feeding System	Tecniplast S.p.A. (Italy)
Tecniplast ZBWTU0011	Tecniplast S.p.A. (Italy)
Thermo Heraeus HERAcell 150 Liter	Heraeus (Germany)
Thermomixer-Mixer HC	Starlab International GmbH (Germany)
Vacuboy	INTEGRA Biosciences AG (Switzerland)
Vacusafe	INTEGRA Biosciences AG (Switzerland)
Varioclav® BlueLine 100 S	HP Labortechnik GmbH (Germany)
Vortex	Starlab International GmbH (Germany)
Water Bath Type 1002	Gesellschaft für Labortechnik (GFL®) mbH (Germany)
Water Bath	Memmert GmbH & Co. KG (Germany)

3.23 Databases and Webpages

Table 23: Databases and Webpages used for this study

Database	URL
Assay design for Universal Probe Library	https://primers.neoformit.com
Basic Local Alignment Search Tool (BLAST®)	https://blast.ncbi.nlm.nih.gov/Blast.cgi
e! Ensembl	https://www.ensembl.org/index.html
GeneCards®	https://www.genecards.org
MultAlin	http://multalin.toulouse.inra.fr/multalin/
NEBcutter V2.0	http://nc2.neb.com/NEBcutter2/

OligoPerfect Primer Design	https://www.thermofisher.com/de/de/home/life-science/oligonucleotides-primers-probes-genes/custom-dna-oligos/oligo-design-tools/oligoperfect.html
Online Mendelian Inheritance in Man® (OMIM®)	https://omim.org
Open Reading Frame Finder	https://www.ncbi.nlm.nih.gov/orffinder/
PubMed®	https://pubmed.ncbi.nlm.nih.gov
Reverse Complement	http://reverse-complement.com
SMART	http://smart.embl-heidelberg.de
The Human Protein Atlas	https://www.proteinatlas.org
The Zebrafish Information Network	https://zfin.org
UniProt	https://www.uniprot.org
Universal ProbeLibrary Assay Design Center	https://lifescience.roche.com/en_de/brands/universal-probe-library.html#assay-design-center

4 Methods

4.1 Zebrafish

4.1.1 Zebrafish husbandry

Zebrafish (*Danio rerio)* were maintained in a zebrafish housing system (Zebtec from Tecniplast). The water temperature was between 27.5 and 29 degrees Celsius (°C), the room temperature (RT) was around 26 °C. Two water treatment units (WTU) (Tecniplast) circulated the water with a water exchange rate of 10 % per hour. They automatically hold the perfect pH and conductivity values by adding sodium bicarbonate ($NaHCO_3$) (Sigma) for pH adjustment and Instant Ocean (Aquarium Systems) for conductivity adjustment. The fish had a 14 hours (h) day and 10 h night rhythm. The first two years they were fed three times per day. In the morning with artemia live food (Aqua Schwarz) and in the noon and afternoon with pellet dry food (Sparos). The last two years an automatic feeding system, called Tritone (Tecniplast), used a dry diet dispenser (Tecniplast) with the same pellet dry food to feed them three times a day. Additionally, we kept feeding them with artemia live food in the morning.

Maintenance as well as manipulation of zebrafish were in line with the European Union Directive 86/609/EEC and approved by the Veterinary Care Unit at Ulm University and Tübingen University as well as the animal welfare commissioner of the regional board Tübingen, Germany.

4.1.2 Mating of zebrafish

Zebrafish were naturally mated in the afternoon with a sloping breeding tank (Tecniplast). The next day the fish were triggered to lay eggs by switching on the light in the morning. These mating tanks helped to collect the eggs using an inlet that could be removed. The eggs were collected with a transfer pipette and rinsed in a 5 cm petri dish with 1x E3 or egg water (Table 2). Eggs were incubated at 28.5 °C until the desired stage. Unfertilized and dead eggs were sorted out prior starting an experiment.

4.1.3 Fish lines

The fish lines AB wild-type, EK wild-type, cmlc2-GFP and Wt1b-GFP (kind gift of Christoph Englert (86)) were used for this study. In addition, Prof. Melanie Philipp produced a Grk4 mutant fishline by CRISPR/Cas9 mediated gene editing, which will be called Grk4 1.2 in this thesis.

4.1.4 Zebrafish injection

Fertilized and rinsed eggs were injected during the one or two cell stadium using a FemtoJet® 4i or a FemtoJet® with a joystick micromanipulator (Narishige Group) and a self-made injection plate. The injection needle was made with a P-1000 Flaming/Brown Micropipette Puller (Sutter Instrument) and following conditions:

Table 24: Program conditions for needle pulling

Line	Value
Ramp	486
Heat	514
Pull	200
Vel.	80
Time	250
Safeheat	X
Pressure	500

The tip of each needle was then clipped a little with fine forceps. For the injection plate a 10 cm petri dish was filled with 1.5 % agarose (Invitrogen) in embryo medium. An injection mold (Eppendorf) was put on top before the gel had solidified to obtain trenches where the

zebrafish eggs were hold. Prior to injection all MOs were diluted as follows: 5 nl of a 2 mM MO stock solution were mixed with 4 µl 5x Phenol red (Sigma-Aldrich Inc.) and 11 µl *aqua ad iniectabilia* (ad. inj.) (Braun) to obtain a 0.5 mM working solution for each MO.

4.1.4.1 Adsl knockdown

Adsl depleted embryos were generated by injection of a translation blocking antisense morpholino oligonucleotide (ATG MO) or a splice blocking antisense morpholino oligonucleotide (splMO). The ATG MO targeted the 5' untranslated region (UTR) and the beginning of the coding region (5'-TCCCTCCATGCCTGCAGCGGTTAAA), whereas the splMO targeted the exon-intron boundary at exon 4 (5'- CCAACTGTGGGAGAGAGCGACTGTA). For each experiment a standard control MO (CTRL MO) was also used. Non-injected (NI) embryos of the same mating tank were used as an internal control for clutch quality. Rescue experiments were performed by co-injection of 5 nl 0.5 mM Adsl ATG or splMO with 5 nl 100 ng/µl capped RNA encoding either zebrafish or human wildtype variants of ADSL or one of the two human genetic variants R426H or V429A.

4.1.4.2 Grk4 knockdown

Grk4 depleted embryos were also generated by using an ATG MO targeting the 5' UTR (5'-GTCAGAAGAAAGATCCCATGCAGTC). A specific 5 bases mismatch MO was injected as CTRL MO (5'-GTGACAACAAACATCCCATCCAGTC) (for easier reading both CTRL MOs, for Adsl and Grk4, will be named CTRL MO, although they are different CTRL MOs). As described above, NI embryos were also used for internal clutch quality observation. Rescue experiments were performed by co-injection of the Grk4 ATG MO with either zebrafish or human GRK4 variants. The following Table 25 describes all rescue RNAs:

Table 25: GRK4 rescue RNAs

RNA	Species	Description

Grk4	human	Flag-tagged full length/WT version of GRK4 (also called α splice variant)
Grk4 β	human	Flag-tagged splice variant of GRK4
Grk4 γ	human	Flag-tagged splice variant of GRK4
Grk4 δ	human	Flag-tagged splice variant of GRK4
Grk4 R65L	human	Flag-tagged patient variant of GRK4(88)
Grk4 A142V	human	Flag-tagged patient variant of GRK4(88)
Grk4 KiDe	human	KiDe version of GRK4 (K216/217M)
Grk4 ΔRH	human	GRK4 version with depleted regulator of G-protein signaling homology (RH) domain (aa 39-180)
Grk4 1.2	human	GRK4 version resembling the generated zebrafish mutation c.580-585del
grk4	zebrafish	capped WT version of Grk4

4.1.4.3 Grk4 mutant genotyping

Adult heterozygous fish were mated naturally to generate mutant embryos. Polymerase chain reactions (PCR) were performed for genotyping adult fish and embryos. We isolated genomic DNA (gDNA) from fin-clipping (adult fish) or cutting of the heads (embryos). The biological material was immersed in 50 µl 50 mM sodium hydroxide (NaOH) and incubated at 95 °C for 20 min. After rapid cooling to RT, 5 µl of 1 M Tris pH 8 were added. The whole mixture was spun with 13,000 rpm at RT for 10 min. 1.5 µl of this isolated gDNA were used for PCR as described in the following table:

Table 26: Reaction setup for Grk4 1.2 genotyping

Genotyping PCR
1.5 µl gDNA
0.5 µl 10 µM Primer Mix (PM)
1 µl 2 mM dNTPs
1 µl Standard *Taq* Reaction Buffer
0.1 µl *Taq* DNA Polymerase (NEB)
6.5 µl H_2O ad. inj.

The PM contained the zf Grk4 CRISPR WT Fw primer (5'-TGG GAT TTA CGG TGC ATT GTT ATT AGT GAA), zf Grk4 CRISPR mut Fw primer (5'-CAT TAC AGG GTA TTG GGC ATT T) and a combined zf Grk4 CRISPR Rev primer (5'-ACC ACT GAT AAC GCC CAT TCA ATC AAA TG). This resulted in 3 bands: 493 bp (WT), 487 bp (mutant) and 385 bp (mutant).

The PCR was performed using a SimpliAmp™ Thermal Cycler (Invitrogen) with the following conditions:

Table 27: PCR running conditions for genotyping

Temperature	Time	Cycles
94 °C	1 min	1x
94 °C	12 sec	
68 °C	15 sec	35x
68 °C	30 sec	
68 °C	3 min	1x
8 °C	∞	

The PCR was analyzed by agarose gel electrophoresis (see 4.3.1.2).

4.1.5 Zebrafish treatment

One method to preserve the transparency of zebrafish embryos is the inhibition of pigmentation by exposing embryos to 1-phenyl-2-thiourea (PTU). With this treatment live phenotype, cyst and cilia analysis became much easier. 24.32 mg PTU (Sigma) were solved in 40 ml embryo medium (Table 2) to obtain a 20x PTU stocksolution. Embryos were then treated with 1x PTU diluted in embryo medium or in 1x E3 from tailbud stage (10 hpf) or 24 hpf on.

All drug treatments were performed with around 25 embryos per condition in a 12-well plate with 1.5 ml medium per well. Each drug was diluted with embryo medium containing 1x PTU as described in Table 28. The solvent reagent of the stock solution of each drug was used as vehicle treatment. Except for the nucleoside treatment, where H_2O was used as vehicle, all other control treatments were performed with Dimethyl sulfoxide (DMSO).

Table 28: Drugs used for zebrafish manipulation

Compound	Stocksolution	Working solution	Application	Experiment
Methotrexate (MTX)	10 mM in DMSO	100 µM	from tailbud stage until 24 hpf	for live phenotype analysis and imaging of neuronal cells
Nucleosides	100x in H_2O	1x	from tailbud stage until 24 hpf	for live phenotype analysis and imaging of neuronal cells
Fenoldopam	10 mM in DMSO	10 µM	from tailbud stage until 48 hpf	for live phenotype and cyst analysis
Rapamycin	10 mM in DMSO	500 nM	from tailbud stage until 48 hpf	for live phenotype, cyst and cilia analysis

4.1.6 Dechorionization

Zebrafish embryos were manually dechorionated after 24 hpf using fine forceps. For imaging of ELAVL3/4- and γH2AX-positive cells and cilia it was important to dechorionate them prior to fixation (4.1.9). For Sox2-positive cells, it was better to dechorionate after fixation for easier imaging.

4.1.7 Live phenotype analysis

Live phenotype analysis of injected embryos was performed at 48 hpf. For this the dechorionated embryos were treated with a few drops of 20x Tricaine (Table 18) to prevent their movement. We looked for different cilia-related phenotypes like edema formation, pinheads, smaller eyes and curled/kinked tails (89).

4.1.8 Cyst analysis

With the help of the transgenic fishline wt1b-GFP (kind gift of Christoph Englert (86), it was easy to analyze cyst formation in developing zebrafish embryos. 48 hpf injected and/or treated embryos were observed under fluorescent light (4.4). The glomerulus, the neck and the proximal convoluted tubule glowed green as shown in Figure 11.

To prevent their movement some drops of 20x Tricaine (Table 18) were added.

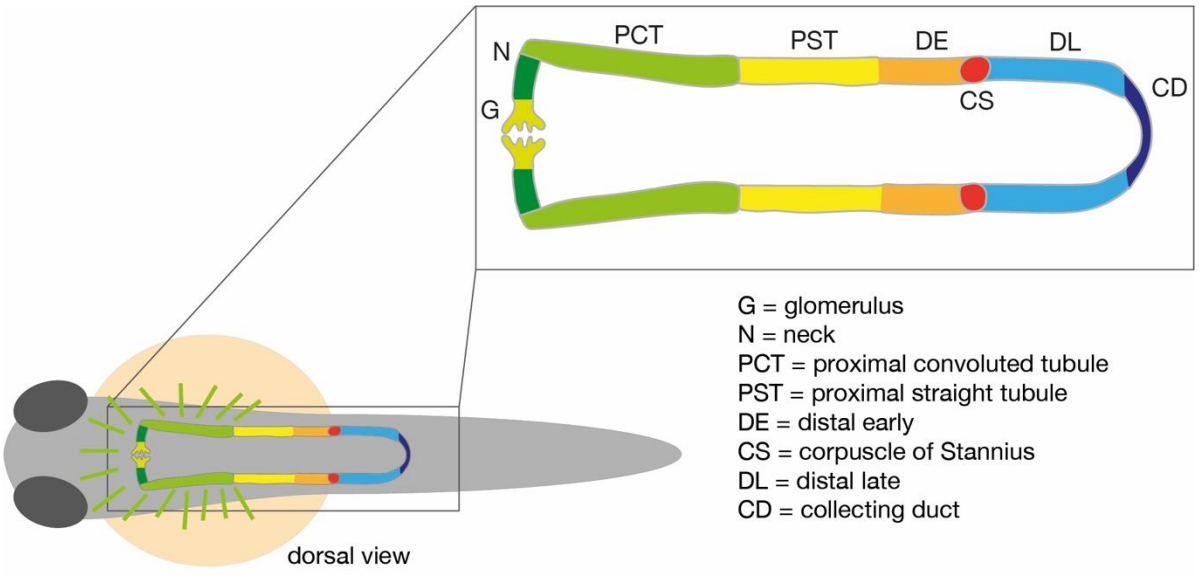

Figure 11: wt1b-GFP transgenic fishline

Cartoon of a 48 hpf old embryo, showing the developing kidney. The glomerulus (G), the neck (N) and proximal convoluted tubule (PCT) glow green in wt1b-GFP embryos. After the PCT the pronephros can be divided in the proximal straight tubule (PST), the distal early (DE), the corpuscle of Stannius (CS) and the distal late (DL) with the collecting duct (CD). Adapted with permission from Chambers et al. (90).

4.1.9 Fixation of zebrafish embryos

After live phenotype analysis or when the embryos reached the desired stage, they were transferred to a 2 ml safe-lock tube and fixed using 500 µl 4 % PFA (Table 18). If the embryos were used for whole-mount in situ hybridization (WMISH), fixation occurred at 4 °C over night (o/n). If embryos were intended for antibody (AB) or Alcian blue staining, they were fixed for around 90 min – 2 h at RT on a shaker (IKA-Werke GmbH & Co. KG).

4.1.10 Storage of zebrafish embryos

In order to store fixed embryos for a longer period, embryos were rinsed once with 1x PBS with 0.1 % Tween® 20 (Sigma) (PBST) and then subsequently dehydrated using a graded methanol (MeOH) series. Starting with 25 % MeOH in PBST, following 50 % MeOH in PBST, 75 % MeOH in PBST and twice 100 % MeOH. Each step was performed for 4-5 min on a shaker at RT. After this, the embryos could be stored at -20 °C for several months.

4.1.11 Immunofluorescence (IF) of zebrafish embryos

All incubation steps were performed with a volume of 500 µl, unless indicated otherwise.

After fixation with 4 % PFA (4.1.9) the embryos were washed 4 times for 5 min with PBST and permeabilized with H_2O for 5 min. Then they were incubated with prechilled acetone for 7 min at -20 °C and washed again with H_2O for 5 min. Then, the embryos were washed with PBST containing 1 % DMSO (= PBDT) and blocked with 10 % NGS in PBDT (= blocking solution) for 2 h at RT. The embryos were incubated with 200 µl primary antibodies diluted in blocking solution at 4 °C o/n. On the next day, the embryos were washed 6 times with PBDT containing 1 % NGS and 0.1 M NaCl for 5 min at RT. Before

the incubation with 200 µl secondary antibodies in blocking solution for 4 h at RT, the embryos were washed once with PBDT containing 1 % NGS. After the incubation with secondary antibodies, the embryos were washed again 6 times with PBDT containing 1 % NGS and 0.1 M NaCl. Then they were rinsed once and stored in PBDT at 4 °C until further use

The different dilutions for all antibodies can be found in Table 15.

This protocol was adapted from Jaffe et al. (91).

4.1.12 Alcian blue staining of zebrafish embryos

All incubation steps were performed with a volume of 1 ml at RT.

Embryos were fixed at 4 days post fertilization (dpf) in a 2 ml tube, according to 4.1.9. Then, embryos were rinsed once with PBS and incubated with 50 % EtOH in PBS for 10 min on a shaker. After this the embryos were incubated o/n with the Alcian blue staining solution (Table 30). On the next day, embryos were rinsed once with H_2O and bleached for 20 min with open lid with 1.5 % H_2O_2 and 1 % potassium hydroxide (KOH) diluted with H_2O. Afterwards the embryos were washed with following Glycerol/KOH series:

- 30 min 20 % Glycerol with 0.25 % KOH in H_2O
- 2 h 50 % Glycerol with 0.25 % KOH in H_2O
- rinsed with 50 % Glycerol with 0.1 % KOH in H_2O.

Embryos were stored in 50 % Glycerol with 0.1 % KOH in H_2O at 4 °C until further use.

Table 29: Alcian blue stocksolution

Reagent	Quantity (for 50 ml)	Final concentration
Alcian blue 8 GX	200 µl	0.4 %
H_2O	20 ml	
EtOH abs.	fill to 50 ml	70 %

Table 30: Alcian blue staining solution

Reagent	Quantity (for 100 ml)	Final concentration
Alcian blue 8 GX stocksolution	5 ml	0.02 %
95 % EtOH	70 ml	70 %
1 M Magnesium chloride ($MgCl_2$)	5 ml	50 mM
H_2O	20 ml	

4.2 Cell culture

4.2.1 Cell culture maintenance

These cell lines were used in the course of this thesis: human retinal pigment epithelial cells (RPE1), human embryonic kidney 293 cells (HEK), human hTERT immortalized 1BR3 wild-type fibroblasts (1BR3) and mouse inner medullary collecting duct cells (IMCD3) (Table 4). All of them were cultured in a 10 cm culture dish with 10 ml of specific medium (see Table 5 for the medium for each cell line) in an incubator with 37 °C, 5 % carbon dioxide (CO_2) and 95 % humidity. All media and supplements were prewarmed to 37 °C prior to use. All cell lines were split once they reached >90 % confluence. To do so, the culture medium was removed and cells were rinsed once with 10 ml Phosphate-Buffered Saline (PBS) and incubated for 5 min with 1 ml 1x Trypsin EDTA (Trypsin) at 37 °C. 9 ml of medium were then added and the cells were transferred to new plates in a 1:2 (for 1BR3 and RPE1) or 1:5 ratio (HEK and IMCD3). Medium was added until each new plate had 10 ml.

4.2.2 Cell counting

For calculating a desired cell number, trypsinized cells were mixed with 9 ml medium and centrifuged for 5 min with 700 rpm. The trypsin-medium solution was discarded and the pellet was resuspended in 1 ml medium. 10 µl of the cells were mixed with 10 µl trypan blue staining and 10 µl of this mixture were transferred into a cell counting chamber slide. This chamber slide was placed in the Countess™ Automated Cell Counter to determine the actual cell number of living cells.

4.2.3 MeOH fixation of cells

For the fixation of cells with methanol (MeOH), cells were rinsed once with PBS and then immersed with 1 ml prechilled MeOH for 4 min at -20 °C. After fixation, cells were washed twice with PBS and could be stored at 4 °C until further use.

4.2.4 Immunofluorescence of cells

Fixed cells were washed three times with 1 ml 1x PBS for 5 min. Then cells were permeabilized with 100 µl 1 % Triton X-100 for 10 min and blocked with 100 µl 1x PBS containing 10 % fetal bovine serum (FBS) for 1h at RT. Primary antibodies were diluted in blocking solution (1x PBS with 10 % FBS) and 100 µl of this mixture were added to each coverslip and incubated o/n at 4 °C (see Table 15 for antibody dilutions). On the next day, the cells were washed three times for 15 min at RT with 1ml 1x PBS and subsequently incubated with secondary antibodies diluted in blocking solution for 90 min at RT in the dark (see Table 15 for antibody dilutions). After an additional three washed with 1 ml 1x PBS for 5 min and post-fixation for 15 min with 1 ml 4 % PFA at RT, the PFA was washed out three times with 1 ml 1x PBS for 5 min at RT. Finally, the coverslips were mounted on a slide using one drop of Vectashield® Mounting Medium for Fluorescence with DAPI H-1200 (Vector Laboratories) and sealed with Essence 2 in 1 Base + Top Coat nail polish (Cosnova GmbH). Stained slides were stored at 4 °C in the dark.

4.2.5 Human Retinal Pigment Epithelial Cells (RPE1)

RPE1 cells were cultured in DMEM:F12 medium containing 10 % FBS and 1 % P/S. Cilia induction was achieved by serum starvation during 72 hours. The starvation medium consisted of DMEM:F12 with 0.1 % FBS and 1 % P/S.

4.2.5.1 Fenoldopam treatment

150,000 cells were transferred to each well of a 6-well plate containing coverslips. 2.5 ml of 10 µM fenoldopam or DMSO as vehicle, both solved in starvation medium were added to each well. The cells were incubated with this solution for 3 days before fixing with prechilled MeOH (4.2.3) and following an AB staining for acetylated tubulin and γ-tubulin (4.2.4). Pictures of these cells were taken with the help of an AxioCam MRc and Axio Imager M1 (Carl Zeiss Sports Optics GmbH). The cilia length was measured with Fiji.

4.2.6 Human Embryonic Kidney 293 Cells (HEK)

HEK cells were cultured in Dulbecco's Modified Eagle's Medium – high glucose (DMEM) medium containing 10 % FBS and 1 % P/S.

4.2.6.1 HEK cell transfection

The Lipofectamine® 3000 Transfection Kit (Invitrogen) was used to transfect HEK cells in a 6-well plate. 125 µl Opti-MEM were mixed with 1 µg DNA (Table 10) and 5 µl P3000 by pipetting up and down. In a well of the 6-well plate 125 µl Opti-MEM™, Reduced Serum Medium, no phenol red (Opti-MEM) were prepared with 3.75 µl L3000. The DNA-P3000 mixture was transferred to the L3000 mixture and the whole reaction was incubated for 5-10 min at RT. To a total volume of 2 ml 600,000 cells in medium were added to the incubated mixture for 24 h.

4.2.6.2 HEK cell treatment

HEK cells were also treated with 30 nM Rapamycin or DMSO as control in a 6-well plate. 600,000 cells per well were plated and treated with the chemical compound for 24 h.

4.2.6.3 HEK cell size and protein content

Cells were washed once with DPBS and trypsinized with 1 ml prewarmed Trypsin for 1 min at 37°C. Then, cells were transferred to a 15 ml falcon tube and centrifuged for 5 min with 700-800 rpm. The supernatant was discarded and the pellet was resuspended with 1 ml DPBS. To measure the cell size, 10 µl of the resuspended cells were mixed with 10 µl trypan blue staining and 10 µl of this mixture were transferred into a cell counting chamber slide. This was made twice for each condition. The chamber slide was placed in the Countess™ Automated Cell Counter for taking pictures of the cells. To calculate the actual cell diameter, pictures of Countess™ test beads (Invitrogen) with defined size were also taken. The test beads and cells were then measured using Fiji. The rest of the resuspended cells was used to determine the total protein content of the cells. For this 3x 200,000 cells per condition were transferred into 3 different tubes. The cells were again centrifuged with 1,000 rpm for 5 min. The supernatant was discarded and 50 µl SDS-lysis buffer (3.18) were added. 2 µl of a 1:10 diluted Universal Pierce-Nuclease (Thermo Fisher Scientific) with H_2O ad. inj. were added per sample and incubated for 15 min at RT. For each sample I prepared 1 ml of Copper (II) sulfate solution diluted 1:50 with bicinchoninic acid solution (BCA). 5 µl of each sample were then added to the BCA mixture. For measuring a blank 5 µl of SDS-lysis buffer were also added to one BCA mixture. After an incubation of 15 min at 60 °C the whole reaction was transferred to a cuvette (Sarstedt AG & Co. KG). Finally, the protein content was measured with a Nanodrop One^C program OD600 and an additional monitored wavelength at 562nm. The actual protein content was calculated in ng/cell using Excel (Microsoft Corporation).

4.2.7 Human hTERT Immortalized 1BR3 Wild-Type Fibroblasts (1BR3)

1BR3 cells were maintained in Minimum Essential Medium (MEM) α with 10% FBS and 1% P/S. For inducing ciliogenesis, cells were switched to starvation medium containing MEM α with 0.1% FBS and 1% P/S and cultured for 72 hours.

4.2.7.1 1BR3 transfection

1BR3 cells were transfected with Lipofectamine® RNAiMax (Invitrogen) in a 6-well plate with 120,000-150,000 cells and one coverslip per well. Following the manufacturers protocol, I diluted 6.25 µl 20 µM siRNA (Table 6) with 250 µl Opti-MEM. In another tube, 4 µl Lipofectamine® RNAiMax Transfection Reagent were diluted with 250 µl Opti-MEM. For complex formation, the siRNA mixture was added to the Lipofectamine® RNAiMax Transfection Reagent mixture and incubated for 15 min at 37°C. During this complex formation, 1BR3 cells were detached using Trypsin and counted. 120,000-150,000 cells were added with 2 ml medium to each well. Afterwards, the transfection complex was added to the cells in the well. One day later the medium was changed to starvation medium and cells were cultured for three days for cilia growth. Then, cells were rinsed once with PBS and fixed with ice cold MeOH as described in 4.2.3, followed by an AB staining (4.2.4) for cilia length analysis (4.5) or lysis for RNA isolation as described in 4.3.4, which in turn was used for cDNA synthesis (4.3.5) and qPCR analysis (4.3.6).

4.2.7.2 1BR3 nucleofection

1BR3 cells were nucleofected with the Amaxa™ Cell Line Nucleofector™ Kit R and Nucleofector® 2b Device (both Lonza Group AG) and eventually plated at a density of 250,000 cells per well in a 6-well plate. According to the manufacturers protocol, the nucleofection solution was adjusted slowly to RT. The cells were counted and 500,000 cells were added to a 15 ml Falcon tube. This was centrifuged for 5 min with 900 rpm at RT. The supernatant was discarded and the pellet resuspended with 100 µl nucleofection solution. 1µg DNA (Table 10) and/or 1.5 µl 20 µM siRNA (Table 6) were added to the cells. The whole mixture was transferred to the cuvette, which was closed afterwards. The cuvette was placed in the Nucleofector® 2b Device and pulsed with program U-023. Then the cuvettes were incubated for 10 min at RT. 500 µl of medium were added and the cells were distributed equally into two different wells of the 6-well plate. One day later, the medium was changed to starvation medium for three days for cilia growth. After these three days the cells were rinsed once with PBS and fixed with ice -cold MeOH as described in 4.2.3, followed by an AB staining (4.2.4) for cilia length analysis (4.5). Alternatively, cells were

lyzed for RNA isolation as described in 4.3.4, for subsequent cDNA synthesis (4.3.5) and qPCR analysis (4.3.6).

4.2.7.3 1BR3 Western Blot

1BR3 cells were lyzed as described in 4.2.6.3. Instead of 1 % SDS lysis buffer, 2 % SDS lysis buffer was used. Then I followed the above mentioned protocol. Protein concentration was assessed by BCA assay and 10 µg protein were calculated. To achieve denaturation, samples were mixed with 5 µl of a 1:7 diluted β-mercaptoethanol:10x loading dye mixture. They were briefly mixed and incubated for 15 min at 60 °C. After incubation, they were spun for 3.5 min with 11,000 rpm at RT. 33 µl of each sample were loaded on a Bolt™ 4-12 % Bis-Tris plus gel (Invitrogen) in a Bolt™ Mini Gel Tank (Thermo Fisher Scientific) with 1x Bolt™ MES SDS Running Buffer (Thermo Fisher Scientific). Additionally, I loaded one pocket of the gel with 8 µl Precision Plus Protein™ Kaleidoscope™ Standard marker (Bio-Rad Laboratories Inc.) Electrophoresis was then performed with 150 V and 500 milliampere (mA) until the 10 kDA band of the marker disappeared. Then, proteins were blotted for 1 h at RT at 10 V on a nitrocellulose membrane (Bio-Rad Laboratories Inc.) using a Mini Bolt Module (Thermo Fisher Scientific) filled with transblot buffer (Table 18) and a Bolt™ Mini Gel Tank (Thermo Fisher Scientific). After an incubation of 5 min with a Ponceau S staining solution (0.2 % Ponceau S with 3 % Trichloroacetic acid (both Sigma-Aldrich Inc.)), the membrane was rinsed with H_2O. Then, the membrane was blocked for 1h at RT in 2 % Nonfat Dried Milk Powder (AppliChem GmbH) in 1x TBST and rinsed once with 1x TBS. Finally, the first ABs were diluted as described in Table 15 with 3 % bovine serum albumin fraction V (BSA) (Roche) in 1x TBST and the membrane was incubated over night at 4 °C. On the next day, the first ABs were removed and the membrane was rinsed once with H_2O and washed 3x for 5 min with Western Wash (Table 18) on a shaker. Then, the membrane was incubated with secondary ABs diluted as described in Table 15 with ½ Odyssey® Blocking Buffer (TBS) (LI-COR Biosciences) with 0.2 % Tween® 20. After 4h of incubation at RT on a shaker the ABs were removed and the membrane was washed 3x for 5 min at RT with Western Wash. Finally, the membrane was rinsed with and stored in 1x TBST. I used the iBright™ FL1500 instrument (Invitrogen) to image the membrane.

4.2.8 Inner Medullary Collecting Duct Cells (IMCD3)

IMCD3 cells were cultured in Mixture F-12 (1:1) (1x) (DMEM/F-12) with 10 % FBS and 1 % P/S. As starvation medium we used DMEM/F-12 with 0.1 % FBS and 1 % P/S.

4.2.8.1 IMCD3 transfection

The Lipofectamine® 3000 Transfection Kit (Invitrogen) was used to transfect IMCD3 cells with either empty vector (pCS2+), zebrafish Grk4 or zebrafish Grk4 KiDe and siGrk4 (Dharmacon) (Table 6) in a 12-well plate. For one well following reaction was assembled: 50 µl Opti-MEM were mixed with 1 µg DNA and 1 µl P3000. 12.5 µl Opti-MEM were mixed with 2.815 µl 20 µM siRNA (total dilution of 1:400). 62.5 µl Opti-MEM with 1.875 µl L3000 were prepared in a well of the 12-well plate. Then the P3000 mixture was added to the diluted siRNA and this was added to the L3000 mixture in the well and mixed by pipetting up and down. The whole reaction was incubated for 10 min at RT. After the 10 min 1 ml of medium containing 100,000 cells were added to the well. One day after transfection, cells were washed once with PBS and detached with 100 µl trypsin for 5 min at 37 °C. The cells were resuspended with 1 ml medium and centrifuged with 800 rpm for 5 min. The supernatant was discarded and the pellet resuspended with 500 µl medium. The cell number was determined and medium added until one had 150,000 cells per ml. For each well 100 µl cell suspension were gently mixed with 100 µl Matrigel® Matrix (Corning Inc.), that has been thawed slowly at 4 °C. The mixture, containing 150,00 cells in total, was quickly transferred to one chamber of a Nunc™ Lab-Tek™ II Chambered Coverglass (Thermo Fisher Scientific). The chambered coverglass was transferred to the incubator at 37 °C for 15-30 min until the whole mixture was solidified. Then 200 µl of medium were added to the hardened cell Matrigel® Matrix layer. On the next day, the medium was switched to starvation medium for cilia growth. When the spheroids appeared to be fully formed (normally 2-3 days after seeding in Matrigel® Matrix) the gel was washed three times with PBS. To prepare the spheroids for antibody staining, 200 µl of 4 % PFA were added and incubated for 30 min on a shaker at RT. Most of the Matrigel® Matrix dissolved in PFA and the spheroids fell down and adhered on the bottom of the well. The spheroids were rinsed

three times and once washed for 5 min with PBS. 200 µl of permeabilization buffer (3.18) were added to the spheroids followed by an incubation for 30 min at RT. During this incubation I diluted the first antibodies in permeabilization buffer (see Table 15 for dilutions). After these 30 min the permeabilization buffer was discarded and 100 µl of the first antibody solution were added and incubated at 4 °C o/N. On the next day, the spheroids were washed a total of four times with permeabilization buffer, once quickly and three times for 10 min while shaking at RT. The secondary antibodies were also prepared in permeabilization buffer (see Table 15 for dilutions). 100 µl of this mixture were added to each well and incubated for 4h at RT in the dark. After this, the spheroids were again washed a total of four times with permeabilization buffer, once quickly and three times for 10 min while shaking at RT. Finally, the spheroids were mounted using some drops of Vectashield® Hard Set™ Mounting Medium with DAPI H-1500 (Vector Laboratories). The spheroids were drying at RT o/n in the dark and then stored at 4 °C until imaging with the Confocal Microscope Platform STELLARIS 5 (Leica Microsystems GmbH). Cilia were measured as described in 4.5. Cells were counted by eye.

4.3 Molecular methods

4.3.1 Cloning and generation of in situ probes and capped RNA

4.3.1.1 PCR amplification

For cloning capped RNA resembling the mutation Grk4 1.2, I had to perform three different PCR amplifications:

Table 31: Mastermix PCR #1 reaction setup

PCR #1
10 µl 5x Q5® Reaction Buffer
5 µl 2 mM dNTPs

2.5 µl 10 µM zfGrk4 FW ClaI
2.5 µl 10 µM zfGrk4 c 580_585del Rev
0.5 µl Q5® High-Fidelity DNA Polymerase
1 µl pCS2+-zfGrk4
28.5 µl H_2O

Table 32: Mastermix PCR #2 reaction setup

PCR #2
10 µl 5x Q5® Reaction Buffer
5 µl 2 mM dNTPs
2.5 µl 10 µM zfGrk4 c580_585del Fw
2.5 µl 10 µM zfGrk4 Rev StuI
0.5 µl Q5® High-Fidelity DNA Polymerase
1 µl pCS2+-zfGrk4
28.5 µl H_2O

Table 33: Mastermix PCR #3 reaction setup

Mastermix PCR #3
10 µl 5x Q5® Reaction Buffer

5 µl 2 mM dNTPs
2.5 µl 10 µM zfGrk4 FW ClaI
2.5 µl 10 µM zfGrk4 Rev StuI
0.5 µl Q5® High-Fidelity DNA Polymerase
1 µl PCR product #1
1 µl PCR product #2
28.5 µl H_2O

All PCRs were run with following conditions:

Table 34: Running conditions PCR amplifications

Temperature	Time	Cycles
98 °C	30 sec	1x
98 °C	10 sec	
72 °C	20 sec	30x
72 °C	1 min	
72 °C	2 min	1x
8 °C	∞	

4.3.1.2 Gel electrophoresis

An agarose (Invitrogen) gel was prepared to visualize DNA, amplified PCR products or different types of RNA. For this 1.5 - 2 % agarose were dissolved in 50 ml 1xTAE using a microwave. After a short cool down 2 µl of Midori Green Advance (Nippon Genetics Europe GmbH) were mixed into and the whole solution were poured in a gel tray with a well comb. The gel was solidified 20 - 30 min at RT. The samples were mixed with 2 µl 10x Loading Buffer. After removing the comb and placing the gel tray into the electrophoresis chamber (VWR), the wells were loaded with either Ladder (NEB) or sample. The gel ran with 120 V until the desired bands were clearly visible and separated (normally around 20 min).

Table 35: 10x Loading Buffer

Reagent	Volume
Glycerol anhydrous p.A. (AppliChem)	6 ml
H_2O	6 ml
Bromphenol blue (Merck KGaA)	small spatula tip

4.3.1.3 Gel extraction

Prior gel extraction of the band of interest, a photo of the gel was taken using the iBright 1500 (Invitrogen). For the following extraction of the band the Monarch® DNA Gel Extraction Kit (New England BioLabs® Inc.) was used. First, the desired band was cut out of the gel and this slice was weighed and 4 volumes of gel dissolving buffer were added. This was incubated at 50 °C for around 5-10 min. After dissolving the whole gel slice, the sample was loaded into a collection tube with a column on top. This was spun for 1 min at 13,000 rpm at RT with a centrifuge (Eppendorf). The flow-through was discarded. The re-inserted column was washed with 200 µl DNA wash buffer and spun for 1 min with 13,000 rpm at RT. This step was repeated once. At the end, the column was put on top of a 1.5 ml reaction tube (Eppendorf). 10 µl of H_2O ad. inj. were added to the center of the column and

incubated for 1 min at RT. Then the DNA was eluted by spinning 1 min with 13,000 rpm at RT. For better elution the last step normally was repeated once. The extracted DNA was stored at -20 °C until further use.

4.3.1.4 Cloning into pCS2+vector

For Cloning reactions into the pCS2+ vector the purified and extracted PCR product needed to digest o/n at 37 °C:

Table 36: Mastermix for PCR-product digest with ClaI and StuI

Mastermix PCR-digest o/n
1.5 µl rCutSmart™ Buffer
0.2 µl ClaI
0.2 µl StuI
3.1 µl H_2O ad. inj.
add to the 10 µl purified PCR product

The pCS2+ vector itself also needed to be digested with the following mixture for 2 h at 37 °C.

Table 37: Mastermix pCS2+ vector digest

Mastermix pCS2+ digest
1 µl pCS2+ vector
1.5 µl rCutSmart™ Buffer

0.2 µl ClaI
0.2 µl StuI
13.1 µl H_2O ad. inj.

After 2 h the digested vector was cleaned using the Monarch® DNA Gel Extraction Kit from NEB (4.3.1.3) and eluted with 7 µl H_2O ad. inj..

The digested PCR product was then ligated into the digested pCS2+ vector using the USB® Ligate-IT™ Rapid Ligation Kit (Affymetrix, Inc. USB) for 15 min at RT.

Table 38: Reaction Mix Ligation

Reaction Mix Ligation of DNA into the pCS2+ vector
6 µl cleaned and digested PCR product
2 µl 5x Ligate-IT Reaction Buffer
1 µl cleaned and digested pCS2+ vector
1 µl Ligate-IT T4 DNA Ligase

After the ligation of the PCR product into the pCS2+ vector, this construct was transformed in competent cells.

4.3.1.5 Transformation and Cloning

First, 4 µl of the extracted and purified PCR product (4.3.1.3) were mixed with 1 µl salt solution and 1 µl pCS2+ vector by pipetting carefully up and down and incubated for 5-10 min at RT. After a maximum of 10 min the mixture was put on ice. One Shot™ TOP10

Chemically Competent *E. coli* (Invitrogen) were thawed on ice. The whole cloning reaction was put to the cells and mixed by carefully flipping the tube. After an incubation of 10 min on ice, a heat shock was made at 42 °C for 1 min. This ensured the uptake of the plasmid into the cells. After the heat shock the cells were put on ice and 80 µl of Super Optimal Broth medium with added glucose (S.O.C. medium) were added (92). This transformation was incubated at 37 °C for 30 min while shaking with 180 rpm. Lysogeny broth (LB) (93) plates were prepared some days before plating and growing cells. For this, 32 mg of Lennox L Agar (Invitrogen) were solved in 1 l H_2O and autoclaved at 121 °C for 15 min. After a short cooldown, 100 µg/ml ampicillin were added, as the pCS2+ vector contains an ampicillin resistance. The LB agar was poured in 10 cm petri dishes and solidified. Two of these plates were then used for plating and growing cells. The transformed cells were then distributed on the two plates and incubated upside down at 37 °C o/n. On the next day, 6 single colonies were picked, solved in 3 ml Lennox L Broth Base (LB Broth Base) medium containing ampicillin and placed in an incubator (H-15, KS-15, Edmund Bühler GmbH) at 37 °C o/n with 260 rpm.

4.3.1.6 Minipreparation of plasmid DNA

On the next day, 1.4 ml of this so-called miniculture were transferred into a 1.5 ml Eppendorf tube and spun for 1 min with 10,000 rpm at RT. The supernatant was discarded. The pellet was resuspended with 300 µl P1 Buffer (Table 18). 300 µl of P2 (Table 18) were added and the tube was inverted three times. Then 300 µl of P3 were added and again the tube was inverted three times and spun for 10 min at 4 °C with 13,000 rpm. While the tube was centrifuged, a new Eppendorf tube was prepared with 600 µl prechilled 2-propanol (Honeywell). 830 µl of the supernatant were transferred into the new tube and mixed by vortexing. This tube was spun at 4 °C with 13,000 rpm for 10 min. After discarding the supernatant, the pellet was washed with 300 µl 70 % EtOH. After short vortexing, the tube was centrifuged for 10 min at 4 °C with 13,000 rpm. The supernatant was discarded and the pellet was air dried for 1-2 min with open lid. Finally, the pellet was dissolved in 30 µl H_2O

ad. inj.. To differentiate which colony was successfully transformed, a control digest was performed with following reaction setup:

Table 39: Reaction setup control digest Miniprep

Reaction setup for n=1
1 µl rCutSmart Buffer™ (NEB)
0.1 µl ClaI (NEB)
0.1 µl StuI (NEB)
5.8 µl H_2O ad. inj.
7 µl total volume/tube
add 3 µl Mini-DNA

The digest was incubated for 15 min at 37 °C. After this, the whole digest was analyzed by gel electrophoresis (4.3.1.2). One positive transformed Miniculture was taken to set up a so-called Midiculture. For this 100 µl of the Miniculture were incubated with 35 ml LB Broth Base medium containing ampicillin (1:1000 diluted) at 37 °C o/n with 260 rpm in an Erlenmeyer flask.

4.3.1.7 Midipreparatiopn of plasmid DNA

On the next day the whole Midiculture was transferred to a 50 ml falcon tube and spun for 10 min with 4,000 rpm at RT. The supernatant was discarded. For the following midipreparation I used the Plasmid *Plus* Midi Kit from QIAGEN®. The pellet was resuspended with 4 ml of P1 buffer (Table 18). 4 ml of P2 buffer (Table 18) were added and the tube was mixed by inverting. After an incubation of 3 min at RT, 4 ml of S3 buffer were added and the tube inverted until all traces of blue were gone (usually 4-6 time were

sufficient). A screw cap was put on a QIAfilter cartridge and the whole mixture was transferred in this. During an incubation of 10 min at RT, the vacuum manifold was prepared with QIAGEN Plasmid *Plus* Midi spin columns. 2 ml of BB buffer were also prepared in a new 50 ml falcon tube. By gently inserting a plunger into the QIAfilter, the mixture was filtered and collected in the prepared 50 ml falcon containing BB. The filtered lysate was transferred to the QIAGEN Plasmid *Plus* Midi spin column with a tube extender attached on the QIAvac 24 Plus. The vacuum source was switched on, the tap was opened and the solution has been drawn through the QIAGEN Plasmid *Plus* Midi spin column. After all of the solution was gone, the tap was closed and 700 µl ETR buffer were added to the column. The tap was again opened until the added buffer was gone. 700 µl of PE buffer were added and the vacuum wash was repeated. To ensure that all of the solution was gone, the tube with spin column was centrifuged for 1 min with 13,000 rpm at RT. After this, the spin column was placed in a new 1.5 ml Eppendorf tube and 150 µl of EB buffer or H_2O ad. inj. were added to the middle of the center and incubated for 1 min at RT. This was spun for 1 min with 13,000 rpm at RT. Finally, the concentration of the plasmid was measured using a Nanodrop One^C, program dsDNA with a baseline correction at 340 nm. Normally all plasmids were then diluted to 1 µg/µl, or to 500 ng/µl if not possible.

To be sure that no mutations occurred during cloning, the plasmid was sent for sequencing.

4.3.1.8 Sequencing with GATC or Microsynth

For sequencing with GATC I prepared following reaction mix:

Table 40: GATC sequencing

Reaction setup
500 ng DNA
2.5 µl 10 µM Sp6 or T7 Primer
x µl H_2O ad. inj. for a total volume of 10 µl

For sequencing with Microsynth, following reaction mix was prepared:

Table 41: Microsynth sequencing

Reaction setup
720 ng DNA
3 µl 10 µM Sp6 or T7 Primer
x µl H_2O ad. inj. for a total volume of 12 µl

4.3.1.9 Linearization of plasmids

In order to transcribe the desired sequence inserted into a given plasmid, the plasmid was linearized. For this, the following reaction setup was prepared and incubated at 37 °C for about an 1 h:

Table 42: Linearization of plasmids

Reaction setup
10 µg Plasmid
5 µl 10x Restriction buffer
(0.5 µl 100x BSA if necessary)
2.5 µl Restriction enzyme
x µl H_2O ad. inj. for a total volume of 50 µl

The linearization was checked by running an agarose gel with 0.3 µg undigested plasmid versus 1 µl of the digest (4.3.1.2). If only one band was visible the digest was ready for purification.

4.3.1.10 Purification of linearized DNA

150 µl H_2O ad. inj. were added to the digest. After mixing, 200 µl Phenol:Chloroform:Isoamylalcohol 25:24:1 (AppliChem GmbH) were added. The tube was vortexed and centrifuged for 10 min with 10,000 rpm at RT. The upper aqueous phase was transferred into a new tube and another 200 µl Chloroform were added. Again, the tube was vortexed and centrifuged with 10,000 rpm at RT and the upper aqueous phase was transferred into a new tube. 25 µl 3 M sodium acetate and 650 µl EtOH abs. were added, everything was vortexed and the DNA was precipitated for at least 1 h or o/N at -80 °C. On the next day, the tube was centrifuged for 15 min at 4°C with 13,000 rpm. The supernatant was discarded and the pellet resuspended with 500 µl 70% EtOH. This was centrifuged again at 4°C with 13,000 rpm for 10 min. The supernatant was discarded and the pellet was dissolved in 20 µl H_2O ad. inj. The DNA was stored at -20°C.

4.3.2 Preparation of capped RNA for injection

For rescue experiments of zebrafish embryos by injection it was necessary to prepare capped RNA. After linearization and purification of the generated plasmid, the capped RNA was transcribed. For this, we used two different kits, depending on the orientation of the gene of interest in its vector. The mMESSAGE mMACHINE™ SP6 Kit (Invitrogen) was used for the transcription using SP6 polymerase. The following was assembled in a reaction tube and incubated for 1 h at 37 °C.

Table 43: SP6 in vitro transcription

Reaction setup
10 µl 2x NTP/CAP
2 µl 10x Reaction buffer
2 µl linearized template DNA

2 µl Enzyme mix
to 20 µl H_2O ad. inj.

For the transcription with T7, the AmpliCap-Max™ T7 High Yield Message Maker Kit (Cellscript) was used. Following the manufactures protocol everything was assembled in a reaction tube and incubated at 37 °C for 30 min.

Table 44: T7 in vitro transcription

Reaction setup
2 µl linearized template DNA
2 µl 10x AmpliCap-Max T7 Transcription Buffer
8 µl AmpliCap-Max Cap/NTP Premix
2 µl 100 mM DTT
0.5 µl ScriptGuard RNase Inhibitor
2 µl AmpliCap-Max T7 Enzyme Solution
to 20 µl H_2O ad. inj.

After the transcription with either SP6 or T7, the RNA was treated with DNase I (included in the kits), purified with Phenol:Chloroform:Isoamylalcohol and precipitated o/n at -80 °C (4.3.2.1 and 4.3.2.2). Finally, an agarose gel was prepared for gel electrophoresis (4.3.1.2) and the concentration of the RNA was measured using the NanoDrop One^C program RNA. For rescue experiments in zebrafish by microinjection, each capped RNA was diluted as described in the following:

Table 45: RNA for injections

Mastermix
X µl capped RNA for a final concentration of 100 ng/µl in 20 µl
4 µl 5x Phenolred
to 20 µl H_2O ad. inj.

The diluted RNA was stored at -20 °C until further use (4.1.4).

4.3.2.1 DNase I recombinant, RNase-free treatment

To get rid of the template DNA, it was necessary to treat the in vitro transcription with DNase I recombinant, RNase-free (Roche) by adding following and mixing by pipetting up and down:

Table 46: DNase treatment

Reaction setup
3.4 µl 10x RNase free DNase Buffer
1 µl DNase I recombinant, RNase-free

This was incubated for 20 min at 37 °C.

4.3.2.2 Precipitation of RNA

Next, the DNase-treated RNA needed to be precipitated. For this 17 µl 7.5 M ammonium acetate and 170 µl abs. EtOH were added. After vortexing, the tube was incubated for at least 1 h, but normally o/n at -80 °C. On the next day, the tube was centrifuged for 15 min

with 13,000 rpm at 4 °C. The supernatant was discarded, the pellet was resuspended in prechilled 70 % EtOH and the tube was centrifuged for 10 min with 13,000 rpm at 4 °C. After discarding the whole supernatant, the pellet was dissolved in 100 µl H_2O ad. inj.. To check for left over linearized plasmid, 1 µl of the RNA were used to run on an agarose gel (4.3.1.2). If necessary, the steps 4.3.2.1 and 4.3.2.2 were repeated. If not, the concentration of the RNA was measured using a NanoDrop One^C with the program RNA and a baseline correction at 340 nm. The RNA was stored at -80 °C until further use.

4.3.3 WMISH for zebrafish embryos

Embryos used for WMISH analysis needed to be incubated in MeOH for at least 1 at -20 °C (see also dehydrating MeOH series at 4.1.10). All incubation steps were performed on a shaker at RT with 500 µl solution, unless otherwise indicated.

After the MeOH incubation the embryos were adjusted to RT and rehydrated with the above described graded MeOH series (backwards) (4.1.10). After the last step (25% MeOH in PBST) the embryos were washed a total of 4 times with PBST for 5 min. For better access of the in situ probe, embryos older than tailbud stage needed to be treated with Proteinase K (Roche). A 10 mg/ml Proteinase K stock solution was diluted 1:1000 with PBST for a final concentration of 10 µg/ml of Proteinase K. The embryos were treated for a specific time with 500 µl of the 1:1000 diluted Proteinase K solution as described in the following:

1-5 somites	2 min
10 somites	3 min
20 somites	5 min
24 hpf	8 min
48 hpf	15 min
72 hpf	30 min

After this treatment the embryos were rinsed once with PBST and then re-fixed using 4 % PFA in PBS for 20 min to inactivate the Proteinase K. The used 4 % PFA in PBS was

collected again and stored it at -20 °C. The embryos were washed 5 times for 5 min with PBST. After removing the PBST, 300 µl of 50 % hybridization buffer were added and the embryos were incubated for at least 1 h in a preheated water bath at 70 °C. The following table describes the 50 % hybridization solution composition:

Table 47: Hybridization solution

Reagent	Quantity (for 50 ml)	Final concentration
Formamide	25 ml	50 % (v/v)
Sodium saline citrate (SSC)	12.5 ml of 20x SSC	5x
Heparin	50 µl 50 mg/ml	50 µg/ml
Ribonucleic acid from torula yeast type VI	spatula tip	500 µg/ml
Tween® 20	500 µl 10 % Tween® 20	0.1 %
Citric acid	460 µl 1M citric acid	0.0092 M
H_2O	add to 50 ml	

The in situ probe of interest was diluted to a final concentration of 250 – 300 ng/200 µl in hybridization solution and denatured for 10 min at 70 °C. For the last step of the first day WMISH, the prehybridization solution was exchanged with the preheated hybridization solution containing the in situ probe of interest and the embryos were incubated o/n at 70 °C. If not already prepared, it was also important to preadsorb anti-digoxigenin alkaline phosphatase (anti-DIG) AB (Roche) for the next day of WMISH. To do so, a few dechorionated, fixed embryos were incubated at 4 °C with a 1:1000 diluted anti-DIG-AB solution. This solution contained 4,400 µl PBST, 100 µl NGS, 500 µl 20 mg/ml BSA and 5 µl anti-DIG AB.

On the next day the first seven wash steps were performed in the water bath at 70 °C for 8 min respectively. Starting with following graded preheated hybridization solution series:

100 % hybridization solution

75 % hybridization solution with 25 % 2x SSC

50 % hybridization solution with 50 % 2x SSC

25 % hybridization solution with 75 % 2x SSC

100 % 2x SSC

100 % 0.2x SSC twice.

After this the embryos were washed with another graded series containing 0.2x SSC and PBST (at RT):

75 % 0.2x SSC with 25 % PBST

50 % 0.2x SSC with 50 % PBST

25 % 0.2x SSC with 75 % PBST

100 % PBST.

Then the embryos were incubated at least for 1 h at RT with a blocking solution containing PBST with 2 mg/ml BSA and 2 % NGS before incubation in antibody at 4 °C o/n. The preadsorbed 1:1000 anti-DIG AB solution was diluted 1:5 with blocking solution to obtain a final concertation of 1:5000 anti-DIG AB in blocking solution.

On the third day, the AB solution was removed and the embryos were washed 8x for 8 min with PBST. During the last wash step, the embryos were transferred to a pre-labeled 24-well plate (Corning Inc.) and subsequently washed twice with alkaline phosphatase (AP) buffer (Table 48).

Table 48: AP-Buffer

Reagent	Quantity for 5 ml	Final concentration

Tris pH 9.5	0.5 ml 1M Tris pH 6.5	100 mM Tris pH 6.5
$MgCl_2$	0.25 ml 1M $MgCl_2$	50 mM $MgCl_2$
NaCl	0.1 ml 5M NaCl	100 mM NaCl
Tween® 20	50 µl 10 % Tween® 20	0.1 % Tween® 20
H_2O	4.1 ml H_2O	

The staining was developed in AP buffer containing 1x nitro blue tetrazolium/5-bromo-4-chloro-3-indolyl phosphate (NBT/BCIP) (Roche) with 0.24 mg/ml Levamisole-HCl (Sigma-Aldrich Inc.). The 24-well plate was wrapped with aluminum foil to minimize light exposure. When the embryos displayed the desired staining, it was stopped by rinsing 4x with PBST and subsequent incubation with 4 % PFA (from day 1) for 20 min at RT. Finally, the embryos were rinsed with and stored in PBST at 4 °C until further analysis.

4.3.4 RNA isolation using the Quick-RNA™ Micro Prep Kit

RNA was isolated with the help of the Quick-RNA™ Micro Prep Kit from Zymo Research (USA) following the manufacturers protocol. All centrifugation steps were performed with 13,000 rpm for 30 sec at RT, unless specified. 300 µl of RNA Lysis Buffer were added to the cells or zebrafish embryos and incubated for around 15 min at RT. 300 µl of 100 % EtOH were added to each sample and everything was mixed well by pipetting up and down. The whole mixture was transferred to a Zymo-Spin™ IC Column in a Collection Tube and centrifuged. After discarding the flowthrough, 400 µl of RNA Wash Buffer were added and the tubes were centrifuged again. The flow-through was discarded. 5 µl of DNase I were mixed with 35 µl DNA Digestion Buffer and directly added on the column matrix without touching it. This was incubated for 15 min at RT. 400 µl of RNA Prep Buffer were then

added on top and the tubes were centrifuged again. The flowthrough was discarded. 700 µl of RNA Wash Buffer were added and the tubes were centrifuged. The flowthrough was discarded again. Then, 400 µl of RNA Wash Buffer were added and the tubes were centrifuged for 2 min with 13,000 rpm at RT. Finally, the column was carefully transferred to a clean, prelabeled 1.5 ml Eppendorf tube and 15 µl H_2O ad. inj. were added to the column matrix. The RNA was then eluted by spinning again. The concentration and purity of the RNA was measured using the NanoDrop One^C program RNA. The RNA was stored at -80 °C.

4.3.5 cDNA Synthesis

The ProtoScript™ II First Strand cDNA Synthesis Kit (New England BioLabs® Inc.) was used for cDNA synthesis. 6 µl of RNA were mixed with 2 µl 50 µM oligod$(T)_{23}$ VN primer and H_2O ad. inj. to a total volume of 8 µl. If more than one sample was transcribed, equal amounts of RNA were used for all reactions. The RNA and oligod$(T)_{23}$ VN primer were denatured for 5 min at 65 °C and transferred to ice. After a brief spin down, 10 µl of the 2x ProtoScript II Reaction Mix and 2 µl of the 10x ProtoScript II Enzyme Mix were added to each sample and the whole reaction was incubated for 1 h at 42 °C. The enzymes were then inactivated by heating the mixture at 80 °C for 5 min. The cDNA was stored at -20 °C.

4.3.6 qPCR

A the Lightycyler® 480 (Roche) and Luna Universal qPCR Master Mix were used (New England BioLabs® Inc.) for qPCR analysis. One row (12 wells) of a 96-well qPCR plate was normally used for the analysis of one cDNA. The total volume of the cDNA (20 µl) was diluted with 28 µl H_2O ad. inj. and 72 µl Luna Universal qPCR Master Mix. 10 µl of this mixture were pipetted into each well of the row. Additionally, 2 µl of a specific primer-universal probe (UP) (Table 11) mixture were added to three of the 12 wells for creating technical triplicates. Normally, 24 wells of the 96-well plate were used for the analysis of one gene. To do so, 24 µl of a 10 µM primer mix (containing forward and reverse primer)

were mixed with 24 µl UP diluted 1:10 with H_2O ad. inj.. When every well was filled with cDNA-Luna mix and primer-UP mix, the 96-well plate was sealed with adhesive clear qPCR seals. The qPCR was run on a Lightycyler® 480 II with the following settings:

-Reaction Volume: 12 µl

-White qPCR semi-skirted plate

-Detection format: Mono Color Hydrolysis Probe/ UPL Probe

-Running conditions:

Table 49: Running conditions for qPCR

Step	Temperature	Time	Ramp Rate (°C/s)	Cycles
Preheating	50 °C	15 sec	4.4	1x
Denaturing	95 °C	1min	4.4	1x
Cycling	95 °C	15 sec	4.4	45x
	60 °C	35 sec	2.2	

The data were analyzed with the Abs Quant/2nd Derivative Max method in the Lightycyler® 480 II software. The calculated values were exported to Excel.

The primers and UP used for qPCR analysis were designed with the help of the Universal ProbeLibrary Assay Design Center. After Roche discontinued this service, the following webpage was used: https://primers.neoformit.com

4.4 Imaging

Live images as well as images of whole mount in situ hybridization embryos were acquired on a Leica M125 microscope with an IC80HD or MC190HD camera (Leica Microsystems GmbH). For fluorescence images of the developing kidney a Leica M205FCA and Leica

DFC9000GT sCMOS camera was used. For fluorescence images of cilia in zebrafish embryos and of cilia in cells, a Leica TCS SP5II confocal microscope or Confocal Microscope Platform STELLARIS 5 (both Leica Microsystems GmbH) were used with optimized z-stack size. The pictures were processed into a 3D stack using the Leica acquisition software LAS AF. Equal adjustment for brightness, contrast and cropping of all images were done by using Adobe Photoshop. With the help of Adobe Illustrator final figures were generated.

4.5 Measuring cilia length

With the Simple Neurite Tracer plugin of Fiji, cilia length was measured in 3D. These data were more accurate than measuring the cilia length of the 2D projection of a 3D picture.

4.6 Statistical analysis

Statistics were assessed by using GraphPad Prism 8. First, all data were analyzed for normal or not normal distribution with the Shapiro-Wilk test. For the comparison of two datapoints a two-tailed t-test with Welch's correction was used or a Mann-Whitney test, if not normally distributed. For the comparison of more than two different datapoints an One-Way ANOVA with Sidak's multiple comparison test was used or a Kruskal-Wallis test with Dunn's correction for not normally distributed data, respectively.

5 Results

5.1 Expression of *adsl* during zebrafish development

In the course of establishing ADSL as a potential new regulator of cilia, an expression pattern of Adsl during zebrafish development was generated using WMISH. During early development, *adsl* is ubiquitously expressed (Figure 12A -D). In 8-somite stage (SS) embryos, *adsl* is transcribed in the optic vesicle (ov) (arrow) (Figure 12E and F). At later stages (18 SS, Figure 12G and H), *adsl* expression still can be found in the ov and in the developing brain, to be more specific in the midbrain (mb) and hindbrain (hb). At 24 hpf, in the pharyngula period, *adsl* is expressed in the epiphysis (ep), the optic tectum (ot), the mesencephalon (me), the midbrain-hindbrain boundary (mhb) with the cerebellum (ce), the hindbrain (hb) and the otic capsule (oc). Additionally, the lens (le), the rhombencephalon (re), the somites (so) and the proctodeum (pr) also show a transcription of *adsl* (Figure 12I + J). After 48 hpf, *adsl* expression is still in neuronal tissue, like the ce, the mhb, the ot, the ep, the telencephalon (te). *Adsl* is also transcribed in the le, the retina pigmented epithelium (rpe), the so and in the pectoral fin buds (pfb) (Figure 12K + L).

Taken together, *adsl* is ubiquitously expressed in the early stages and in the later stages it mainly showed a transcription in ciliated tissues.

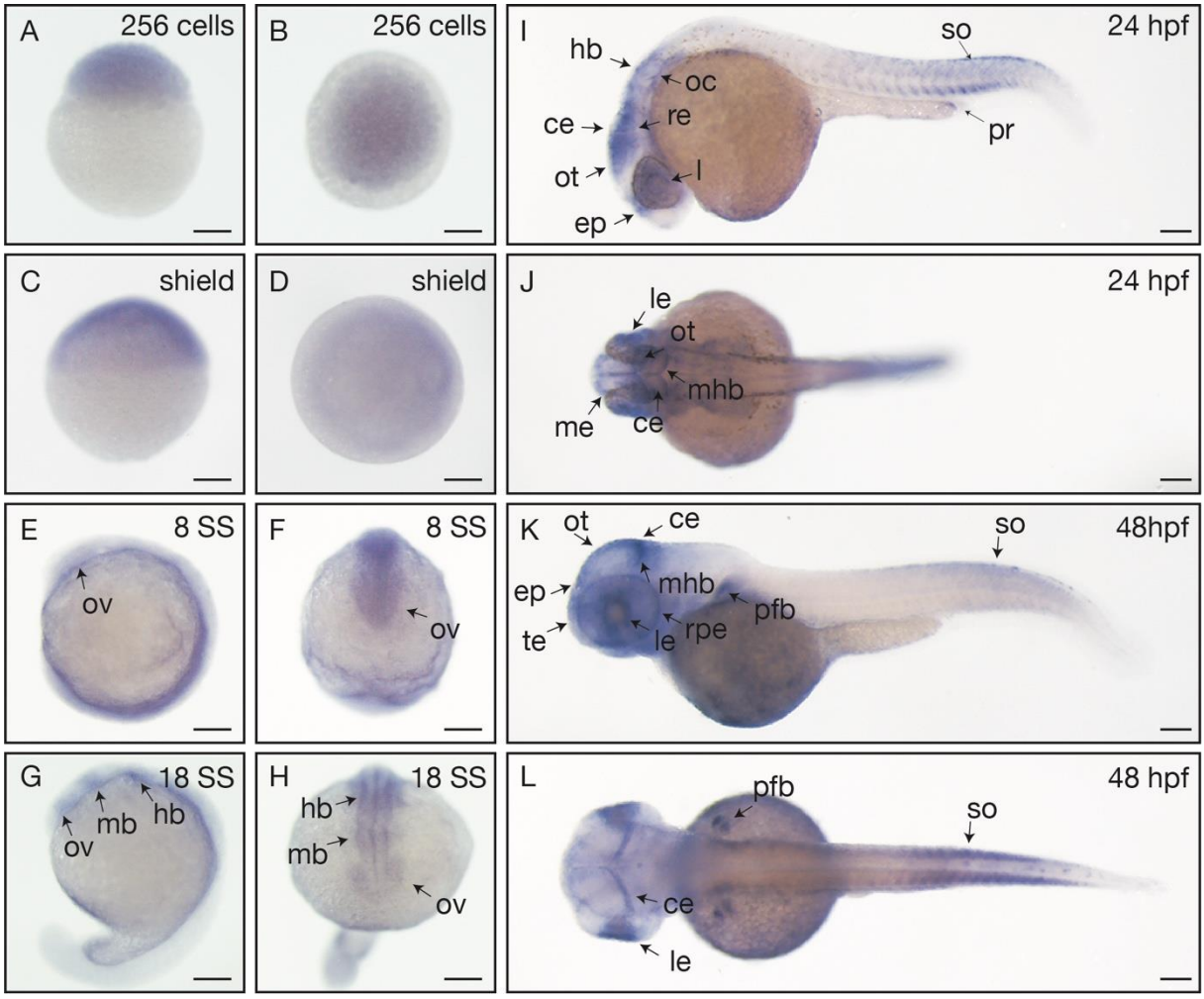

Figure 12: *Adsl* expression in the developing zebrafish embryo

Adsl mRNA was detected by WMISH. ov = optic vesicle, mb = midbrain, hb = hindbrain, ep = epiphysis, ot = optic tectum, me = mesencephalon, mhb = midbrain-hindbrain boundary, ce = cerebellum, oc = otic capsule, le = lens, re = rhombencephalon, so = somites, pr = proctodeum, te = telencephalon, rpe = retina pigmented epithelium, pfb = pectoral fin buds. All scale bars = 100 µm. A, C, E, G, I and K anterior view. B, C, F, H, J and L dorsal view. WMISH of stages 256 cells to 18 SS kindly provided by Sophia Aicher, a former lab member.

5.2 Adsl knockdown resembles ciliopathy-like phenotypes

To achieve a KD of Adsl in zebrafish I used a Adsl ATG MO (3.3, 4.1.4.1). Fertilized eggs were injected into the yolk during the first cell stage and allowed to develop until 48 hpf. As shown in Figure 13, Adsl depleted embryos displayed a cilia dysfunction resembling phenotype (89). One was clearly able to see that the embryos developed pericardiac edema (green arrow), hydrocephalus (red arrow), did have a kinked tail (yellow arrow) or had a pinhead (blue arrow). Only a small percentage of CTRL MO injected embryos or NI embryos showed any of these phenotypes (Figure 13). Around 60 % of the Adsl ATG MO

injected embryos developed pericardiac edema (Figure 13B), almost 80 % a kinked tail (Figure 13C) and pinhead (Figure 13E). Less than 20 % developed a hydrocephalus after Adsl KD (Figure 13D).

In summary, Adsl depleted embryos developed typical cilia dysfunction related phenotypes (89), such as pinheads or edema.

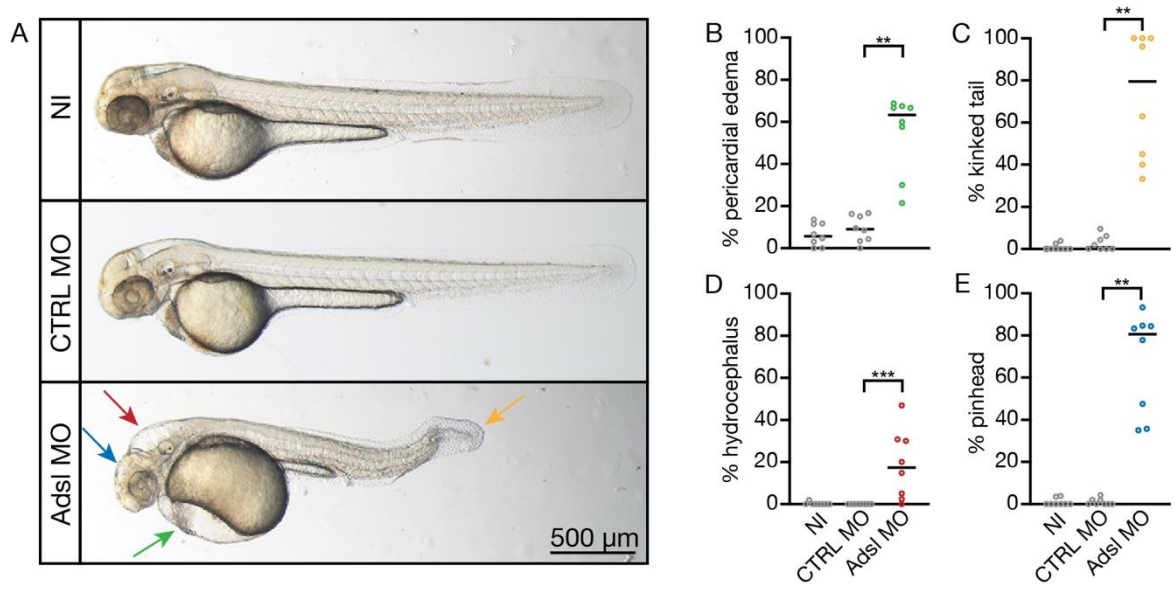

Figure 13: Adsl depleted embryos displayed ciliopathy associated phenotypes

A: Representative pictures of NI embryos, CTRL MO injected embryos and Adsl ATG MO injected embryos at 48 hpf. Red arrow = hydrocephalus, blue arrow = pinhead, green arrow = pericardiac edema, yellow arrow = kinked tail. B: Adsl depletion led to increased pericardial edema formation. C: More embryos developed a kinked tail after Adsl KD. D: Some embryos showed hydrocephalus after Adsl MO injection. E: Pinhead formation after Adsl depletion. Lines indicate the median. N = 8 experiments with NI embryos = 311, CTRL MO = 275 and Adsl MO injected embryos = 227. Kruskal-Wallis test with Dunn's multiple comparison test. **: p = 0.0042 for B, p = 0.0032 for C and p = 0.0011 for E, ***: p = 0.0005.

5.3 Adsl depletion causes cilia dysfunction

In the next step I tested whether these observed phenotypes are truly cilia related. For this, I assessed LR asymmetry formation, which depends on functional cilia in the KV (Figure 3 and Figure 4). I analyzed the correct heart looping and the correct placement of the liver by the expression of two genes, namely *cmlc2* (*cardiac myosin light chain 2*) and *angptl3* (*angiopoietin-like 3*).

cmlc2 is expressed in the heart of zebrafish embryos, with a stronger expression in the ventricle (V) than in the atrium (A). The ventricle is normally located on left side above the atrium (Figure 14A). After injection of Adsl ATG MO, the zebrafish embryos showed a significantly higher percentage of wrongly looped hearts, meaning non-looped or inverse looped hearts, in comparison with NI or CTRL MO injected embryos (Figure 14B and C)

angptl3 is expressed in the liver of zebrafish embryos on the left side of the body axis (dorsal view) (Figure 14D). Adsl-depleted embryos also displayed LR asymmetry defects as shown for the heart looping. More than 20 % of the embryos that have been injected with the Adsl ATG MO displayed a liver on the wrong (right) side of the body. This was also significant in comparison to the two control conditions (NI and CTRL MO) (Figure 14E and F).

To verify the observed impaired LR asymmetry I also tested for other marker genes during earlier embryonic development.

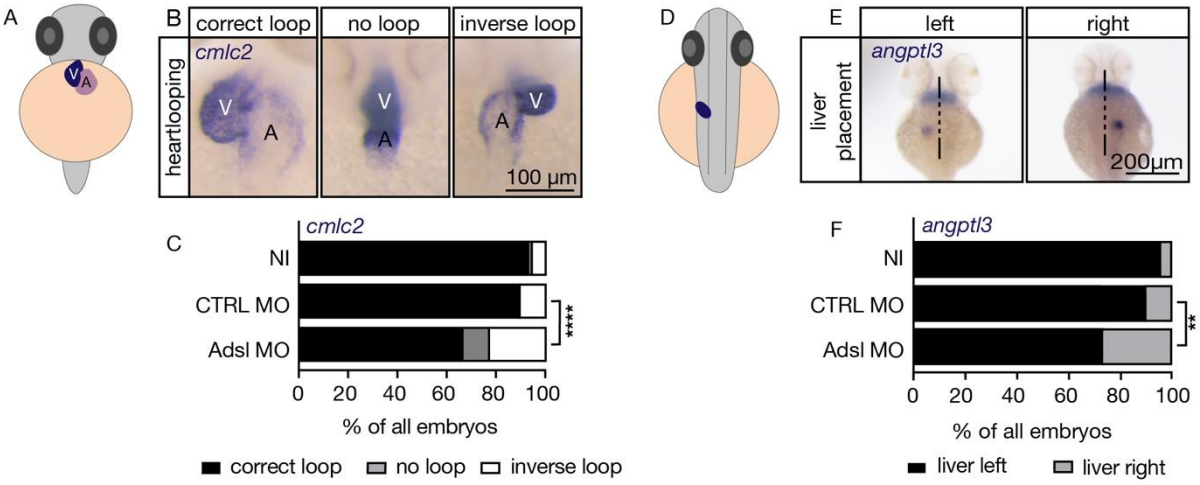

Figure 14: LR asymmetry defects after Adsl KD

A: Cartoon of proper heart looping in 48 hpf zebrafish embryos. V = ventricle, A = atrium. Ventral view. B: Representative pictures of the heart looping of zebrafish embryos after WMISH for *cmlc2*. C: Heart looping was affected after Adsl KD. N= 6 experiments with NI embryos = 266, CTRL MO = 176 and Adsl MO = 188. D: Cartoon of correct liver placement in 48 hpf zebrafish embryos. The liver is normally located on the left side of the body (dorsal view). E: Representative pictures of embryos showing the liver placement on either the left or the right side after WMISH for *angptl3*. F: Random distribution of *angptl3* after Adsl depletion. N= 3 experiments with NI embryos = 185, CTRL MO = 121 and Adsl MO = 99. Two-tailed Fisher's exact test for C and F. ****: $p < 0.0001$, **: $p = 0.0015$.

As already mentioned in Figure 4 is the KV, or to be more precisely the counterclockwise fluid flow in the KV, responsible for the initiation of the LR asymmetry. This so-called

nodal flow activates the asymmetric expression and signaling cascade of *nodal*. In zebrafish there have been identified three different *nodal*-related genes: *nodal-related 1 (ndr1) nodal-related 2 (ndr2) and southpaw (spaw)* (94). *spaw* is known to be one of the earliest markers of LR asymmetry (94–96). Therefore, I performed a WMISH for *spaw* to check the LR asymmetry development in the earliest points.

Under control conditions, meaning NI or CTRL MO injected embryos, around 90 % showed a proper *spaw* expression on the left side of the body axis (dorsal view) (Figure 15A and B). After depletion of Adsl more than 40 % displayed an altered expression of *spaw* shifted to right or both sides. Important to say is that co-injection of Adsl ATG MO with 500 ng capped RNA encoding zebrafish Adsl partially rescued the shifted expression of *spaw* in a significant manner (Figure 15C). On the one hand this is a first verification for the specificity of the Adsl MO. On the other hand, it shows that Adsl indeed is important during early embryogenesis, or to be more specific for proper LR asymmetry development. I also confirmed this early impaired LR patterning with another gene, called *lefty1*.

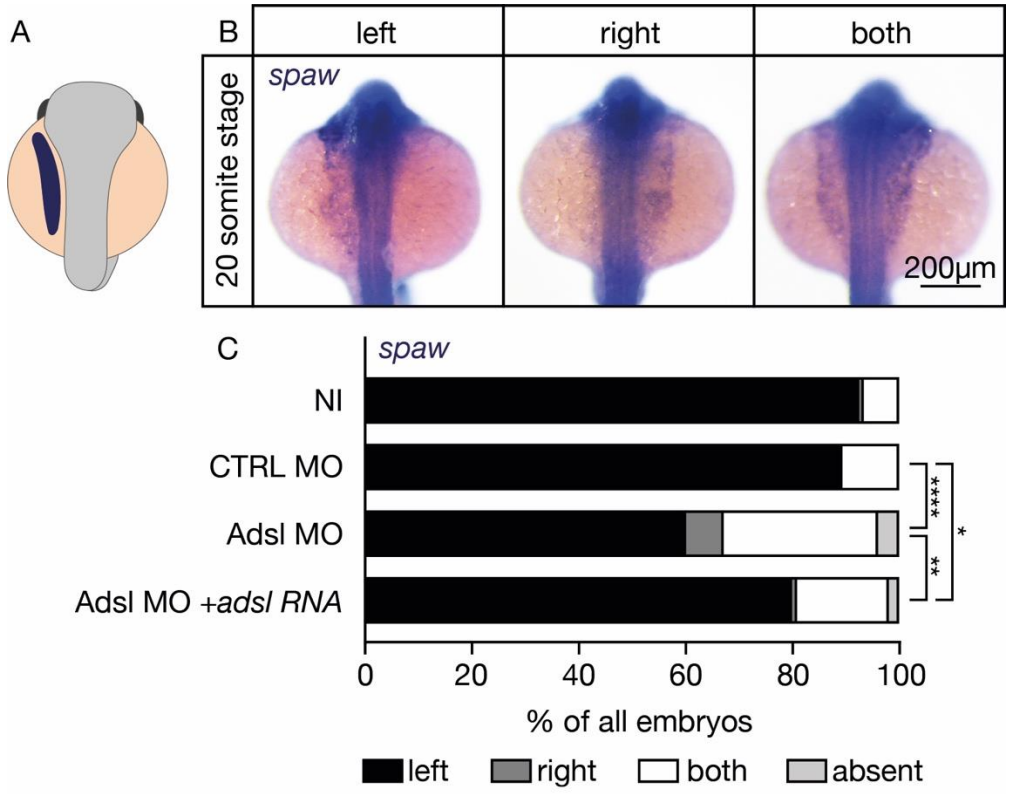

Figure 15: Altered *spaw* expression after Adsl depletion

A: Cartoon showing the correct expression of *spaw* on the left side of the body axis (dorsal view). B: Representative pictures of the expression of *spaw* after WMISH. C: Randomized *spaw* expression after Adsl KD was partially rescued with capped RNA encoding zebrafish Adsl. N = 5 experiments with NI

embryos = 121, CTRL MO = 142, Adsl ATG MO = 128 and Adsl ATG MO + *adsl* RNA = 105. Two-tailed Fisher's exact test. *: p = 0.0451, **: p = 0.0016, ****: p < 0.0001.

lefty1 is another marker gene for the *nodal* cascade, downstream of *spaw*. During 22-somite stage it is expressed in the epiphyseal region of the diencephalon on the left side of the body (95) (Figure 16A). In this experiment I only used CTRL and Adsl MO. Even though 20 % of the CTRL MO injected embryos showed an impaired expression of *lefty1*, one can clearly see that the depletion of Adsl amplified this effect. Almost 60 % of these embryos displayed a LR asymmetry defect (Figure 16C).

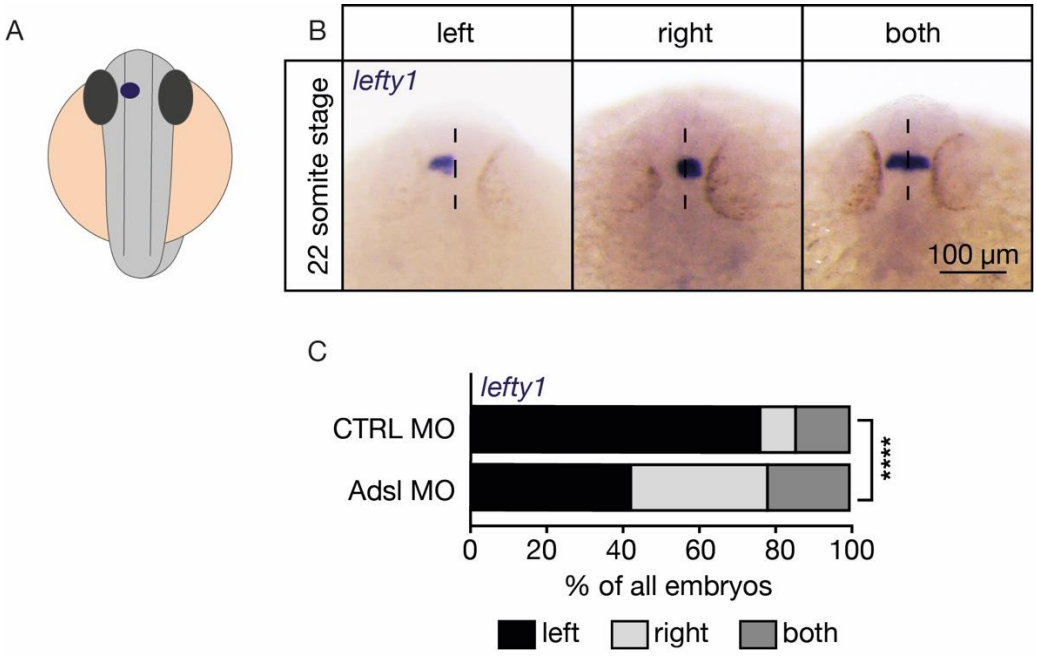

Figure 16: Altered *lefty1* expression upon Adsl KD

A: Cartoon showing the normal expression of *lefty1* in the epiphyseal region of the diencephalon. It is located on the left side of the brain (dorsal view). B: Representative pictures of *lefty1* after WMISH during the 22-somite stage. C: Randomized *lefty1* expression after Adsl depletion. N = 7 experiments with CTRL MO = 88 embryos and Adsl ATG MO = 103 embryos. Two-tailed Fisher's exact test. ****: p < 0.0001.

These experiments indicate that Adsl is important for proper embryogenesis. Already in the earliest phases of LR asymmetry development, zebrafish that had been depleted of Adsl, showed a significantly higher percentage of embryos that expressed *spaw* and *lefty1* on the wrong side of the body. Further downstream of this *nodal* cascade I found a randomized organ placement or formation, as shown by the expression of *angptl3* and *cmlc2*. These data suggest that cilia in the KV, the organ of laterality, may be malfunctional.

5.4 Adsl is required for proper cilium formation

As already mentioned in Figure 4, cilia are crucial for proper LR asymmetry development. They create a counterclockwise fluid flow in the KV, which is then sensed and translated into the *nodal* cascade that gives rise for left and right side of the body (Figure 17A). The KV is already visible during the 1-4-somite stage in zebrafish embryos. After injection of CTRL MO, Adsl ATG MO or Adsl ATG MO with capped RNA encoding zebrafish Adsl, I performed an AB staining for acetylated tubulin (red) and PKCζ (green). Acetylated tubulin stained cilia within the KV, whereas PKCζ stained for apical cell borders. With this approach I could take pictures of the stained KV using confocal microscopy (Figure 17B). Depletion of Adsl led to a reduction in cilia length from 3.3 µm (CTRL MO) to 2.4 µm. Interestingly, I was able to partially rescue the reduced cilia length by co injection of the Adsl ATG MO with capped RNA encoding zebrafish Adsl. The cilia got longer, to a level of 2.6 µm (Figure 17C). The number of cilia within the KV did not differ between the different conditions (Figure 17D). I also measured the outline of each KV and calculated the area of it. Even though it is not significant, one can see a small reduction of the KV area after Adsl depletion and a tendency that capped RNA of *adsl* increased the reduced KV size again (Figure 17E).

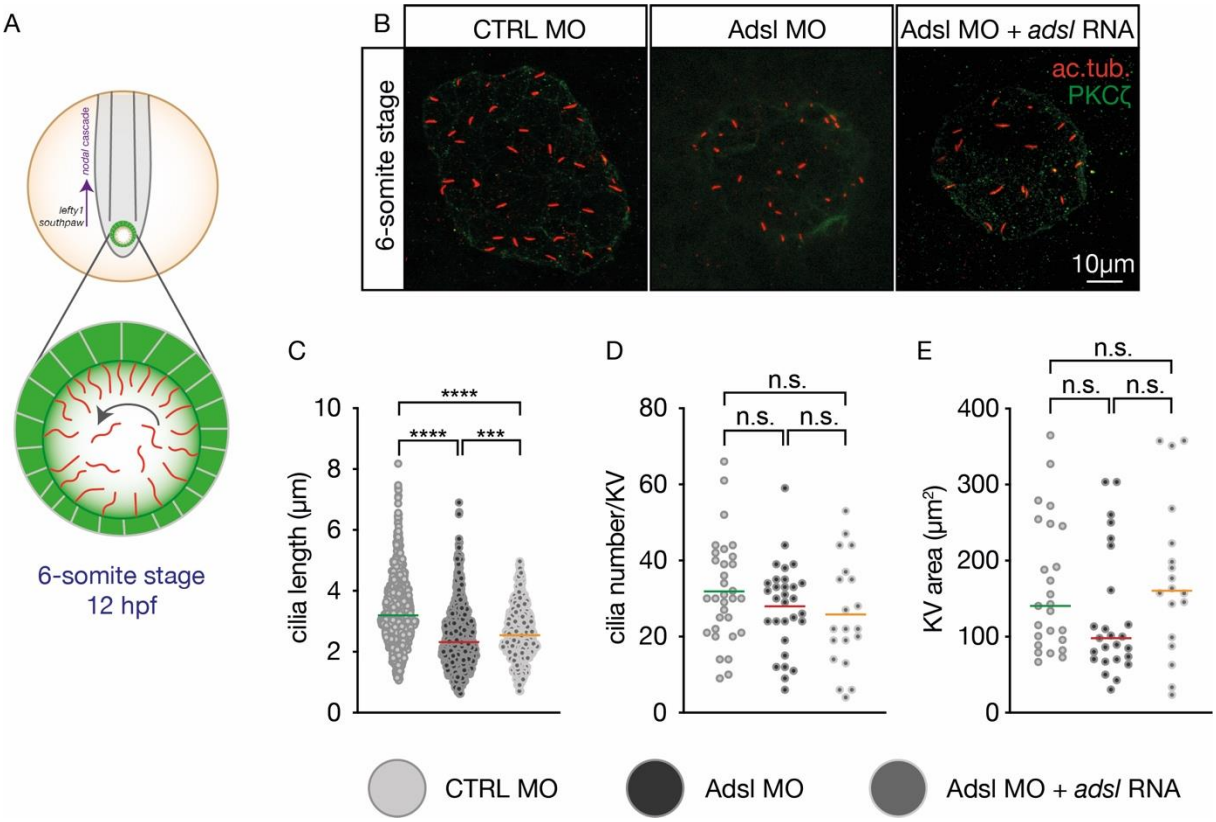

Figure 17: Cilia formation in the KV after Adsl MO injection

A: Cartoon of the KV, the organ of laterality, in the developing zebrafish (6 SS). B: Representative confocal z-stacks converted to a 2D picture of the KV at 6 SS. Acetylated tubulin (ac.tub., red) stained cilia, PKCζ (green) stained the apical cell borders. C: Cilia got significantly shorter after Adsl ATG MO injection. Co-injection of the Adsl ATG MO with capped RNA encoding zebrafish Adsl partially rescued the shortened cilia in the KV. CTRL MO = 960 cilia, Adsl ATG MO = 798 cilia, Adsl ATG MO + *adsl* RNA = 540 cilia. Kruskal-Wallis test with Dunn's correction. Horizontal line indicates median. ***: p = 0.0008, ****: p < 0.0001. D: Cilia number per KV was not affected in the different conditions. CTRL MO = 32 KVs, Adsl ATG MO = 30 KVs, Adsl ATG MO + *adsl* RNA = 20 KVs. Each circle represents the KV of one embryo. One-way ANOVA with Sidak's multiple comparison test. Lines indicate the means. p-values: CTRL MO vs. Adsl ATG MO = 0.5538, CTRL MO vs. Adsl ATG MO + *adsl* RNA = 0.2844, Adsl ATG MO vs. Adsl ATG MO + *adsl* RNA = 0.9225. E: Adsl depletion did not significantly reduce the KV area. CTRL MO = 25 KVs, Adsl ATG MO = 25 KVs, Adsl ATG MO + adsl RNA = 18 KVs. Each circle represents the KV of one embryo. Kruskal-Wallis test with Dunn's correction. Lines indicate the medians. p-values: CTRL MO vs. Asl ATG MO = 0.2582, CTRL MO vs. Adsl ATG MO + *adsl* RNA > 0.9999, Adsl ATG MO vs. Adsl ATG MO + *adsl* RNA = 0.1684.

5.5 Adsl affects neurodevelopment

With the first experiments I was able to show that Adsl is important for proper cilium formation and function. In the next experiment I performed an AB staining after injection with either CTRL or Adsl MOs of 24 hpf old embryos to check where Adsl localizes. I used an AB for acetylated tubulin, to stain the axons, and for Adsl. In panel A of Figure 18 I used CTRL MO and the Adsl ATG MO, as in the above-mentioned experiments. Under control

conditions, Adsl colocalizes with axons. Only by looking at the green channel (staining for Adsl) one can see the form of axons in the head. The merged picture confirms this colocalization of Adsl and acetylated tubulin. After injection of the Adsl ATG MO the structure of the axons did not really change, but we barley were able to see any Adsl signal. Also, the merged pictures shows that we do not have any Adsl signal that overlaps the signal of the axons. On the one hand this experiment showed that Adsl indeed colocalizes with axons in the head region of the developing embryo. On the other hand, it was a clear readout that the KD of Adsl by MO injection works.

Using an Adsl splMO instead of the ATG MO confirmed these observations. Panel B of Figure 18 shows the same result as panel A. Adsl colocalizes with axons under control conditions, but Adsl splMO injection reduced Adsl signals.

Taken together, Adsl colocalizes with axons in the head of zebrafish embryos.

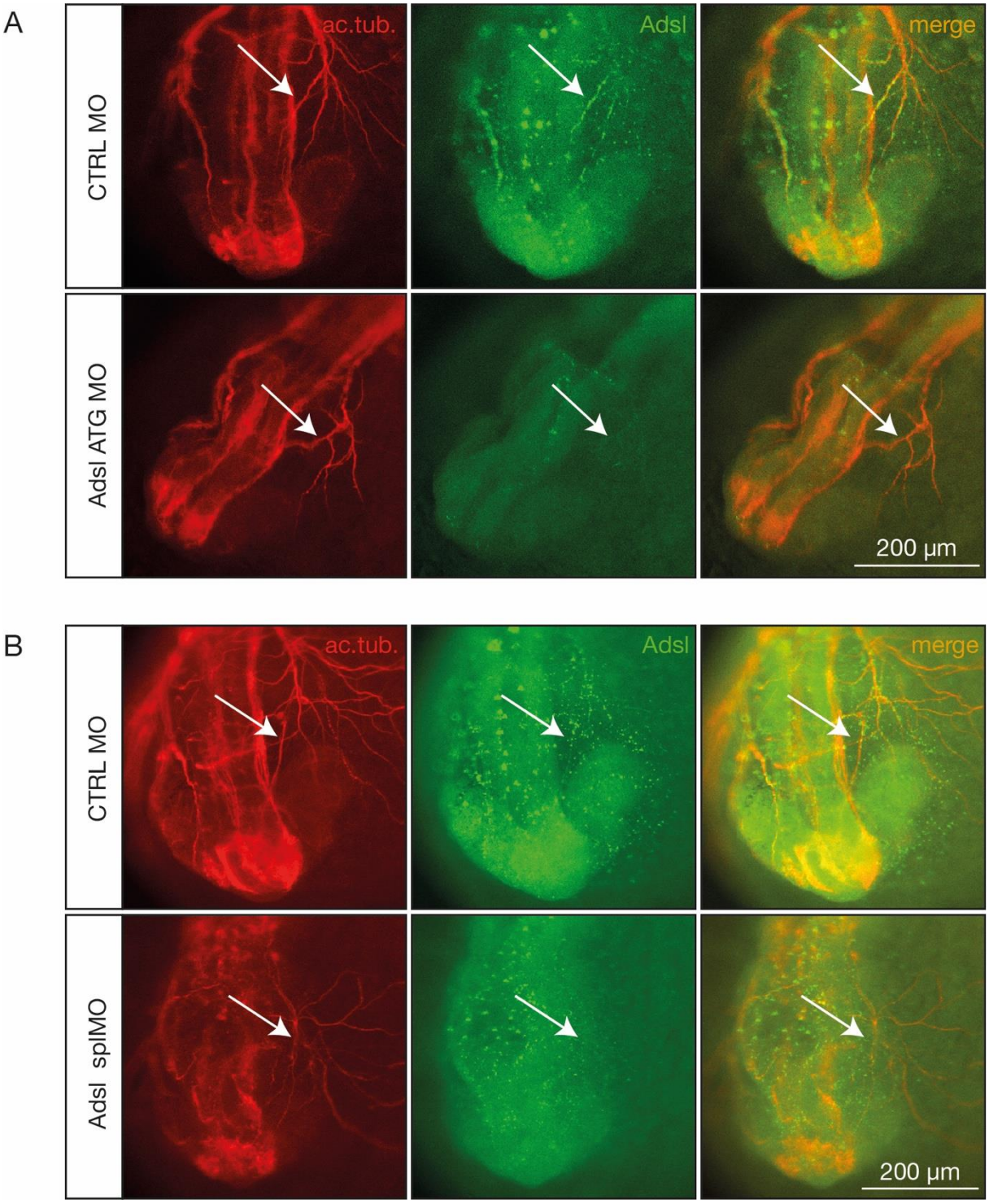

Figure 18: Adsl colocalized with axons

AB staining for acetylated tubulin (red), which stains axons, and Adsl (green). Merged pictures show a colocalization of Adsl and axons (arrow) and a reduction in the signal of Adsl after Adsl MO injections. Pictures were taken of 24 hpf old embryos in the anterior view. A: Representative pictures of CTRL MO and Adsl ATG MO injection embryos. B: Representative pictures of CTRL MO and Adsl splMO injection embryos.

Additionally, the tail region of the stained embryos showed a colocalization of Adsl with cilia of the pronephric duct (Figure 19). Adsl depletion led to a reduction of the Adsl signal in the proximal part of the developing kidney. This observation added a new hint that Adsl may be connected to cilia.

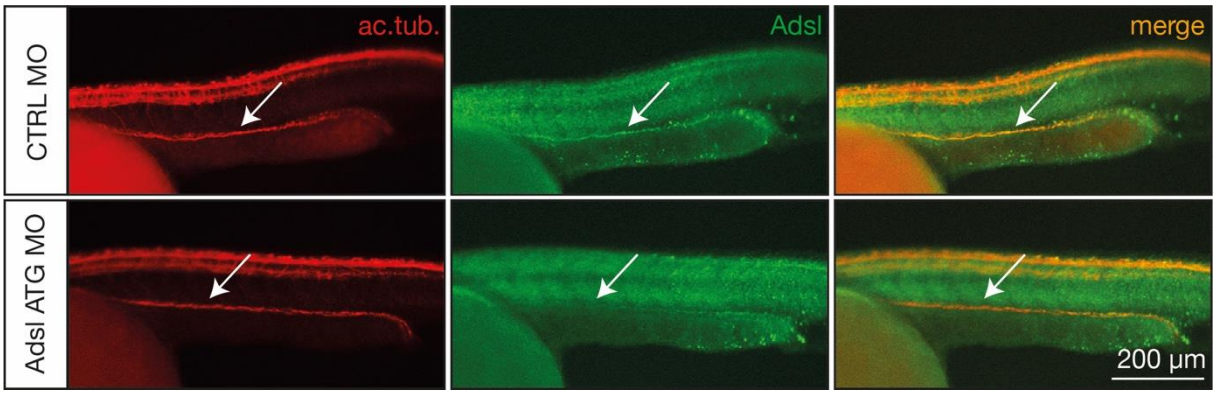

Figure 19: Adsl colocalized with cilia in the pronephric duct

AB staining of 24 hpf old embryos that had been injected with either CTRL MO or Adsl ATG MO. I stained for acetylated tubulin (red) and Adsl (green). Representative pictures showing a colocalization of Adsl with acetylated tubulin, or to be more specific with cilia, within the pronephric duct (arrow). Depletion of Adsl resulted in a weaker signal of Adsl, especially in the proximal part of the tubule.

Next, I analyzed neuronal progenitor cells in the head of zebrafish embryos after Adsl KD. In an initial experiment I made an AB staining of 24 hpf CTRL MO and Adsl ATG MO embryos, respectively. I stained for acetylated tubulin and Sox2. Sox2 is a transcription factor in neuronal stem cells. It is required for the maintenance of stem cells and reprogramming differentiated cells into stem cells (97,98). The zebrafish head is composed out of the hindbrain, midbrain and forebrain. In this study I will mainly focus on the forebrain, which can be divided in the diencephalon and telencephalon (Figure 20A and B). Under control conditions the embryos had around 35 Sox2 positive cells per forebrain. After Adsl depletion the number of neuronal progenitor cells decreased to 21 Sox2 positive cells per forebrain (Figure 20C).

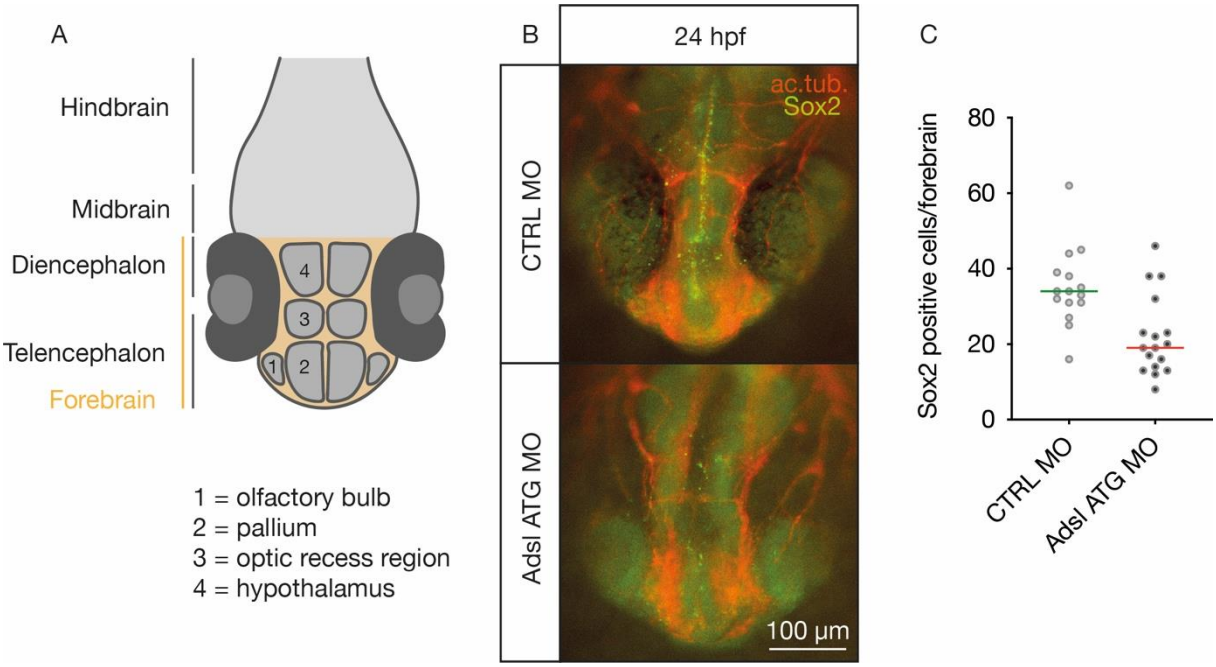

Figure 20: Adsl depletion reduced neuronal progenitor cells in the forebrain

A: Cartoon of the head of a 24 hpf old zebrafish embryo with the hindbrain, midbrain and forebrain. The forebrain can be divided into the diencephalon with the hypothalamus (4) and the telencephalon with the olfactory bulb (1), the optic recess region (2) and the pallium (3). B: Representative AB staining pictures of the head of CTRL MO and Adsl ATG MO injected embryos. Acetylated tubulin (red) stains axons, Sox2 (green) neuronal progenitor cells. C: Reduction of Sox2 positive cells per forebrain after Adsl depletion. N = 1 initial experiment with CTRL MO = 15 embryos, Adsl ATG MO = 17 embryos.

It is not known whether the effects of ADSLD arise from a lack in nucleotide production or from the accumulation of the toxic intermediates SAICAr and S-Ado (2.4). To get a better understanding of this I administered Methotrexate (MTX), which inhibits the first and second step of the THF cycle and by that the production of 10-Formyl-THF (Figure 7). 10-Formyl-THF is necessary for the following DNPS, as it is required for the reaction steps 6 and 12. As a consequence, there is no accumulation of any toxic intermediates after malfunctional Adsl, because MTX inhibits the whole pathway downstream of the THF cycle.

To test the possibility, that the lack of nucleosides may be responsible for the phenotypes observed in ADSLD, embryos were exposed to nucleosides after injection.

As already shown in the initial experiment (Figure 20), the depletion of Adsl led to a reduction in Sox2 positive cells (Figure 21B and D). Treating the embryos with 100 µM MTX did not change the number of these cells under control conditions, but partially

rescued it in morphants (Figure 21B). Interestingly, the treatment with 1x nucleosides did not affect neuronal progenitor cells (not under control conditions nor in morphants) (Figure 21C and D).

This is a first hint that the neural phenotype rather comes from the accumulation of SAICAr and S-Ado than from the lack of nucleosides.

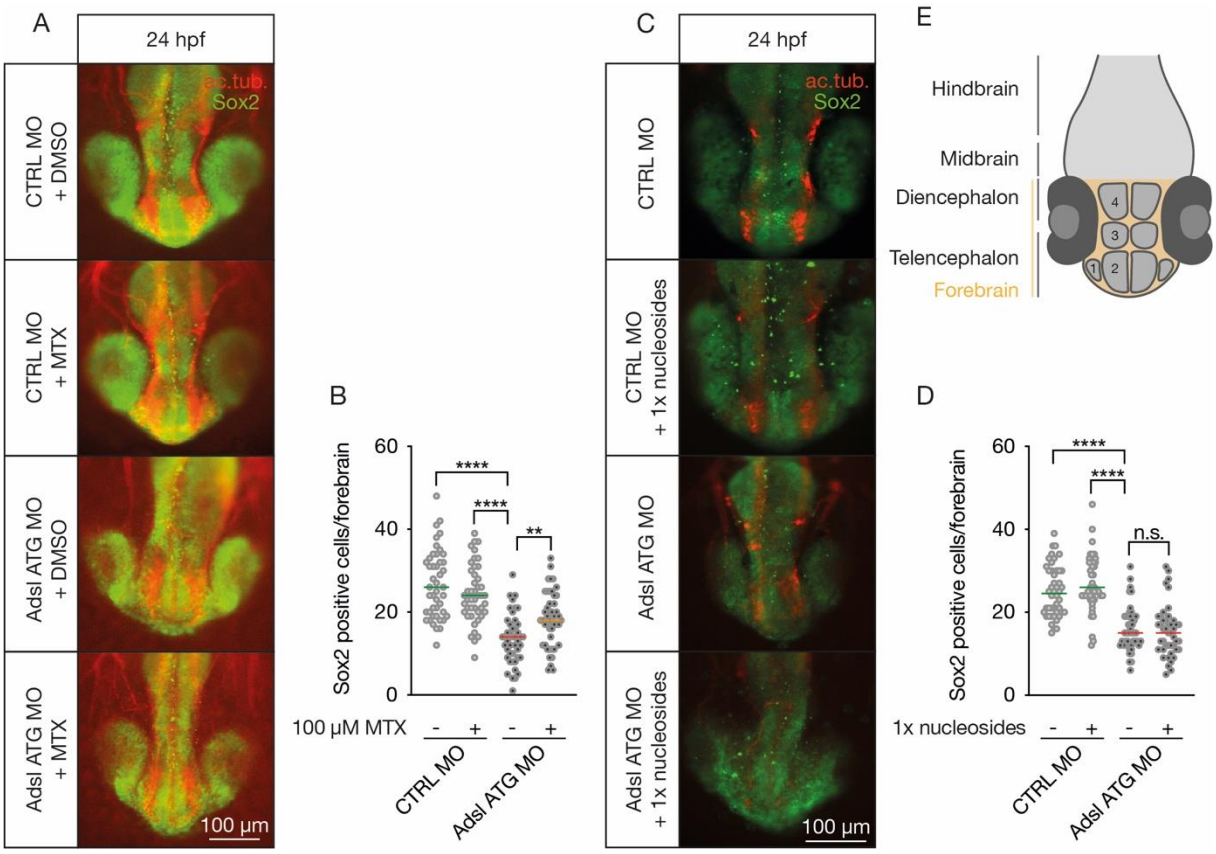

Figure 21: MTX treatment partially rescued neural progenitor reduction upon Adsl KD, while nucleoside treatment did not

A: Representative AB staining pictures of the forebrain of 24 hpf old embryos. They were either injected with CTRL MO or Adsl ATG MO. Furthermore, they were treated with 100 µM MTX or DMSO respectively. Acetylated tubulin is stained in red, Sox2 in green. B: Adsl depletion led to a reduction of Sox2 positive cells. MTX treatment did not affect CTRL MO injected embryos but partially rescued the reduced number of progenitors in Adsl morphants. N = 3 experiments with 45 embryos per condition. Each circle represents one embryo. Lines indicate medians. One-way ANOVA with Sidak's multiple comparison test. ****: $p < 0.00001$, **: $p = 0.0059$. C: Representative AB staining pictures of the forebrain of 24 hpf old embryos. They were either injected with CTRL MO or Adsl ATG MO. Furthermore, they were treated with 1x nucleosides or embryo medium. Acetylated tubulin is stained in red, Sox2 in green. D: Adsl depletion led to a reduction in Sox2 positive cells. Nucleoside treatment did not affect control conditions nor morphants. N = 3 experiments with 46 embryos (CTRL MO) or 45 embryos (every other condition). Each circle represents one embryo. Lines indicate the medians. Kruskal-Wallis test with Dunn's correction. ****: $p < 0.0001$, n.s.: $p > 0.9999$. E: Cartoon of the head of a 24 hpf old zebrafish embryo with the hindbrain, midbrain and forebrain. The forebrain can be divided into the diencephalon with the

hypothalamus (4) and the telencephalon with the olfactory bulb (1), the optic recess region (2) and the pallium (3).

Next, I analyzed the number of differentiated neurons by the marker Elavl3/4 (99). Therefore, I injected zebrafish embryos and fixed them at 24 hpf. I made an AB staining for acetylated tubulin and Elavl3/4 and counted the number of neuronal cells within the neural tube (Figure 22A and B). Depletion of Adsl significantly reduced the number of Elavl3/4 positive cells, which was rescued by co-injection of the Adsl ATG MO with RNA encoding zebrafish Adsl (Figure 22C).

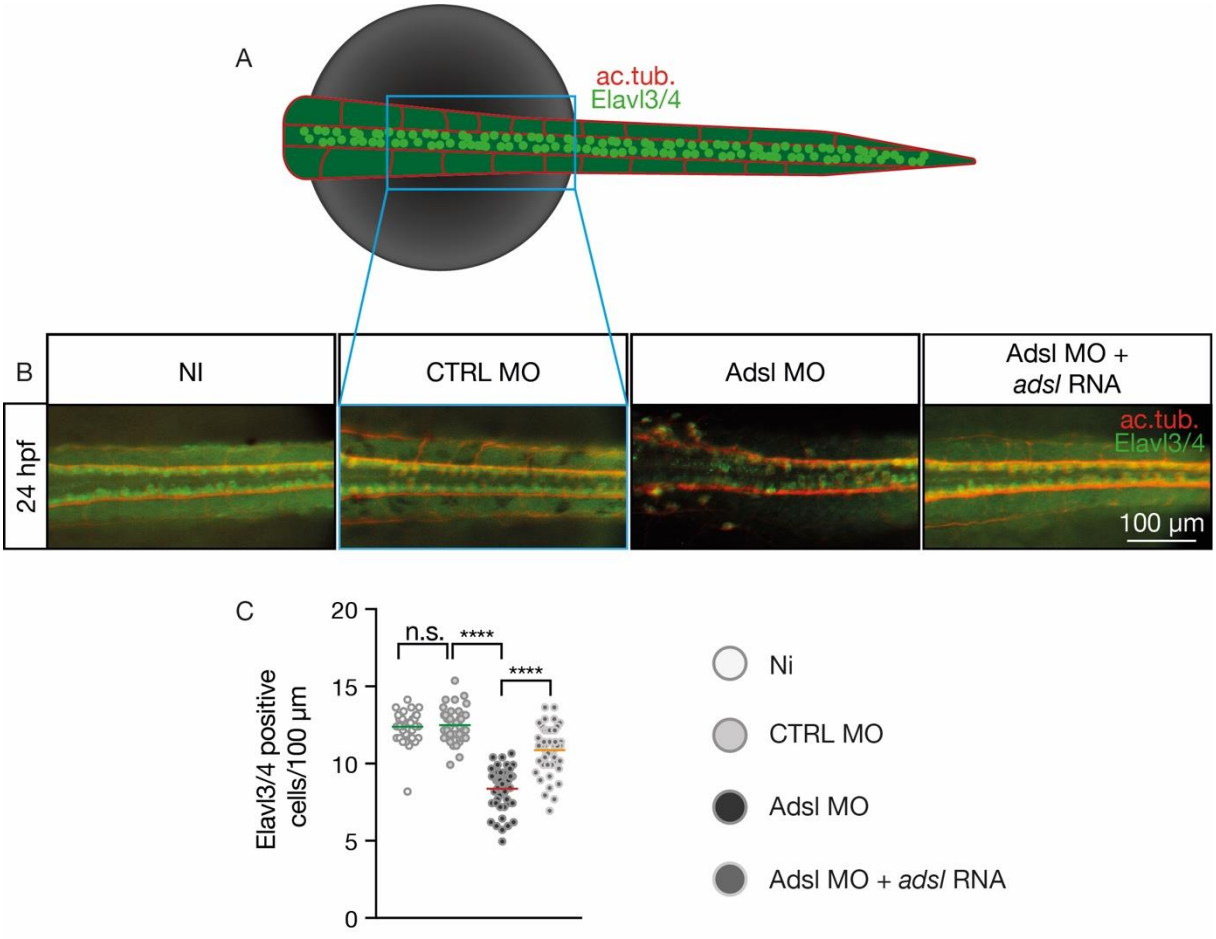

Figure 22: Adsl depletion led to a reduction of mature neurons

A: Cartoon of the AB staining of a 24 hpf old embryo. I imaged a part of the neural tube (dorsal view). Axons were stained for acetylated tubulin (red) and differentiated neuronal cells were stained for the marker Elavl3/4 (green). B: Representative pictures of NI, CTRL MO, Adsl ATG MO injected or Adsl ATG MO + *adsl* RNA injected embryos. Dorsal view of the neural tube of 24 hpf old embryos. C: Adsl depletion reduced the number of Elavl3/4 positive cells in the neural tube. Co-injection of Adsl ATG MO with RNA encoding Adsl partially rescued this phenotype. N = 3 experiments with 45 embryos per condition. Each

circle represents one embryo. Lines indicate the medians. Kruskal-Wallis test with Dunn's correction. ****: $p < 0.0001$, n.s.: $p > 0.9999$.

MTX effectively rescued the reduced number of neural progenitor cells in the forebrain of zebrafish embryos after Adsl depletion (Figure 21). Therefore, I also tried to rescue the reduced number of differentiated neurons in the neural tube. I used the two different MOs: Adsl ATG MO and Adsl splMO. CTRL MO as well as Adsl MO injected embryos were treated with 100 µM MTX, or DMSO as vehicle, from tailbud stage on until 24 hpf. After fixation and AB staining for acetylated tubulin (red) and Elavl3/4 (green), I counted the Elavl3/4 positive cells. Depletion of Adsl, by ATG and splMO, reduced the number of neurons from around 17 positive cells per 100 µm to 13Figure 23B and D). Adding MTX to the medium of the embryos (from tailbud stage on) did not affect the number of Elavl3/4 positive cells under control conditions, however it increased the number of neurons in morphants (almost to control condition levels) (Figure 23B and D).

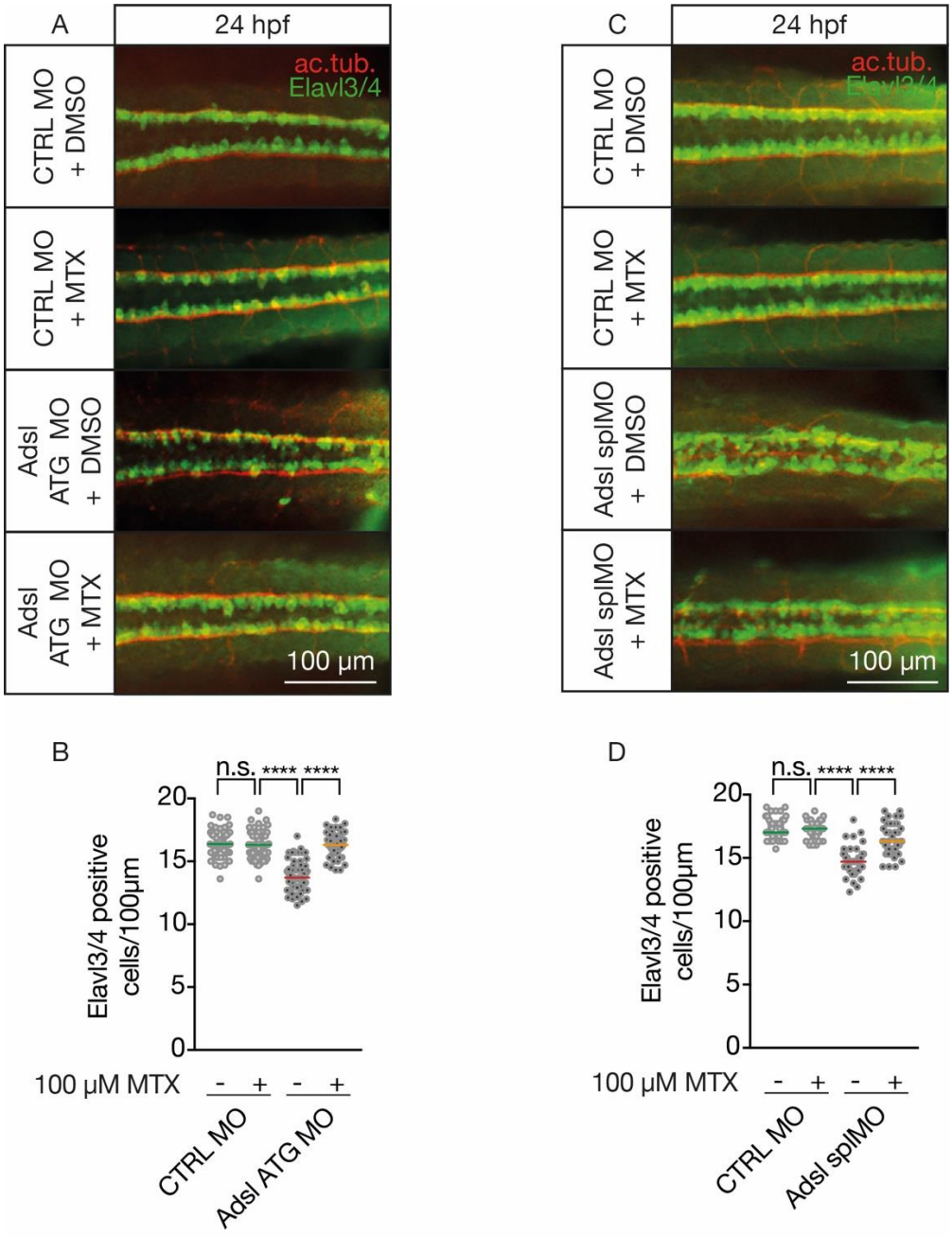

Figure 23: MTX increased Elavl3/4 positive cells in morphants

A: Representative pictures of the neural tube of CTRL MO or Adsl ATG MO injected embryos treated with 100 µM MTX or DMSO from tailbud stage on until 24 hpf. AB staining for acetylated tubulin (red) and Elavl3/4 (green). Dorsal view. B: Adsl depletion by ATG MO significantly reduced the number of differentiated neurons. Adding 100 µM MTX treatment rescued this neuronal phenotype. N = 5 experiments with CTRL MO + DMSO = 69 embryos, CTRL MO + MTX = 75, Adsl ATG MO + DMSO = 63 and Adsl ATG MO + MTX = 58. Each circle represents one embryo. Lines indicate medians. One-way ANOVA with Sidak's multiple comparison test. ****: $p < 0.0001$, n.s.: $p = 0.9740$. C: Representative pictures of the neural tube of CTRL MO or Adsl splMO injected embryos treated with 100 µM MTX or DMSO from tailbud stage on until 24 hpf. AB staining for acetylated tubulin (red) and Elavl3/4 (green). Dorsal view. D: Adsl depletion by splMO decreased the number of Elavl3/4 positive cells. MTX treatment rescued reduced number of neurons. N = 3 experiments with 45 embryos per condition. Each circle represents one embryo. Lines indicate the medians. One-way ANOVA with Sidak's multiple comparison test. ****: $p < 0.0001$, n.s.: $p = 0.9979$.

It already has been published that loss of Adsl also causes DNA damage in cells (48). DNA damage response is crucial for the maintenance of genome stability. Some examples for DNA damage responses are the repair of damaged DNA, cell cycle checkpoints or apoptosis. These responses play an important role in neurodevelopment, as defects can lead to neurological disorders like microcephaly (100). γH2AX is a marker for DNA damage and repair (101). Therefore, I performed an AB staining for γH2AX and acetylated tubulin to analyze DNA damage in the neural tube of 24 hpf embryos (Figure 24A and B). Embryos were injected with either CTRL MO or Adsl ATG MO and treated from tailbud stage on with 1x nucleosides or vehicle (embryo medium). γH2AX signals were increased after Adsl ATG MO injection. This was rescued by adding 1x nucleosides to the medium of the embryos (Figure 24C).

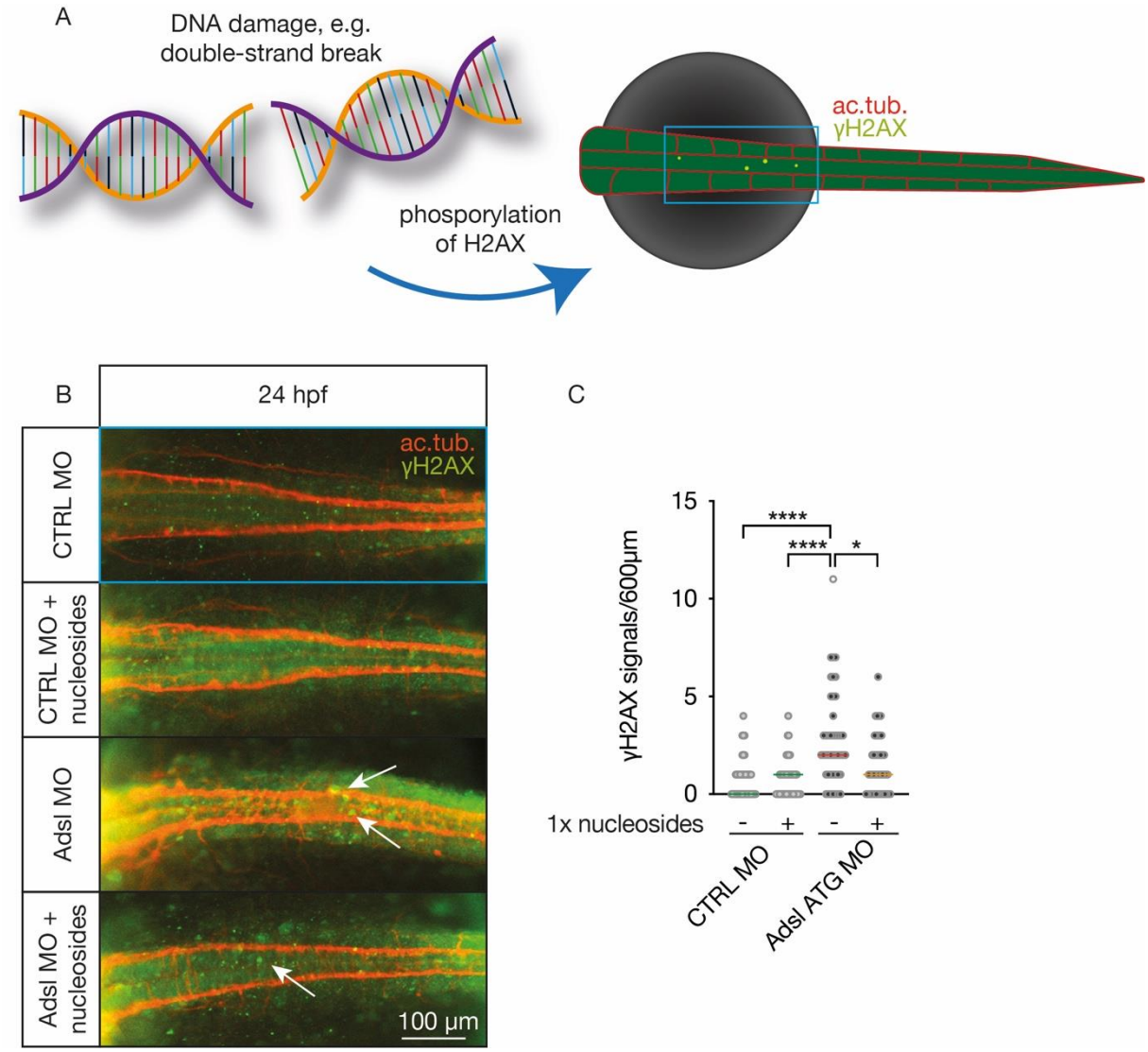

Figure 24: Adsl depletion led to enhanced DNA damage

A: Cartoon of double-strand breaks (one example for DNA damage) leading to γH2AX signals in the neural tube of 24 hpf old zebrafish embryos. Acetylated tubulin red, γH2AX green. Dorsal view. B: Representative pictures of injected embryos. Arrows indicate γH2AX positive signals. C: Adsl depletion led to increased DNA damage in the neural tube. Nucleoside treatment was able to rescue this phenotype. N = 3 experiments with 45 embryos per condition. Each circle represents one embryo. Lines indicate medians. Kruskal-Wallis test with Dunn's correction. ****: $p < 0.0001$, *: $p = 0.0273$.

5.6 Lack of nucleosides may not be responsible for cilia related phenotypes

Next I assessed how the lack of nucleosides contributes to the cilia related live phenotype of the embryos. MTX was able to rescue the number of neuronal cells, including neural progenitor and already matured and differentiated neuronal cells. Nucleoside treatment failed to do so, although nucleosides were able to rescue the enhanced DNA damage in the neural tube of Adsl depleted embryos. I injected embryos with either CTRL MO or Adsl

ATG MO and treated them from tailbud stage on with 1x nucleosides or just embryo medium as vehicle. At 48 hpf I analyzed the live phenotype of these embryos as I already did in Figure 13. Interestingly, nucleoside treatment failed to rescue any of the cilia related phenotypes after Adsl depletion (Figure 25).

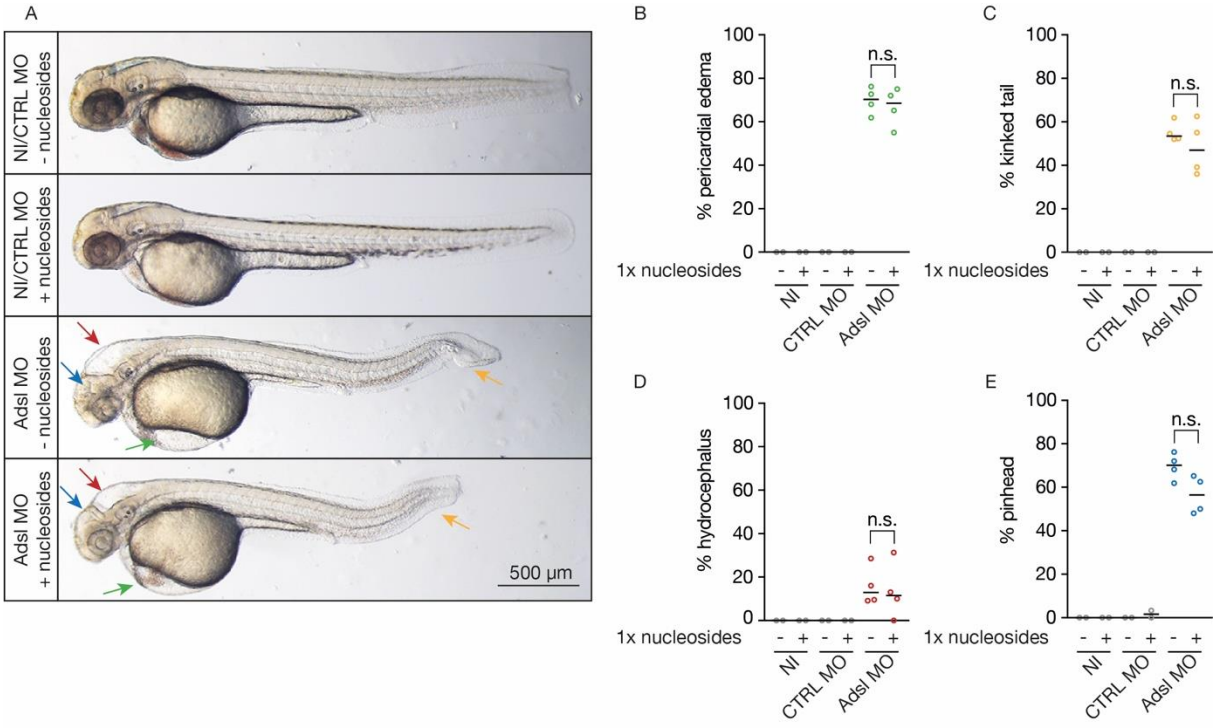

Figure 25: Nucleoside treatment did not rescue cilia related phenotypes

A: Representative live phenotype pictures of 48 hpf embryos. Cilia dysfunction phenotypes are indicated by arrows: Pericardial edema (green), kinked tail (yellow), hydrocephalus (red) and pinhead (blue). Lateral view. B-E: Nucleoside treatment failed to rescue pericardial edema formation, kinked tail, hydrocephalus or pinhead formation. Each circle represents one experiment. N = 2-4 experiments with NI = 39 embryos, NI + 1x nucleosides = 35, CTRL MO = 40, CTRL MO + 1x nucleosides = 54, Adsl ATG MO = 89 and Adsl ATG MO + 1x nucleosides = 84. Lines indicate medians. Unpaired t test with Welch's correction. n.s.: p = 0.6133 (B), 0.3579 (C), 0.7901 (D) and 0.0526 (E).

5.7 Adsl has an impact on cartilage density and formation

Microcephaly is one of the clinical symptoms of ADSLD patients. With the experiments of 5.5, I was able to show that Adsl has an impact on proper neuronal cells numbers, including neuronal progenitor cells and neuronal differentiated, matured cells. These results correlate with the phenotype of neurodevelopment retardation and microcephaly. Another readout for microcephaly is the assessment of cartilage formation during embryogenesis. For

example: One can measure the angle between Meckel's cartilage and the palatoquadrate (Figure 26A), as this one is affected in craniofacial malformations like microcephaly (102). Therefore, I injected cmlc2-GFP zebrafish embryos with CTRL MO, Adsl ATG MO or Adsl ATG MO with RNA encoding Adsl and tried to let them grow until the fifth day, as bone formation starts 4 – 5 dpf. Unfortunately, Adsl morphants were not viable and died after the fourth day. Nevertheless, the first cartilage structures are already present on the second day. After fixation at 4 dpf I performed an Alcian blue staining, that specifically stains the cartilage. NI and CTRL MO injected embryos showed normal cartilage formation which includes the clearly visible Meckel's cartilage, the palatoquadrate, the ceratohyal and the hyosymplectic. The ceratobranchial arches and the basihyal were barely visible as they are not fully formed, yet (Figure 26A and B). Upon Adsl depletion a higher percentage of embryos showed a weaker staining for the cartilage or completely absent cartilage structures. It was very hard to define any of the known cartilage structures in these morphants (Figure 26B). Co-injection of Adsl ATG MO with RNA encoding Adsl partially rescued this phenotype (Figure 26C).

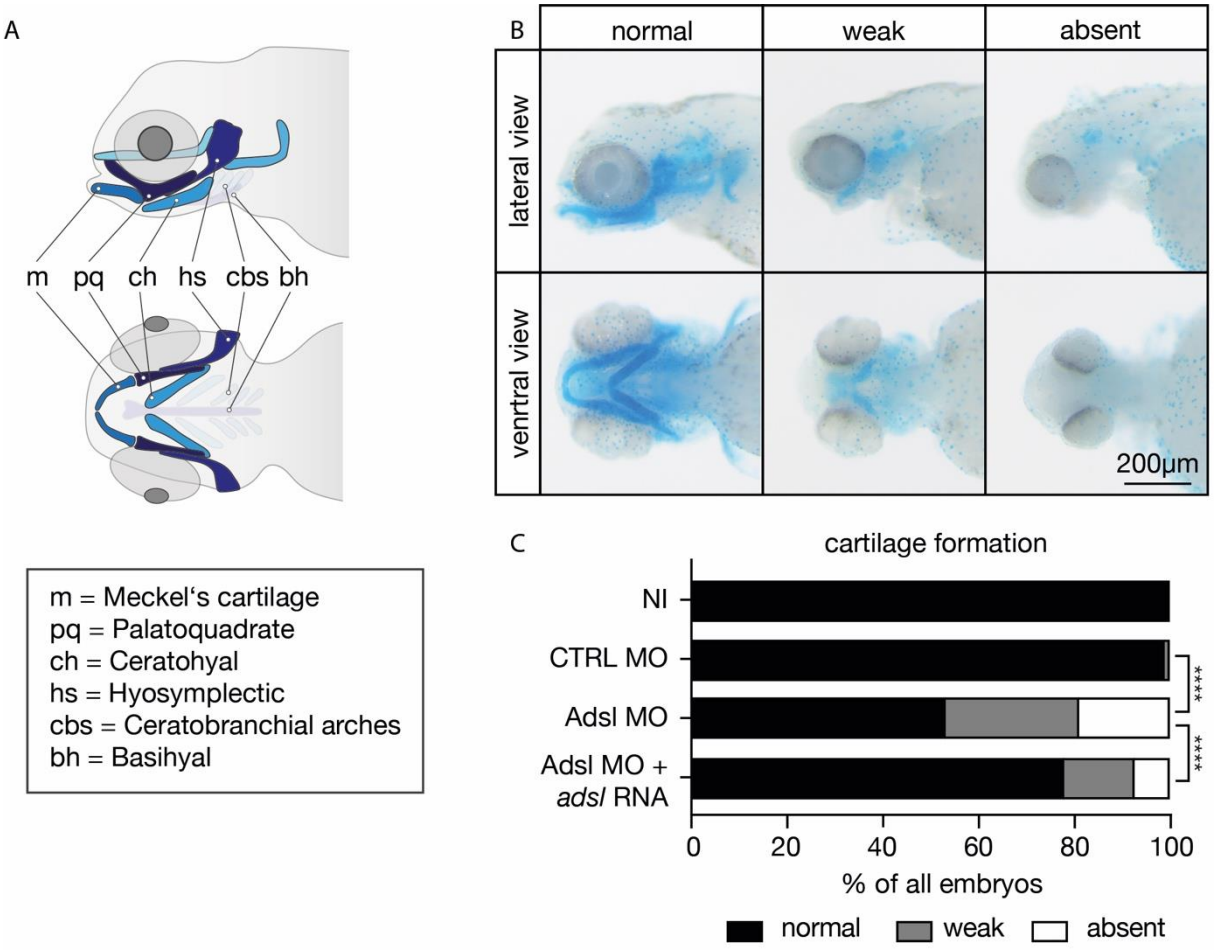

Figure 26: KD of Adsl altered cartilage formation

A: Cartoon of the cartilage structures in 4 dpf zebrafish embryos. Lateral (upper picture) and ventral (lower picture) view. Meckel's cartilage (m), palatoquadrate (pq), ceratohyal (ch) and hyosymplectic (hs) were clearly visible. The ceratobranchial arches and the basihyal were barely visible. Not all structures shown and named. B: Representative pictures of zebrafish embryos 4 dpf showing either normal cartilage formation, weaker or completely absent structures. Lateral (upper pictures) and ventral (lower pictures) views. C: Adsl depleted embryos showed defects in cartilage formation that were partially rescued with RNA encoding Adsl. N = 6 – 8 experiments with NI = 178 embryos, CTRL MO = 133, Adsl ATG MO = 169 and Adsl ATG MO + *adsl* RNA = 123. Two-tailed Fisher's exact test. ****: $p < 0.0001$.

In the next experiment I wanted to identify whether the two genetic variants of ADSL, namely *R426H* and *V429A*, are less functional than the *WT* version, as both of them are associated with ADSLD (103,104). cmlc2-GFP zebrafish embryos were injected with CTRL MO or Adsl MO. Additionally, they were also co-injected with *ADSL WT* RNA and the two genetic variants *R426H* and *V429A*. 4 dpf their cartilage formation was analyzed. Almost 50 % of all the embryos which were injected with the Adsl ATG MO had malformations in the cartilage, meaning a weaker cartilage density or the complete absence of cartilage. Co-injection with human *WT ADSL* significantly rescued this phenotype.

Interestingly, none of the two genetic variants was able to rescue the cartilage formation defects (Figure 27).

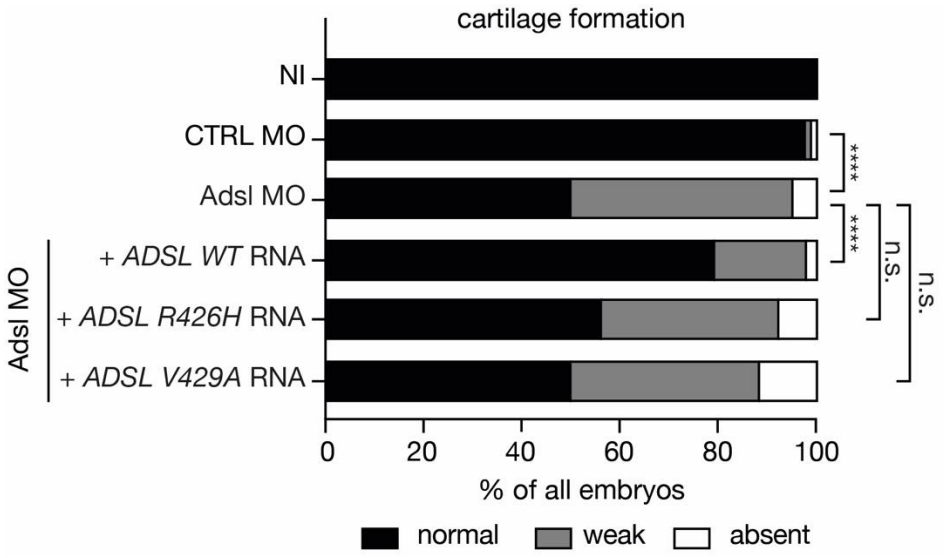

Figure 27: Genetic variants of *ADSL* failed to rescue cartilage defects

Human *WT ADSL* was able to rescue reduced cartilage formation, while both genetic variants, *R426H* and *V429A*, failed so. N = 4 experiments with NI = 116 embryos, CTRL MO = 81, Adsl ATG MO = 80, Adsl ATG MO + *ADSL WT RNA* = 91, Adsl ATG MO + *ADSL R426H RNA* = 89 and Adsl ATG MO + *ADSL V429A RNA* = 68. Two-tailed Fisher's exact test. ****: $p < 0.0001$, n.s.: $p = 0.4436$ for Adsl ATG MO vs. Adsl ATG MO + *ADSL R426H RNA* and n.s.: $p > 0.9999$ for Adsl ATG MO vs. Adsl ATG MO + *ADSL V429A RNA*.

I also wanted to test whether the genetic variants themselves have an impact on proper cartilage formation. Therefore, I repeated this experiment, but instead of a co-injection of Adsl ATG MO with the genetic variants, I injected them without MO. Again, Adsl depletion led to defects in cartilage formation. In this experiment the effects were even stronger than in Figure 27, as I used a fishline with another genetic background. Human *WT ADSL* was able to rescue this phenotype. Injections of the genetic variants, without MO, did not affect cartilage formation at all (Figure 28).

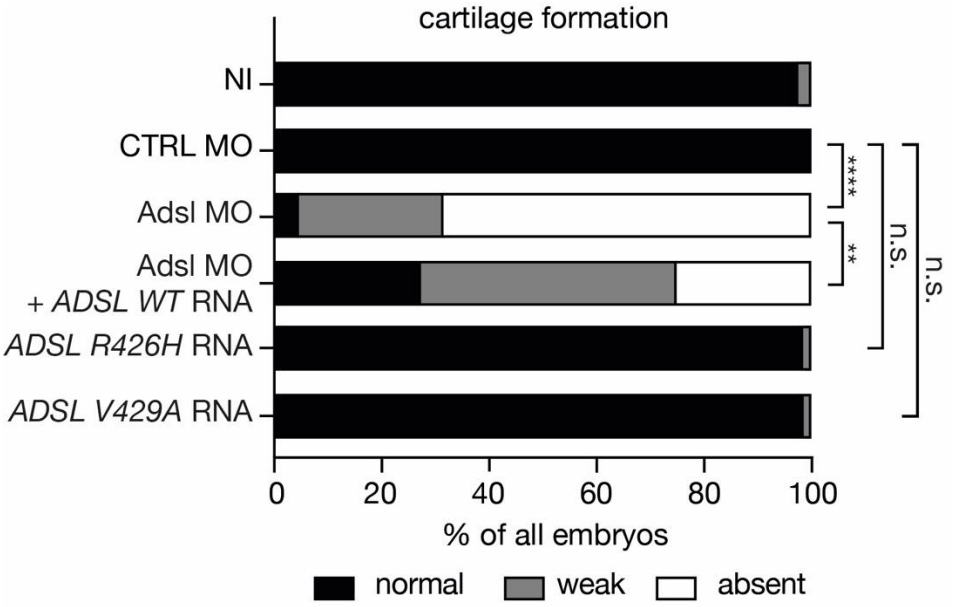

Figure 28: Genetic variants of *ADSL* did not affect cartilage formation on their own

Depletion of Adsl led to a reduction of cartilage formation in 4 dpf old zebrafish embryos. Human WT ADSL RNA, co-injected with the Adsl ATG MO, was able to partially rescue this phenotype. Injections of the genetic variants themselves, did not affect cartilage formation at all. N = 2 experiments with NI = 85 embryos, CTRL MO = 58, Adsl ATG MO = 41, Adsl ATG MO + *ADSL WT* RNA = 40, *ADSL R426H* RNA = 69 and *ADSL V429A* RNA = 74. Two-tailed Fisher's exact test. ****: $p < 0.0001$, **: $p = 0.0066$, n.s.: $p > 0.9999$ for both genetic variants.

Taken together these results show the effect of Adsl depletion on cartilage formation and by that on bone formation. RNA encoding zebrafish or human WT ADSL was able to rescue the cartilage defects observed in Adsl KD. The two genetic variants, associated with microcephaly and ADSLD, were not able to rescue the phenotype. Injection of these variants without MO did not affect cartilage formation at all.

In summary, we found that Adsl is required for proper zebrafish development. Depletion of Adsl led to cilia-related phenotypes, LR asymmetry defects and shorter cilia within the KV. Additionally, zebrafish embryos depleted of Adsl showed less neuronal progenitor and differentiated cells in the forebrain and in the neural tube, which we were able to rescue with MTX but not with nucleosides. Nucleoside treatment rescued the enhanced DNA damage after Adsl MO injection. Furthermore, we analyzed two genetic variants of ADSL, which are associated with ADSLD and found that they are less functional compared to the

WT version of ADSL. Last but not least, we also saw that Adsl depletion led to impaired cartilage formation.

5.8 Expression of *grk4* during zebrafish development

Previous experiments of our lab, made by Dr. Lars D. Maerz, already showed that Grk4 is expressed in ciliated organs like the brain or the eye (yellow arrow) and most interestingly in the developing kidney of zebrafish embryos (black arrow) (Figure 29).

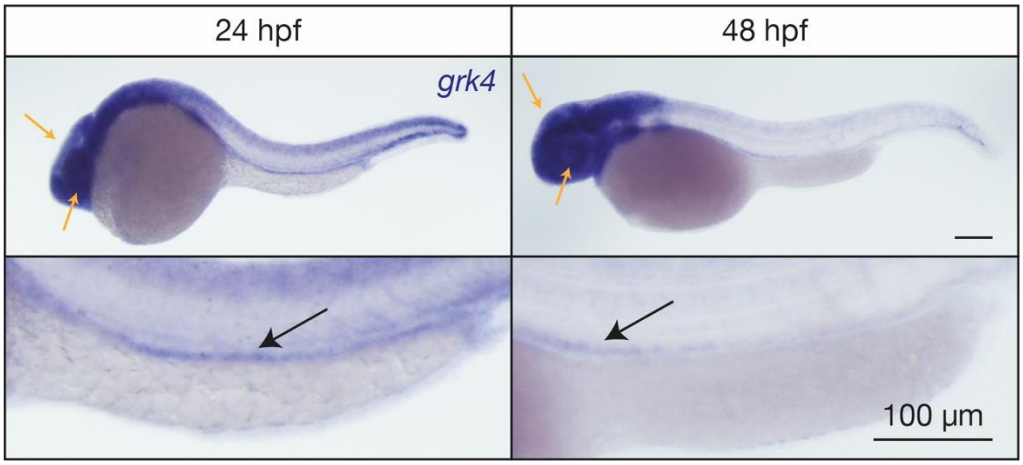

Figure 29: Expression pattern of *grk4* during zebrafish development

WMISH showing expression of *grk4* at 24 hpf and 48 hpf in zebrafish embryos. Grk4 can be found in ciliated organs like the head and eye (yellow arrows) or the pronephric duct (black arrow): Lower panels show the pronephric duct in a higher magnification. Lateral views. WMISH and pictures made by Dr. Lars D. Maerz.

5.9 Grk4 KD resembles cilia associated phenotypes

I performed MO injections into the yolk of 1-cell stadium embryos to achieve a KD of Grk4. In Figure 30 we can see the analysis of the live phenotype after 48 hpf. NI and CTRL MO injected embryos did not develop any phenotypes, whereas Grk4 ATG MO injected embryos showed a significantly higher number of embryos with edema formation (hydrocephalus was very prominent), a curled tail and otolith defects. The size of the head and eyes was not affected after Grk4 KD. I also performed rescue experiments. For this I co-injected the Grk4 ATG MO with RNA of all four different splice variants of human *GRK4*. Interestingly, all of them were able (or showed a tendency) to partially rescue edema

formation, the curled tail and otolith defects (Figure 30). This shows that all human splice variants of GRK4 are functional and that GRK4 is conserved between humans and zebrafish.

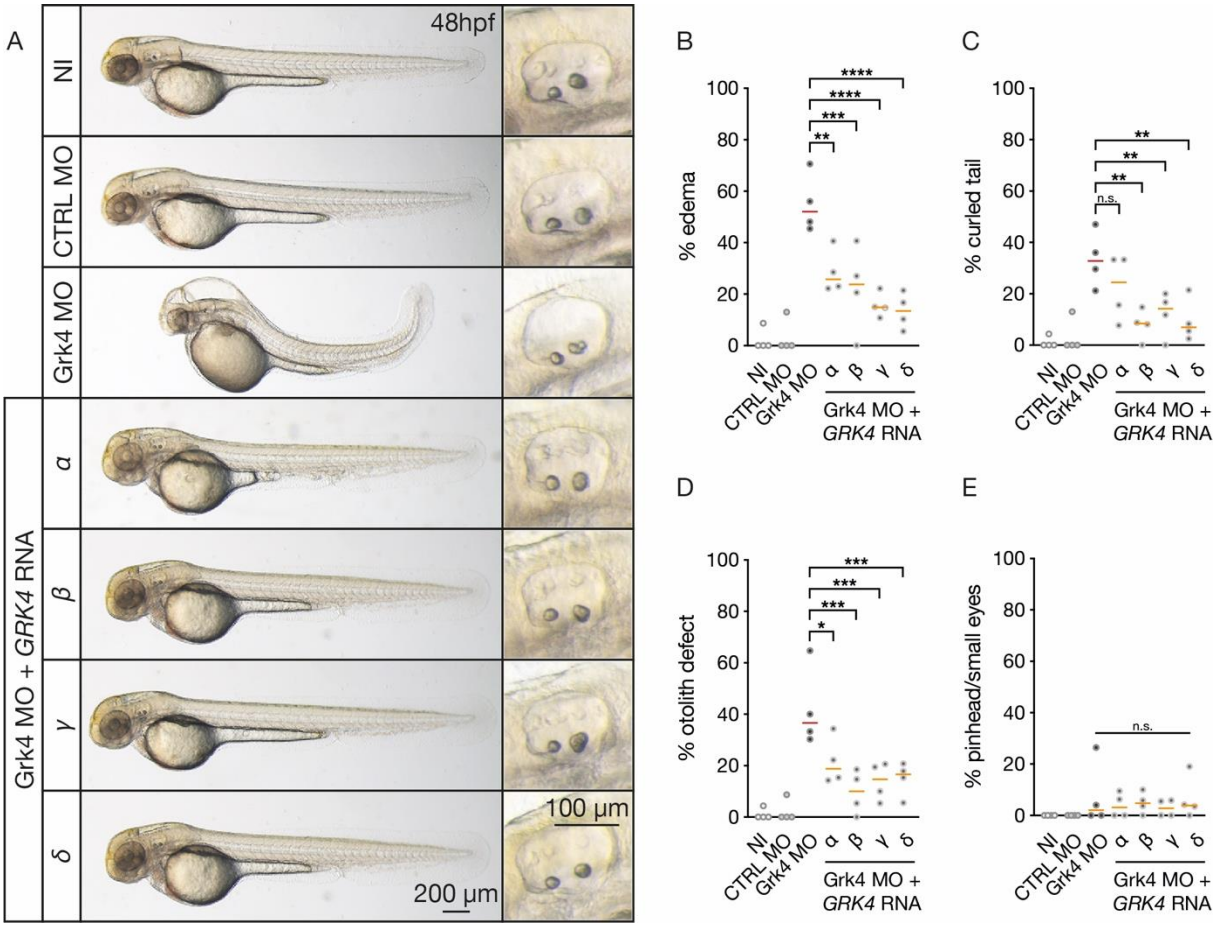

Figure 30: Live phenotype analysis after Grk4 MO injection

A: Representative pictures of embryos at 48 hpf. Higher magnification shows otoliths in the otic placode. B: Grk4 depletion led to edema formation. All splice variants partially rescued this phenotype.**: p = 0.0028, ***: p = 0.0003, ****: p < 0.0001. C: A higher percentage of Grk4 depleted embryos showed a curled tail after injection. n.s.: p = 0.0848, **: p = 0.0016, 0.0041 and 0.0022. D: Grk4 ATG MO led to increased otolith defects. All GRK4 isoforms were able to partially rescue this. *: p = 0.0119, ***: p = 0.0001, 0.0006 and 0.0009. E: Grk4 morphants did not develop a significantly higher percentage of pinheads and smaller eyes. n.s.: p = 0.8083, 0.8083, 0.7633 and 0.8400. For B – E: Each circle represents one experiment. N = 4 experiments with N = 121 embryos, CTRL MO = 118, Grk4 ATG MO = 119, Grk4 ATG MO + *GRK4* α RNA =75, Grk4 ATG MO + *GRK4* β RNA = 118, Grk4 ATG MO + *GRK4* γ RNA = 127, Grk4 ATG MO + *GRK4* δ RNA = 109. Lines indicate medians. One-way ANOVA with Sidak's multiple comparison test.

Next, I analyzed whether all four isoforms of GRK4 are expressed in zebrafish embryos after injection. Therefore, I injected fertilized zebrafish eggs with RNA encoding for Flag-tagged isoforms. At 24 hpf I fixed the injected embryos with 4 % PFA and made an AB staining for acetylated tubulin and Flag. All four isoforms of human GRK4 were expressed in zebrafish

embryos. Interestingly, GRK4 and acetylated tubulin show an overlay in the pronephros, suggesting that GRK4 and cilia colocalize. An AB staining without first ABs served as control (Figure 31).

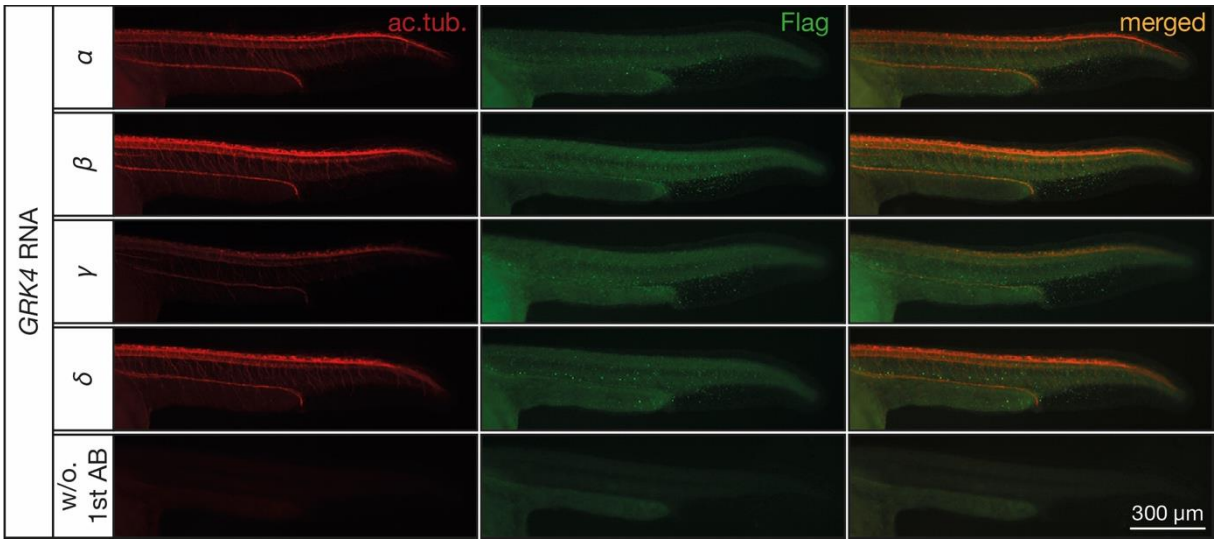

Figure 31: All isoforms of GRK4 were expressed upon injection

An AB staining for acetylated tubulin (red) and Flag (green) shows that all isoforms of GRK4 were expressed upon injection.

5.10 Depletion of Grk4 affects kidney morphology

We concluded that the edema formation in the morphants comes most likely from a defect in the kidney. The expression and colocalization of Grk4 with cilia in the pronephric duct (Figure 29 and Figure 31), together with the already known function of Grk4 in the kidney, strengthen the hypothesis. Therefore, I analyzed the developing kidney of zebrafish embryos using a transgenic fishline, called wt1b-GFP (86). *wt1b* (*Wilms tumor suppressor protein 1b*) is expressed in the glomerulus (G), the neck (N) and the proximal convoluted tubule (PCT) (Figure 32A and B). I injected this transgenic fishline with either CTRL MO or Grk4 ATG MO. Additionally, I co-injected the four different isoforms of GRK4 with the Grk4 ATG MO. Upon depletion of Grk4, almost 50 % of the embryos developed large cyst in their glomeruli (Figure 32B and C). Co-injection with the splice variants of GRK4 significantly rescued cyst formation.

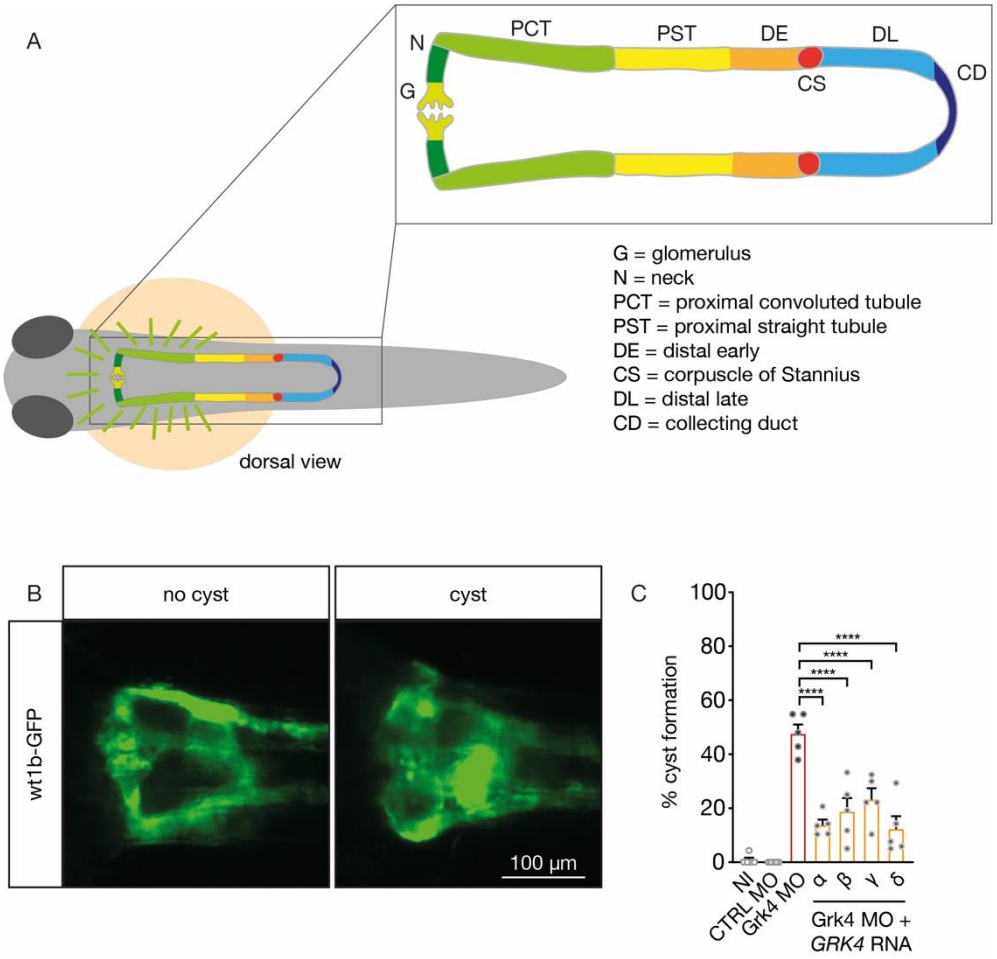

Figure 32: Grk4 depletion led to formation of cysts in the glomeruli

A: Cartoon of a 48 hpf old embryo, showing the developing kidney. The glomerulus (G), the neck (N) and proximal convoluted tubule (PCT) shine green in wt1b-GFP embryos. After the PCT the pronephros can be divided in the proximal straight tubule (PST), the distal early (DE), the corpuscle of Stannius (CS) and the distal late (DL) with the collecting duct (CD). Adapted with permission from Chambers et al. (90). B: Representative pictures of a normal formed glomerulus (no cyst) and a cystic one at 48 hpf in wt1b-GFP embryos. Dorsal view. C: Grk4 depletion led to the formation of large cysts. Co-injection of RNA encoding GRK4 partially rescued cyst formation. Each circle represents one experiment. N = 5 experiments with NI = 149 embryos, CTRL MO = 145, Grk4 ATG MO = 144, Grk4 ATG MO + *GRK4* α RNA =128, Grk4 ATG MO + *GRK4* β RNA = 144, Grk4 ATG MO + *GRK4* γ RNA = 158, Grk4 ATG MO + *GRK4* δ RNA = 138. Mean with SEM. One-way ANOVA with Sidak's multiple comparison test. ****: $p < 0.0001$.

As Glomerulus cysts are often due to cilia defects (1,28), we were interested in pronephric cilia. This next initial experiment was made by Dr. Lars D. Maerz. He injected zebrafish embryos with either CTRL MO, Grk4 ATG MO or Grk4 ATG MO + *grk4* RNA. Depletion of Grk4 led to two very prominent phenotypes in the developing kidney: A dilatation of the proximal part of the pronephros and cilia elongation. CTRL MO injected embryos had a pronephros diameter of 2.3 µm, whereas Grk4 depleted embryos had a diameter of 5 µm. Interestingly, co-injection of Grk4 ATG MO with RNA encoding Grk4 partially rescued

this dilatation. They had a diameter of 3.1 µm (Figure 33B and C).. As cilia in the proximal part of the kidney were very dense, we were not able to measure their length in this region. Therefore, we measured cilia length in the distal part of the kidney. NI and CTRL MO injected embryos had an average cilia length of 3.3 µm. Upon Grk4 depletion cilia got almost 25 % longer (4.1 µm) (Figure 33D).

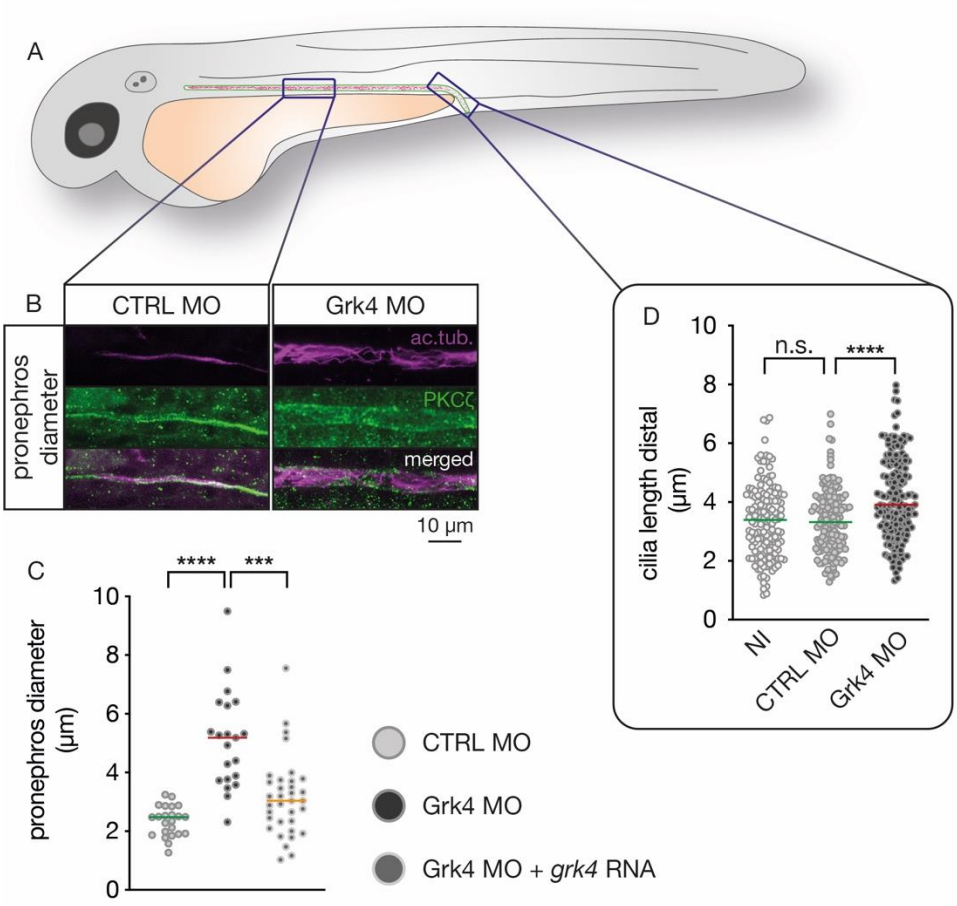

Figure 33: Disturbed kidney morphology upon Grk4 depletion

A: Cartoon of a 48 hpf old zebrafish. After AB staining for acetylated tubulin (magenta) and PKCζ (green), we imaged the proximal part (left side) and the distal part (right side) of the developing kidney. The proximal part was used to assess the pronephros diameter. The distal part was used to measure cilia length. B: Representative pictures of the pronephros after CTRL MO or Grk4 ATG MO injection. C: Grk4 depletion led to a dilatation of the pronephric duct, which was rescued by injection of RNA encoding zebrafish Grk4. Each circle represents one embryo. CTRL MO embryos = 23, Grk4 ATG MO = 21, Grk4 ATG MO + *grk4* RNA = 34. Lines indicate medians. Kruskal-Wallis test with Dunn's correction. ****: $p < 0.0001$, ***: $p = 0.0003$. D: Depletion of Grk4 led to cilia elongation. Each circle represents one cilium. NI = 147 cilia, CTRL MO = 151 and Grk4 ATG MO = 179. Lines indicate medians. Kruskal-Wallis test with Dunn's correction. n.s.: $p > 0.9999$, ****: $p < 0.0001$.

5.11 Grk4 mutants mimic MO-mediated Grk4 KD

For the next experiment I used the mutant line called Grk4 1.2. Prof. Melanie Philipp successfully edited the genome of zebrafish by CRISPR/Cas9. I used these mutant fish for phenotype analysis. We did not see any differences in the live phenotype (48 hpf) between WT, heterozygous or homozygous embryos (data not shown). Therefore, we analyzed the developing kidney. For this purpose, I performed an AB staining for PKCζ and acetylated tubulin to stain cilia in the zebrafish kidney. Then I cut each embryo in two halves (Figure 34B). The head was used for a genotyping PCR (Figure 34C) and the tail was used for imaging the cilia and the pronephric duct (Figure 34D - F). Interestingly, we were able to detect the same phenotype as in Grk4 MO injected embryos. We saw a dilatation of the pronephric tubule in homozygous *grk4* mutants, compared to WT embryos. Moreover, cilia in the developing kidney of these mutants got also longer (again compared to WT fish). This led us to the suggesting that Grk4 1.2 mutants mimic, in some cases, the depletion of Grk4 by MO injection.

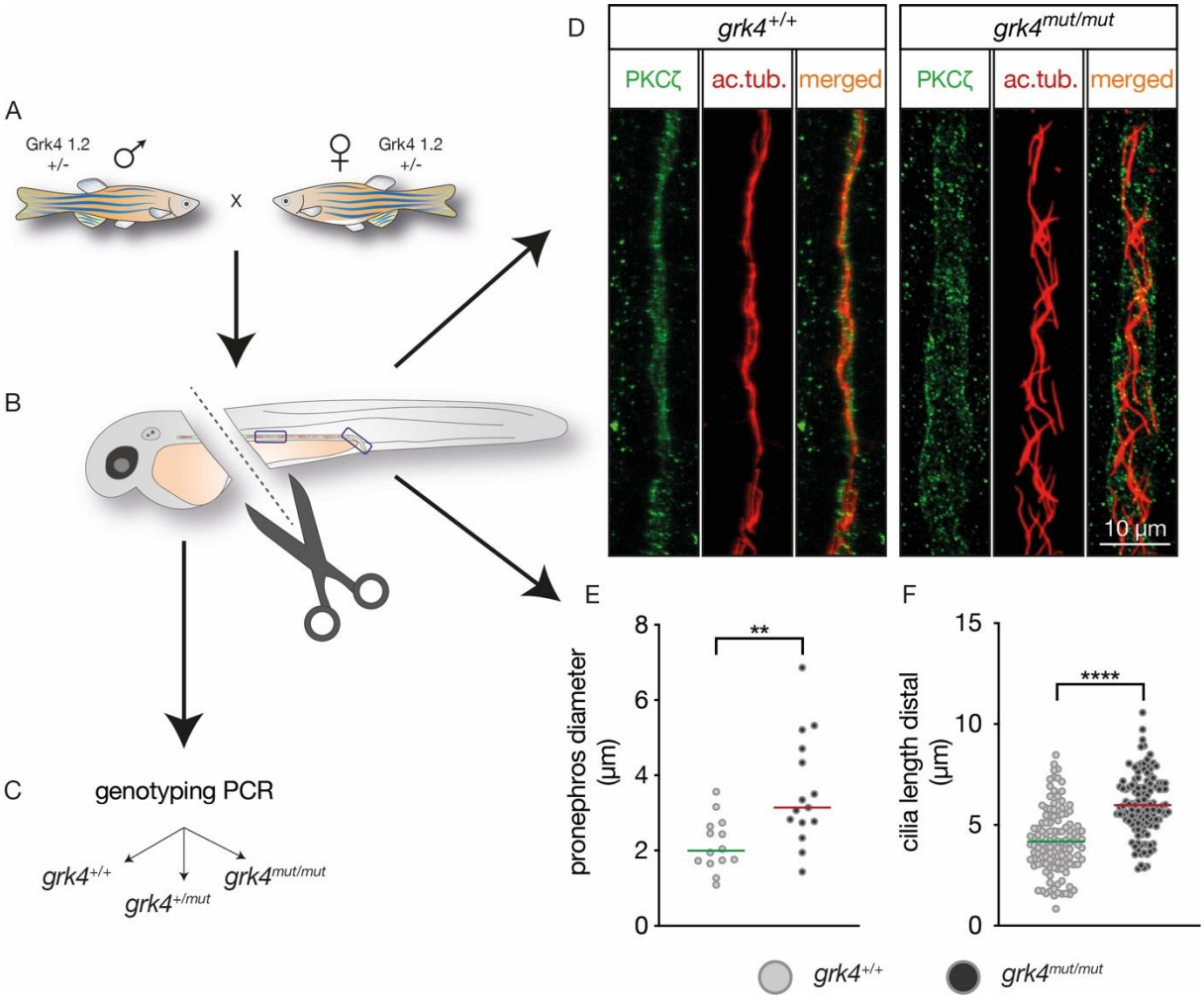

Figure 34: Grk4 mutants resembled kidney phenotype

A: Mating of heterozygous adult Grk4 1.2 fish generated embryos, that were fixed 48 hpf. After fixation I performed an AB staining for acetylated tubulin and PKCζ. B: The head was separated from the rest of the body. C: To know which tail had which genotype, I made genotyping PCRs. D: Representative pictures of the proximal part of the pronephros of WT embryos (*grk4*$^{+/+}$) and homozygous mutant embryos (*grk4*$^{mut/mut}$). PKCζ was stained in green, acetylated tubulin in red. E: Homozygous grk4 mutant showed a dilatation of the pronephros. Each circle represents one embryo. *grk4*$^{+/+}$ = 14 embryos, *grk4*$^{mut/mut}$ = 15. Lines indicate medians. Unpaired t-test with Welch's correction. **: p = 0.003. F: Homozygous Grk4 1.2 mutants showed elongated cilia. Each circle represents one cilium. *grk4*$^{+/+}$ = 124 cilia, *grk4*$^{mut/mut}$ =123. Lines indicate medians. Unpaired t-test with Welch's correction. ****: p < 0.0001.

5.12 Mutated Grk4 shows impaired function

In the next experiment we wanted to verify that Grk4 mutation 1.2 is less functional. Therefore, we generated a capped RNA for injection resembling the original 6 bp in-frame deletion we found in the mutants. I injected embryos with CTRL MO, Grk4 ATG MO or Grk4 ATG MO with capped RNA encoding either WT or mutation 1.2 Grk4. Moreover, I injected embryos only with the capped RNA for *WT grk4* or *grk4 1.2*. The embryos were

analyzed 48 hpf. Depletion of Grk4 led to the already observed phenotypes like edema formation, the curled tail or an otolith defect. Co-injections of Grk4 ATG MO with RNA encoding WT Grk4 were able to partially rescue edema formation, curled tails and otolith defects. Interestingly, co-injections with RNA encoding Grk4 1.2 did not rescue any of these phenotypes (Figure 35B, C and E). With this experiment we had the first verification, that Grk4 1.2 is indeed less functional in comparison with WT Grk4. Worth mentioning is, that we were not able to see a significantly higher number of embryos with pinhead and smaller eyes after Grk4 depletion (Figure 35D). NI embryos were analyzed for clutch quality.

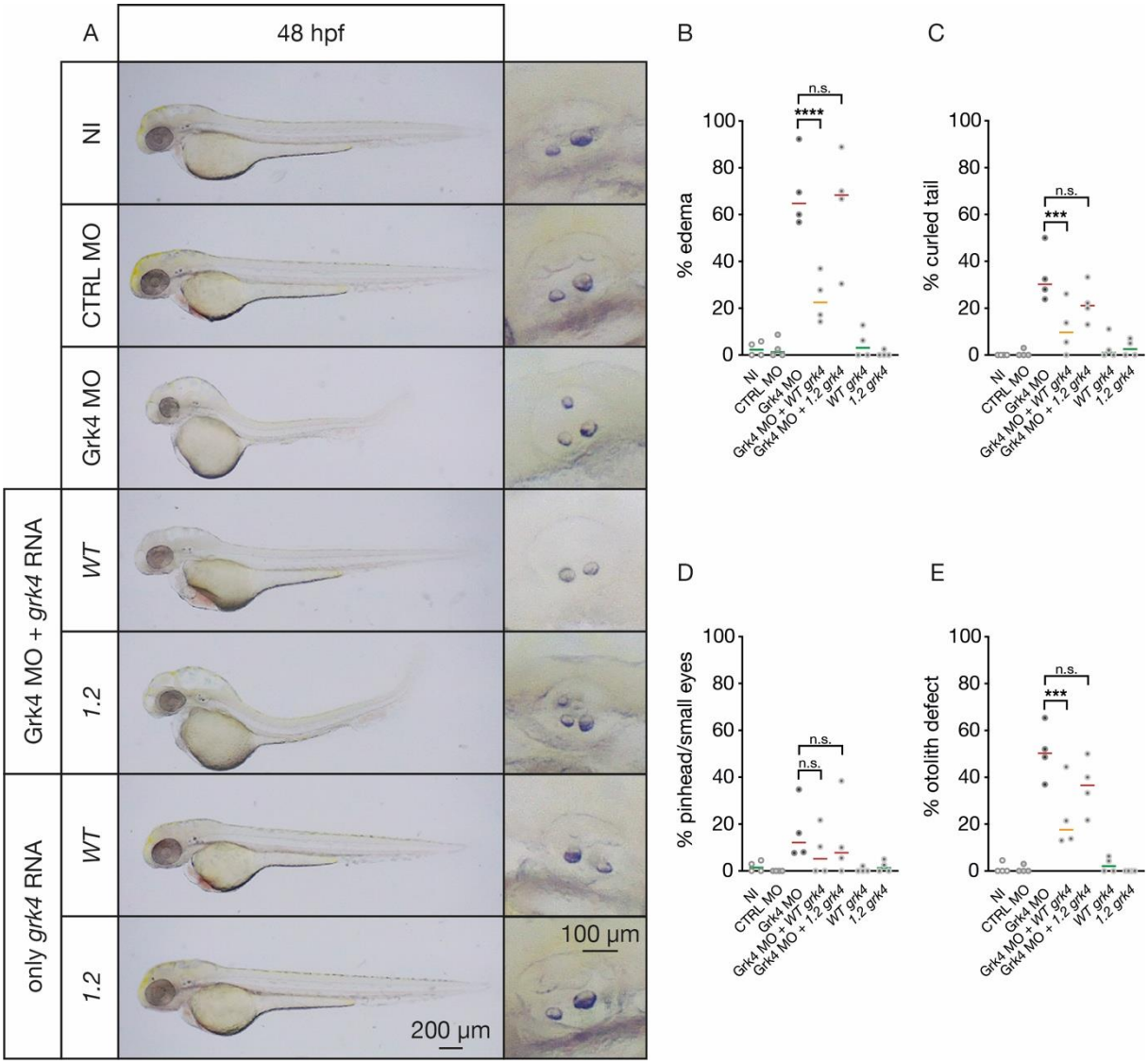

Figure 35: Grk4 mutation 1.2 failed to rescue live phenotypes

A: Representative pictures of embryos 48 hpf. Higher magnification shows otoliths in the otic placode. B: Co-injection with RNA encoding Grk4 1.2 failed to rescue the edema formation. ****: $p < 0.0001$, n.s.: $p = 0.5156$. C: *grk4 1.2* RNA did not rescue the formation of a curled tail after Grk4 depletion. ***: $p = 0.0006$,

n.s.: p = 0.0751. D: Both co-injections did not rescue the low percentage of pinheads and smaller eyes. n.s.: p = 0.3456 and 0.8601. E: WT Grk4 was able to partially rescue the otolith defect, whereas Grk4 1.2 failed so. ***: p = 0.0003, n.s.: p = 0.0510. For B – E: Each circle represents one experiment. N = 4 experiments with NI = 130 embryos, CTRL MO = 113, Grk4 ATG MO = 134, Grk4 ATG MO + *grk4 WT* RNA = 121, Grk4 ATG MO + *grk4 1.2* RNA = 110, *grk4 WT* RNA = 90 and *grk4 1.2* RNA = 91. Lines indicate medians. One-way ANOVA with Sidak's multiple comparison test.

Furthermore, we analyzed cyst formation of these embryos. Grk4 depletion led to a higher percentage of embryos with cysts. The co-injection of Grk4 ATG MO with RNA encoding WT Grk4 partially prevented this. Co-injection with RNA encoding Grk4 1.2 did not lower the number of embryos with cysts. As expected after the live phenotype analysis, the injections with the RNAs alone did not alter cyst formation in comparison to NI and CTRL MO injected embryos (Figure 36B).

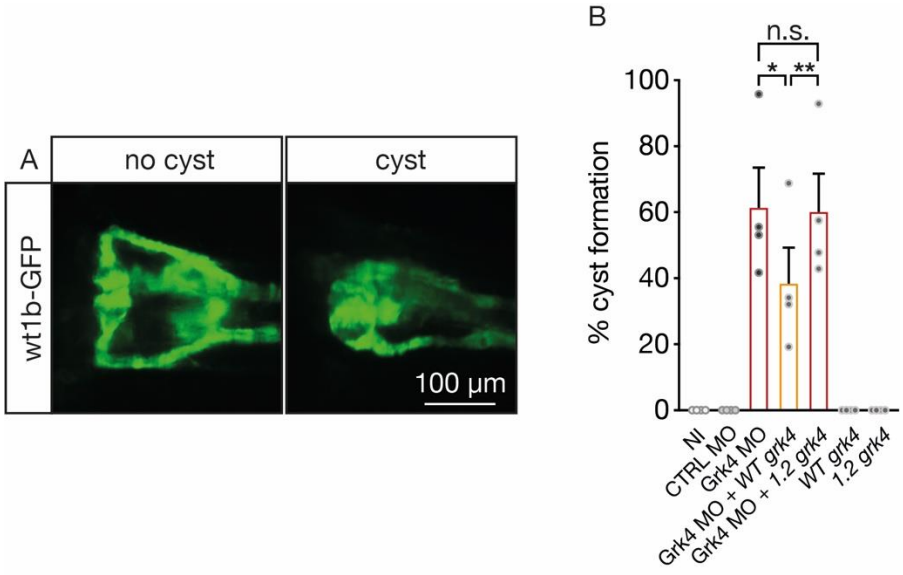

Figure 36: Grk4 1.2 did not prevent cyst formation

A: Representative pictures of a normal formed glomerulus (no cyst) and a cystic one after 48 hpf in wt1b-GFP embryos. Dorsal view. B: Co-injection with *WT grk4* partially reduced the number of cystic embryos, while *grk4 1.2* co-injections failed so. Each circle represents one experiment. N = 4 experiments with NI = 126 embryos, CTRL MO = 101, Grk4 ATG MO = 125, Grk4 ATG MO + *WT grk4* = 114, Grk4 ATG MO + *1.2 grk4* = 98, *WT grk4* = 87 and *1.2 grk4* = 85. Mean with SEM. RM one-way ANOVA with Holm-Sidak's multiple comparison test. *: p = 0.0416, **: p = 0.0051 and n.s.: p = 0.7399.

Taken together, these experiments showed that Grk4 1.2 is impaired in its function as co-injections with RNA encoding Grk4 1.2 did not rescue any of the analyzed phenotypes.

5.13 GRK4 depletion alters ciliogenesis in human fibroblasts

Human fibroblasts were transfected with a smartpool of siRNA for GRK4 or siCTRL respectively. Additionally, I also nucleofected cells with siGRK4 and a plasmid encoding zebrafish Grk4. A qPCR analysis showed that the nucleofection with siGRK4 effectively reduced the relative expression of *GRK4* (Figure 37A) and that zebrafish Grk4 is expressed after nucleofection with the encoding plasmid (Figure 37B). With this proof of principle, we analyzed ciliogenesis after GRK4 depletion. GRK4 KD increased cilia length from around 4.6 µm (siCTRL) to 5.8 µm. Interestingly, we were able to fully rescue elongation of cilia after GRK4 depletion with the co-nucleofection of the plasmid encoding zebrafish Grk4 (Figure 37C and D). These experiments suggest, that GRK4 is necessary for proper ciliogenesis.

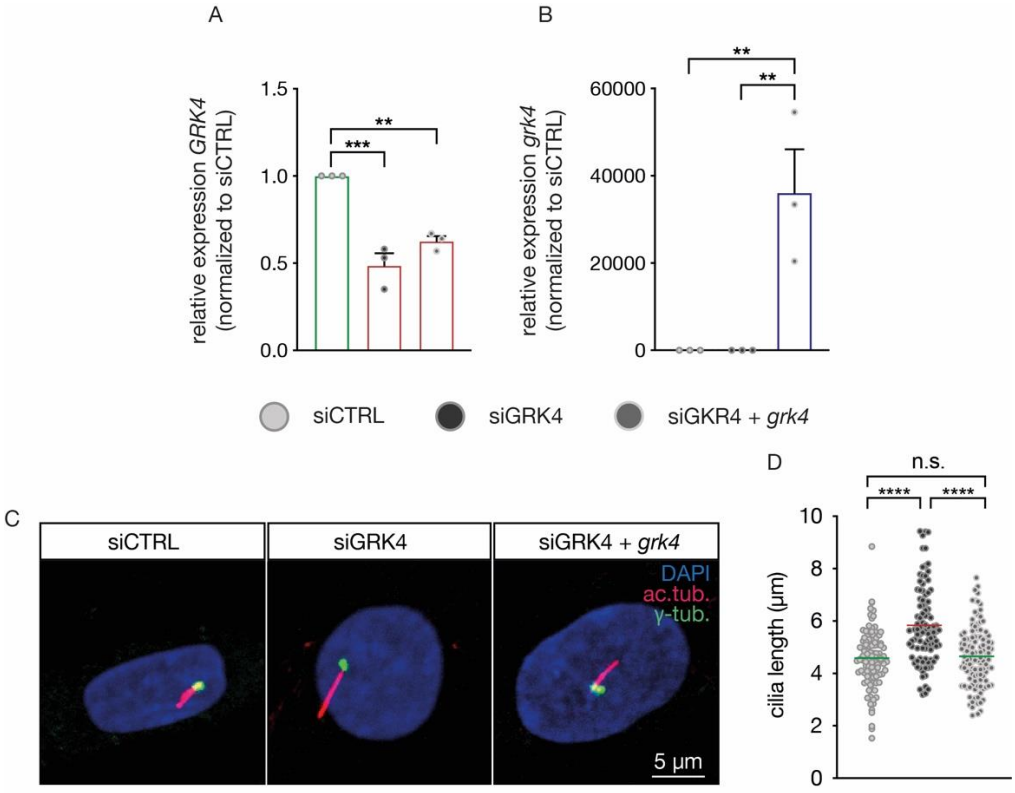

Figure 37: GRK4 depletion elongated cilia in human fibroblasts

A: siGRK4 effectively reduced expression of human *GRK4*. B: Expression of zebrafish *grk4* after nucleofection with a plasmid encoding zebrafish Grk4. siCTRL and siGRK4 co-nucleofected with an empty vector showed no expression of *grk4*. A and B: Expression levels were normalized to the housekeeping gene *SDHA*. Each circle represents one experiment. N = 3 experiments. Bar graphs show mean with SEM. One-way ANOVA with Sidak's multiple comparison test. **: p = 0.0019 (A), **: p = 0.0087 (B), ***: p = 0.0003. C: Representative 2D pictures of confocal z-stacks of human fibroblasts. Acetylated tubulin (cilia)

is stained in magenta, γ-tubulin (for basal body) is stained in green. D: Depletion of GRK4 led to increased cilia length. Reconstitution with zebrafish Grk4 reduced elongated cilia to control level. Each circle represents one cilium. N = 3 nucleofections with siCTRL = 105 cilia, siGRK4 = 91 and siGRK4 + *grk4* = 117. Lines indicate means. Kruskal-Wallis test with Dunn's correction. ****: $p < 0.0001$, n.s.: $p > 0.9999$.

5.14 Kinase function of GRK4 is not required for proper ciliogenesis

Until now the major role of GRK4 seems to be the desensitization of dopamine receptors in the proximal tubule by its kinase activity. Therefore, we wanted to analyze the importance of Grk4 during zebrafish kidney development independently of its kinase function. We cloned a previously reported kinase-dead (KiDe) version of human GRK4 and the zebrafish analogue (105,106), called GRK4 K216M, K217M (or GRK4 KiDe during this study). Collaborators of our lab verified that this version of GRK4 is indeed KiDe (Data not shown).

We repeated the above mentioned nucleofection of human fibroblasts, but instead of using a plasmid encoding the Grk4 WT version we used a plasmid encoding the KiDe version of Grk4. As already shown in Figure 37, depletion of GRK4 led to an elongation of cilia. Reconstitution with the KiDe version of Grk4 completely rescued altered cilia length. Interestingly, cilia got even shorter after co-nucleofection of siGRK4 with *grk4 KiDe* in comparison to those nucleofected with siCTRL and empty vector (ev) (Figure 38A and B).

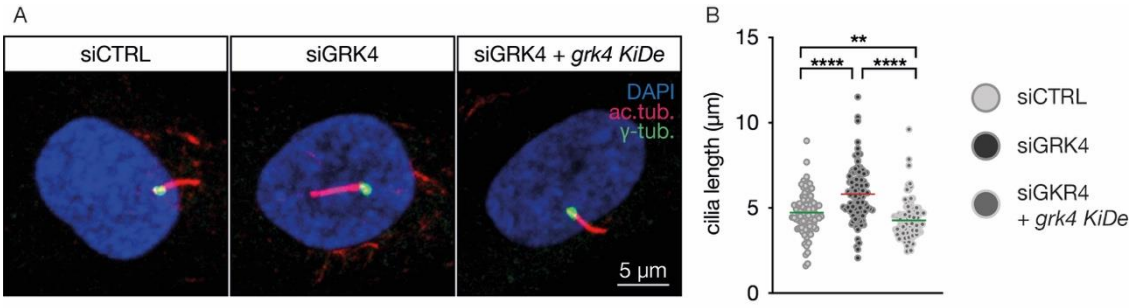

Figure 38: KiDe version of Grk4 fully rescued increased cilia length

A: Representative 2D pictures of confocal z-stacks of human fibroblasts. Acetylated tubulin (cilia) is stained in magenta, γ-tubulin (basal body) is stained in green. B: Depletion of GRK4 led to an increased cilia length. Reconstitution with zebrafish KiDe Grk4 completely rescued elongated cilia. Each circle

represents one cilium. N = 3 nucleofections with siCTRL = 98 cilia, siGRK4 = 95 and siGRK4 + *grk4 KiDe* = 104. Lines indicate means. Kruskal-Wallis test with Dunn's correction. ****: p < 0.0001, **: p = 0.0026.

.

After these first results we decided to perform similar rescue experiment in zebrafish using the newly generated KiDe versions of GRK4. I injected embryos with CTRL MO, Grk4 ATG MO or Grk4 ATG MO + RNA encoding human GRK4 KiDe. NI embryos were used as quality control. At 48 hpf the embryos were analyzed as in Figure 30. Depletion of Grk4 resulted in edema formation, some curled tails and pinheads with smaller eyes and otolith defects (Figure 39). Reconstitution with a KiDe version of human GRK4 significantly rescued edema formation and the otolith defects (Figure 39B and D). Although the rescue for curled tails and pinheads is not significant, a little tendency is visible (Figure 39C and E). To strengthen our hypothesis that the edema formation of Grk4 morphants is associated with kidney function, we analyzed cyst formation in the glomerulus.

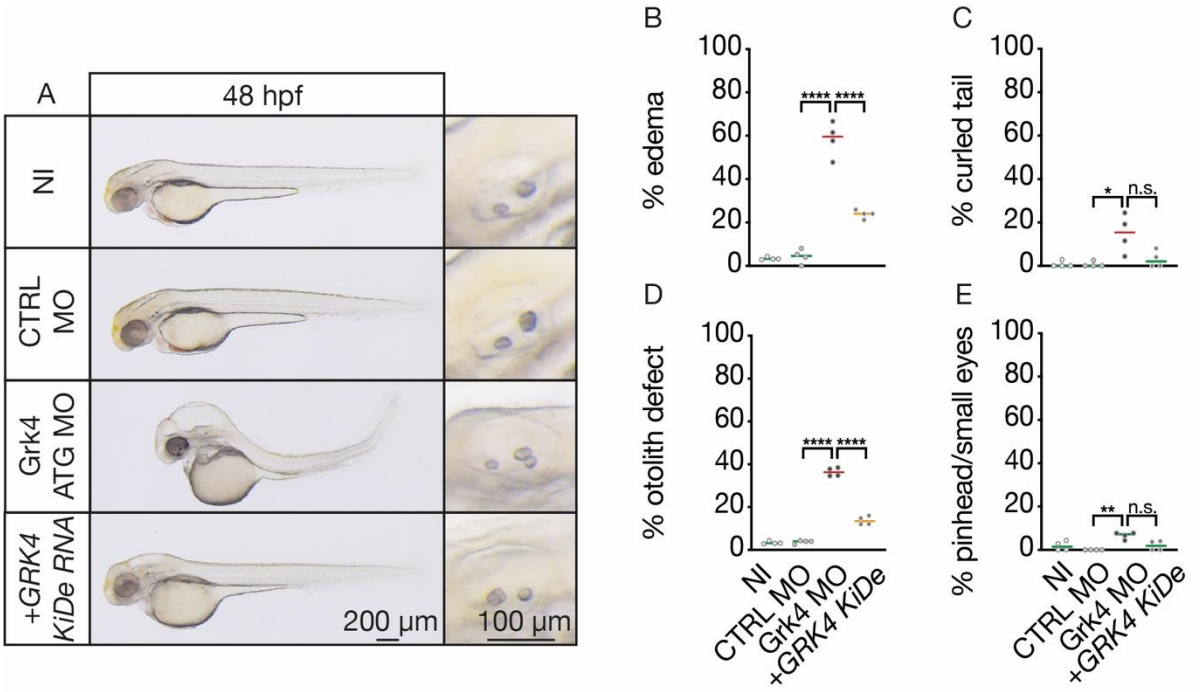

Figure 39: KiDe GRK4 partially rescued live phenotypes

A: Representative pictures of embryos at 48 hpf. Higher magnifications show otoliths in the otic placode. B: Co-injection with RNA encoding KiDe GRK4 significantly prevented edema formation. C: Although co-injection with the *KiDe GRK4* RNA did not rescue the formation of a curled tail in a significant manner, a tendency is visible. D: Co-injections with RNA encoding Grk4 KiDe partially rescued otolith defects. E: Like in earlier injections the phenotype of pinhead with smaller eyes was very mild. For B – E: Each circle represents one experiment. N = 4 experiments with NI = 121 embryos, CTRL MO = 111, Grk4 ATG MO = 120 and Grk4 ATG MO + *GRK4 KiDe* = 110. Lines indicate medians. B and C: One-way ANOVA with

Sidak's' multiple comparison test. C and E: Kruskal-Wallis test with Dunn's correction. ****: $p < 0.0001$, **: $p = 0.0051$, *: $p = 0.0186$, n.s.: $p = 0.1708$ for C, n.s.: $p = 0.0867$ for E.

The depletion of Grk4 led to formation of large cysts in the glomerulus. Co-injection of Grk4 ATG MO with RNA encoding the KiDe version of GRK4 significantly prevented cyst formation (Figure 40). This result goes in line with the rescued edema formation of these embryos, meaning that the kinase activity of Grk4 is not required for proper kidney development.

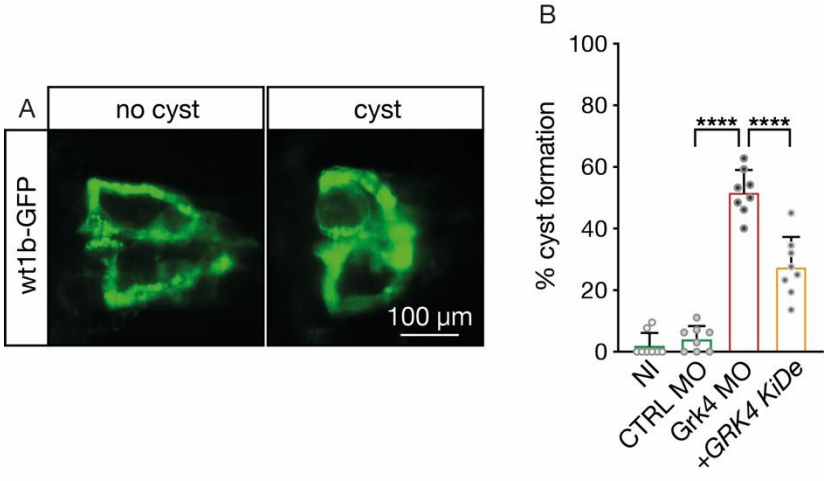

Figure 40: KiDe version of GRK4 rescued cyst formation

A: Representative pictures of a normal formed glomeruli (no cyst) and cystic glomeruli at 48 hpf in wt1b-GFP embryos. Dorsal view. B: Co-injection with RNA encoding KiDe version of GKR4 partially rescued the number of cystic embryos. Each circle represents one experiment. N = 8 experiments with NI = 197 embryos, CTRL MO = 198, Grk4 ATG MO = 229 and Grk4 ATG MO + *GRK4 KiDe* = 253. Mean with SEM. One-way ANOVA with Sidak's multiple comparison test. ****: $p < 0.0001$.

Additionally, we transfected IMCD3 cells with siRNAs against Grk4 and a plasmid encoding either WT or KiDe version zebrafish Grk4. After transfection, cells were seeded in Matrigel to form spheroids and we induced ciliogenesis. I performed an AB staining for acetylated tubulin and ZO-1 (Zonula occludens-1 or Tight junction protein-1). ZO-1 marks polarized cell borders, which is the inner membrane of the spheroids (Figure 41A). The results of this experiment go in line with the previous findings. Depletion of Grk4 led to an increase of cilia length. Both, zebrafish WT Grk4 and KiDe version were able to rescue the elongated cilia (Figure 41B). Interestingly, we also found that spheroids, lacking Grk4, showed more cells per spheroid than under control conditions. Again, both versions of zebrafish Grk4 were able to rescue this phenotype as well (Figure 41C).

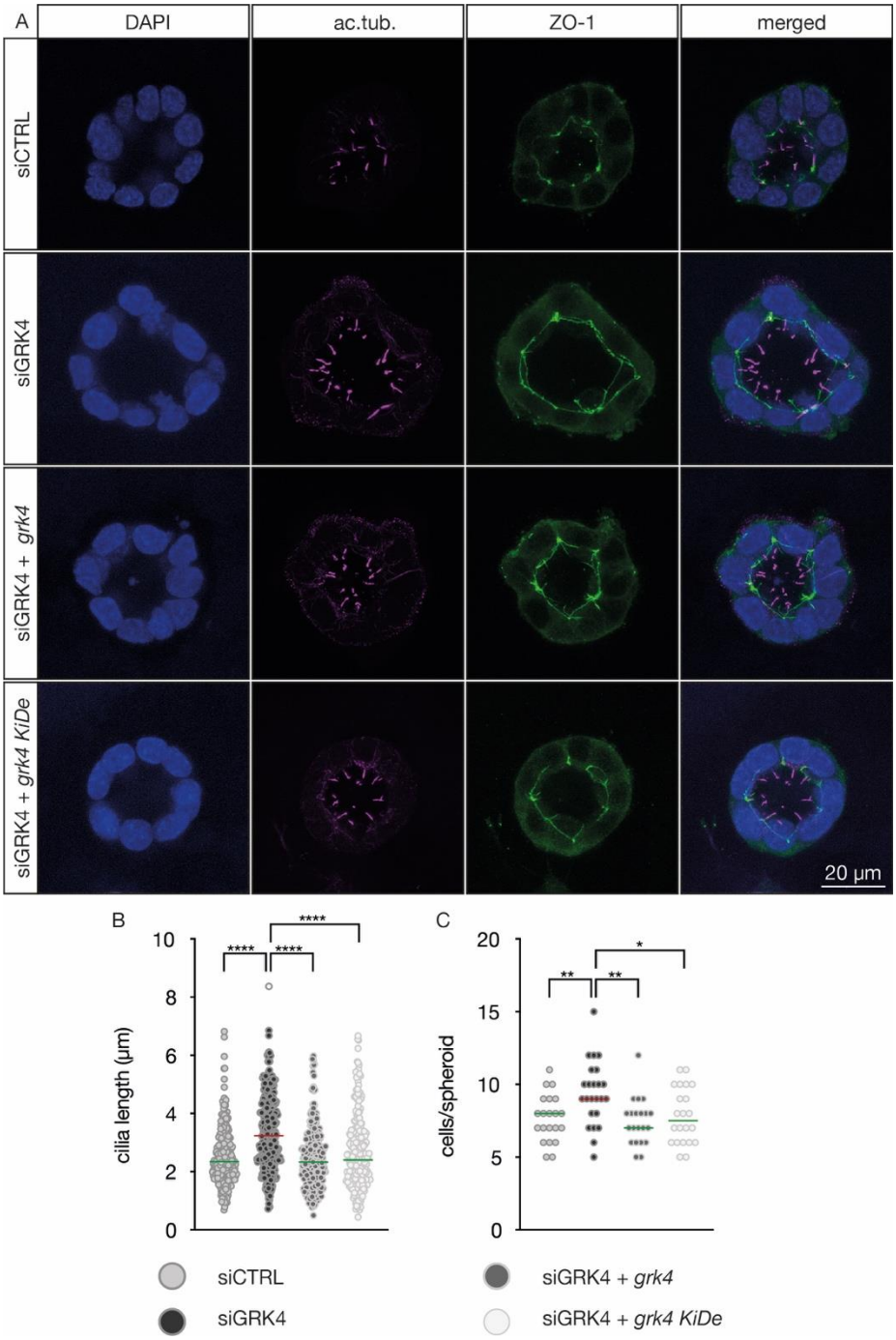

Figure 41: KiDe Grk4 rescued cilia length in spheroids

A: Representative 2D pictures of confocal z-stacks of IMCD3 spheroids. Acetylated tubulin (cilia) is stained in magenta, ZO-1 (polarized cell borders) is stained in green. DAPI is blue. Cells were transfected with siCTRL, siGRK4, siGRK4 with *grk4* or siGRK4 with *KiDe grk4*. B: Depletion of Grk4 led to an elongation of cilia within the lumen of the spheroids. Reconstitution with WT Grk4 or KiDe Grk4 completely rescued elongated cilia. Each circle represents one cilium. N = 21 – 24 spheroids with siCTRL = 266 cilia, siGRK4 = 360, siGRK4 + *grk4* = 284 and siGRK4 + *grk4 KiDe* = 292. Lines indicate means. Kruskal Wallis test with Dunn's correction. ****: $p < 0.0001$. C: Spheroids depleted of Grk4 had more cells than under control conditions or those co-transfected with either WT *grk4* or the KiDe version of *grk4*. Each circle represents one spheroid. 21 spheroids for siCTRL, 24 for siGRK4, 21 for siGRK4 + *grk4* and 22 for soGRK4 + *grk4*

KiDe. Lines indicate means. One-way ANOVA with Holm-Sidak's multiple comparison test. **: p = 0.0088 or 0.0031, *: p =0.0118.

Taken together, GRK4 controls ciliogenesis in three different model systems: human fibroblast, murine kidney cells and in zebrafish. Interestingly, kinase activity of GRK4 is not necessary for normal cilium elongation, suggesting a kinase-independent function of GRK4.

5.15 Constitutively active genetic variants of GRK4 fail to rescue cilia elongation

It already has been published that the three genetic variants of GRK4 (Figure 10), namely *R65L* (rs2960306), *A142V* (rs1024323) and *A486V* (rs1801058), are associated with hypertension and salt-sensitive hypertension. They show an increased activity towards dopamine receptor phosphorylation (83,88). We performed rescue experiments with two of these genetic variants to test whether they are less functional compared to the WT version. Figure 42 proofs that both genetic variants, *R65L* and *A142V,* were expressed in zebrafish embryos after injection.

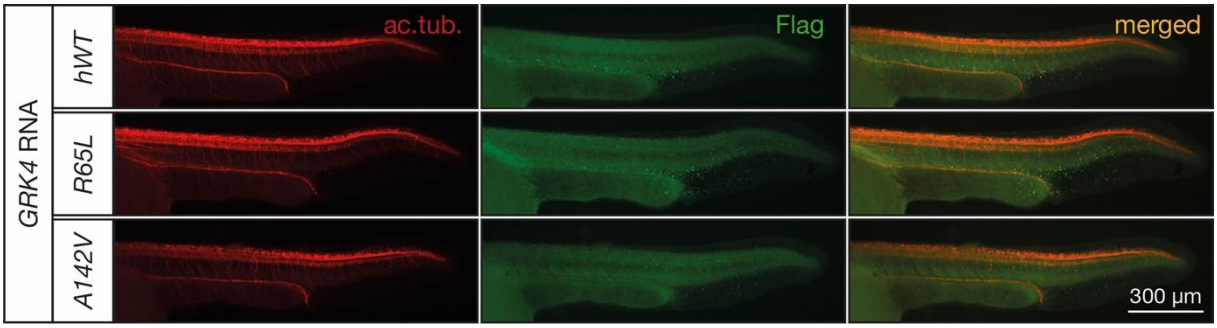

Figure 42: Genetic variants of GRK4 were expressed upon injection

Zebrafish embryos were injected with RNA encoding Flag-tagged patient variants or the WT version of GRK4. At 24 hpf I performed an AB staining for acetylated tubulin (red) and Flag (green) to show that all variants were expressed upon injection.

Dr. Lars D. Maerz injected embryos with CTRL MO, Grk4 ATG MO or Grk4 ATG MO with either *GRK4 WT, R65L* or *A142V* and analyzed edema and cyst formation at 48 hpf. Interestingly, he found that the patient variants were not able to rescue edema or cyst formation after Grk4 depletion (data not shown). Furthermore, he made an AB staining for

acetylated tubulin and PKCζ and took pictures of the developing kidney (see Figure 33 as reference). Then, we measured cilia length (Figure 43). As previous experiments already showed, led the depletion of Grk4 to an elongation of cilia. Co-injection with human WT version of GRK4 significantly reduced cilia length (from 6.4 µm to 5.8 µm). Co-injection with RNA encoding patient variant R65L even increased cilia length (from 6.4 µm to 7.1 µm). The second patient variant, A142V, also failed to rescue cilia length (5.8 µm) (Figure 43).

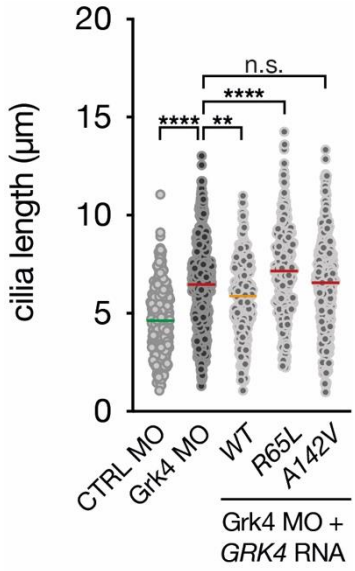

Figure 43: Genetic variants of GRK4 failed to rescue cilia elongation

Grk4 depletion led to cilia elongation that was partially rescued by co-injection of RNA encoding human WT GRK4. Both patient variants of GRK4, R65L and A142V, failed to rescue elongated cilia. Each circle represents one cilium. CTRL MO = 345 cilia, Grk4 ATG MO = 651, Grk4 ATG MO + *GRK4 WT* = 278, Grk4 ATG MO + *GRK4 R65L* = 322 and Grk4 ATG MO + *GRK4 A142V* = 379. Lines indicate medians. Kruskal-Wallis test with Dunn's correction. ****: $p < 0.0001$, **: $p = 0.0036$, n.s.: $p > 0.9999$.

5.16 Dopaminergic receptors are not responsible for elongated cilia

A previous paper showed evidence that dopamine receptor stimulation may be one cause for cilia elongation in the kidney. The authors of this study used porcine kidney proximal tubule cells (LLCPK) and treated them with either dopamine or fenoldopam (both are activator of D1-like dopamine receptor, meaning D1 and D5). Upon treatment, primary kidney cilia became much longer (from 3.3 µm to 7.8 and 11.8 µm, data not shown) (107). Thus, we decided to repeat their experiment using two different cell lines, namely 1BR3

and RPE1 cells. We treated both cell types with 10 µM fenoldopam or DMSO as vehicle (Figure 44). Unfortunately, we were not able to reproduce their findings. In our experiments, treatment with fenoldopam did not increase cilia length in a significant manner (Figure 44C and D). Appendix 1 shows that dopamine receptor 1 and 5 are expressed in human fibroblasts.

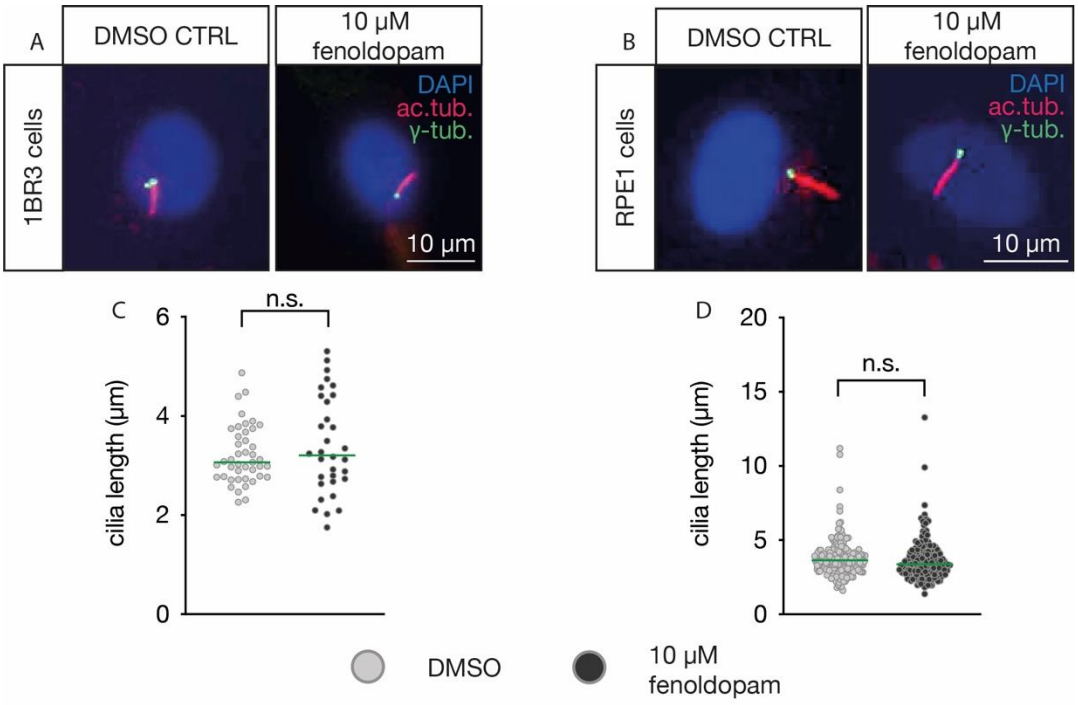

Figure 44: Fenoldopam did not affect cilia length

A and B: Representative pictures of 1BR3 (A) and RPE1 (B) cells. Acetylated tubulin (cilia) is stained in magenta, γ-tubulin (basal body) is stained in green. C: Cilia of 1BR3 cells were not affected upon fenoldopam treatment. N = 1 treatment with DMSO = 43 cilia and 10 µM fenoldopam = 32. Lines indicate means. Two-tailed Mann-Whitney test. n.s.: p = 0.5106. D: Cilia of RPE1 cells did not change their length after treatment with 10 µM fenoldopam. N = 3 treatments with DMSO = 194 cilia and 10 µm fenoldopam = 172. Lines indicate means. Two-tailed Mann-Whitney test. n.s.: p = 0.0950.

As cilia were not affected, we treated zebrafish embryos with fenoldopam. We scored for typical cilia-associated phenotypes like edema formation, otolith defects and cyst formation. Treatment with 10 µM fenoldopam did not lead to an increase in edema formation or otolith defects (Figure 45A, B and C). Furthermore, fenoldopam treated fish did not show any cysts in their glomeruli (Figure 45D and E).

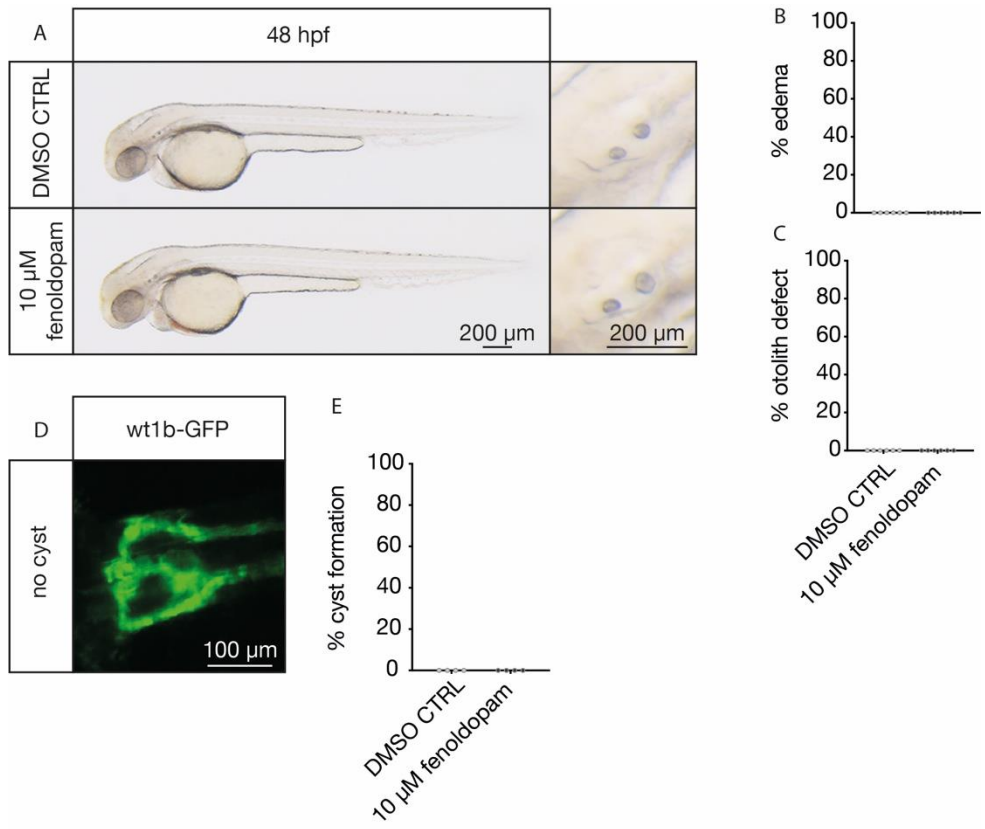

Figure 45: Fenoldopam treatment did not alter zebrafish development

A: Representative pictures of embryos at 48 hpf. Higher magnifications show otoliths in the otic placode. B and C: Embryos treated with 10 µM fenoldopam showed no increase in edema formation nor any otolith defects. Each circle represents one experiment. N = 6 treatments with DMSO CTRL = 132 embryos and 10 µM fenoldopam = 135. D: Representative picture of a normally formed glomerulus (no cyst) at 48 hpf in wt1b-GFP embryos. Dorsal view. E: Treatment with 10 µM fenoldopam did not lead to glomerulus cyst formation. Each circle represents one experiment. N = 4 treatments with DMSO CTRL = 94 embryos and 10 µM fenoldopam = 96. For B, C and E: no statistics were made.

These experiments led us to the conclusion that dopamine receptor signaling may not be the cause of cilia elongation and the observed phenotypes in our experiments. To verify this, we used an antagonist of dopamine receptors, namely SCH 39166, to check whether antagonism of dopamine receptor may reduce cilia length after GRK4 depletion. I transfected 1BR3 cells with either siCTRL or siGRK4. After 48 h I switched to starvation medium to induce ciliogenesis. The starvation medium contained 50 nM or 1 µM SCH 39166 or DMSO as vehicle. GRK4 depletion led to an increased cilia length (from 3.5 µm to 4.9 µm). Treatment with the dopamine receptor antagonist did not alter cilia length (neither in siCTRL transfected cells, nor in siGRK4 transfected cells) (Figure 46).

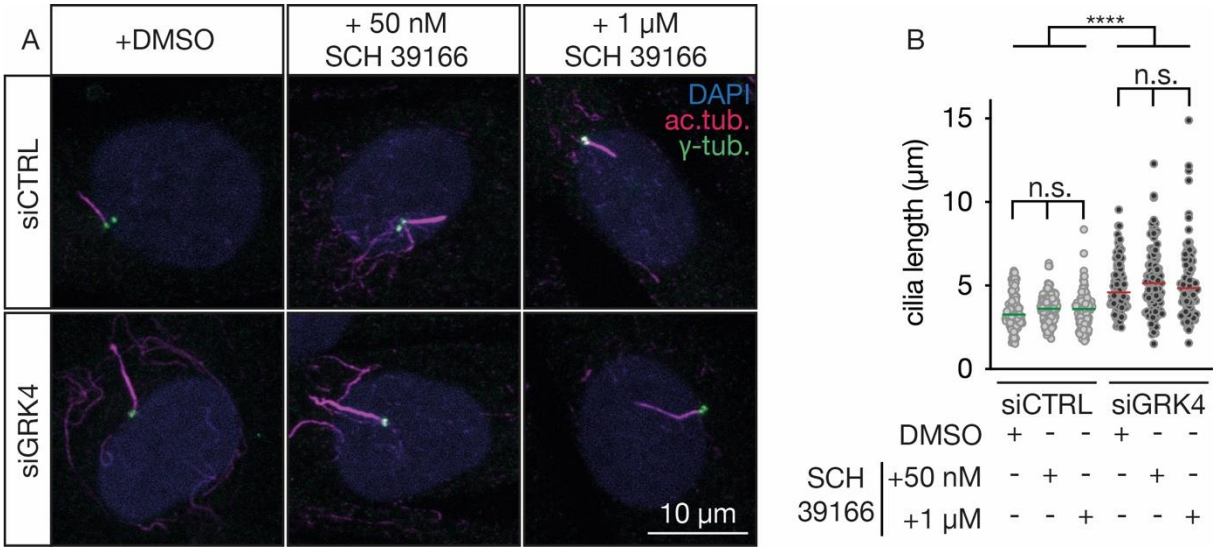

Figure 46: SCH 39166 treatment did not prevent cilia elongation

A: Representative 2D pictures of confocal z-stacks of human fibroblasts. Acetylated tubulin (cilia) is stained in magenta, γ-tubulin (for basal body) is stained in green. B: Depletion of GRK4 led to elongated cilia. Treatment with both concentrations of SCH-39166 did not rescue increased cilia length. Each circle represents one cilium. N = 3 transfections with siCTRL + DMSO = 104 cilia, siCTRL + 50 nM SCH 39166 = 95, siCTRL + 1 µM SCH 39166 = 131, siGRK4 + DMSO = 100, siGRK4 + 50 nM SCH 39166 = 105 and siGRK4 + 1 µM SCH 39166 = 97. Lines indicate means. Kruskal-Wallis test with Dunn's correction. ****: $p < 0.0001$, n.s.: $p > 0.9999$.

With the help of these experiments, we were able to strengthen the hypothesis that dopamine receptor signaling may not be responsible for the observed phenotypes.

Taken together we showed that kinase activity of GRK4 may be unnecessary for the observed phenotypes, as a KiDe version of GRK4 was able to rescue edema and cyst formation and cilia elongation and the kinase hyperactive patient variants failed to do so. Interestingly, both patient variants are located in the regulator of G-protein signaling (RGS) homology (RH) domain, which is known to be important for interactions with other proteins (108). Therefore, we deleted the RH domain and performed rescue experiments with it (Prof. Melanie Philipp did the whole cloning for this) (Figure 47A).

5.17 RH domain of GRK4 is required for proper kidney development and ciliogenesis

I injected zebrafish embryos with CTRL MO, Grk4 ATG MO or Grk4 ATG MO with *ΔRH GRK4* RNA. I also injected the RNA itself and used NI embryos for quality control. At 48 hpf I analyzed the typical phenotypes we were able to observe upon Grk4 depletion. Consistent with the previous findings, Grk4 ATG MO injected embryos showed a higher percentage of edema formation and otolith defects. Co-injection with *ΔRH GRK4* did not rescue these phenotypes (Figure 47C and D).

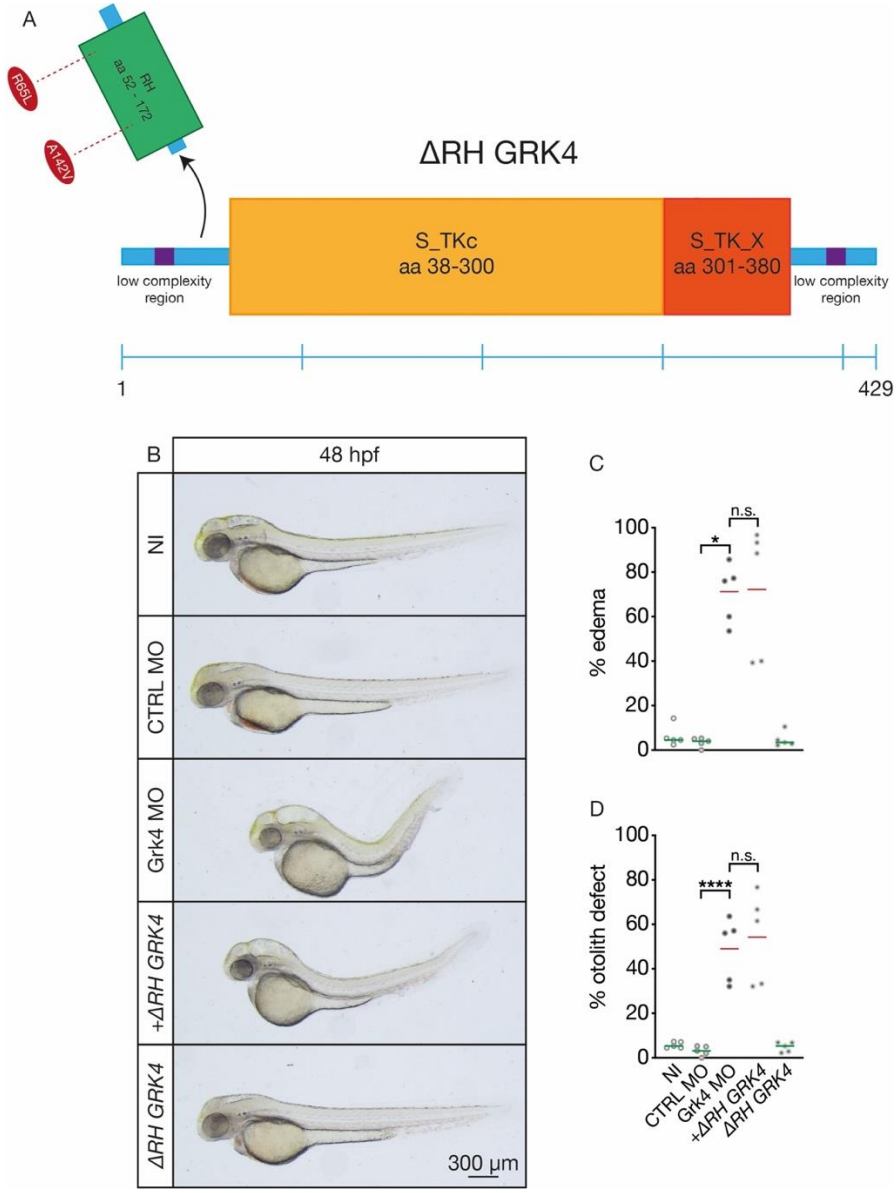

Figure 47: ΔRH version of GRK4 failed to rescue live phenotypes

A: Prof. Melanie Philipp deleted the aa 39-180 from GRK4. This resulted in a ΔRH version of GRK4. B: Representative pictures of embryos at 48 hpf. C: Co-injection with *ΔRH GRK4* failed to rescue edema

formation. D: Reconstitution with ΔRH GRK4 did not rescue otolith defects. Each circle represents one experiment. N = 5 injections with NI = 118 embryos, CTRL MO = 134, Grk4 ATG MO = 123, Grk4 ATG MO + *ΔRH GRK4* = 144 and *ΔRH GRK4* = 173. Lines indicate means. For C: Kruskal-Wallis test with Dunn's correction. For D: One-way ANOVA with Sidak's multiple comparison test. ****: $p < 0.0001$, *: $p = 0.0189$, n.s.: $p > 0.9999$.

Further, cyst formation of these embryos was analyzed, which was neither prevented by ΔRH GRK4 co-injection (Figure 48).

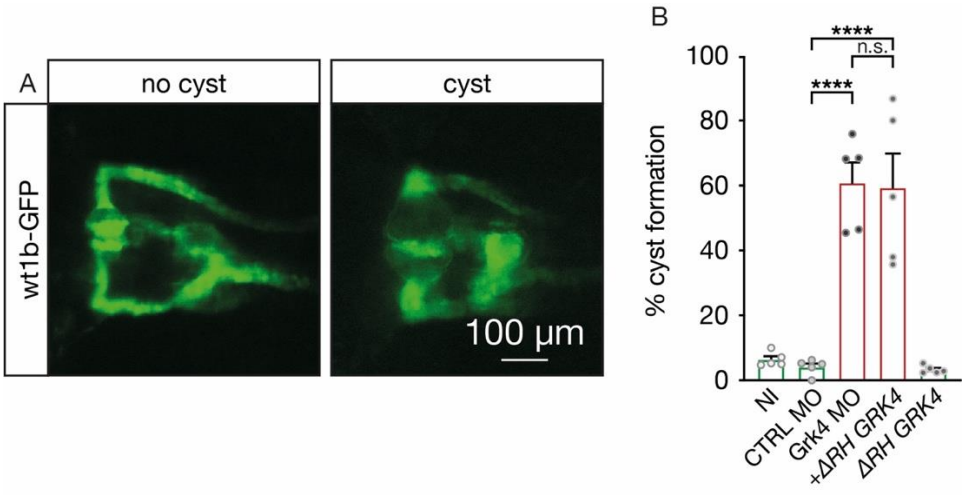

Figure 48: ΔRH GRK4 did not prevent cyst formation

A: Representative pictures of a normally formed glomerulus (no cyst) and a cystic one at 48 hpf in wt1b-GFP embryos. Dorsal view. B: Co-injection with RNA encoding ΔRH GRK4 did not rescue the number of cystic embryos. Each circle represents one experiment. N = 5 injections with NI = 114 embryos, CTRL MO = 133, Grk4 ATG MO = 120, Grk4 ATG MO + *ΔRH GRK4* = 140 and *ΔRH GRK4* = 164. Mean with SEM. One-way ANOVA with Sidak's multiple comparison test. ****: $p < 0.0001$, n.s.: $p = 0.9966$.

Additionally, we performed an AB staining for acetylated tubulin and PKCζ to check for the already described kidney phenotype. In line with the other rescue experiment with *ΔRH GRK4*, we neither rescued the dilatation of the pronephros, nor the elongation of distal cilia (Figure 49). This led us to the conclusion, that the RH domain of GRK4, or to be more specific the interaction with other proteins, may potentially play a crucial role in proper ciliogenesis and kidney developing, at least in our in vivo model. Therefore, we also made rescue experiments in human fibroblasts.

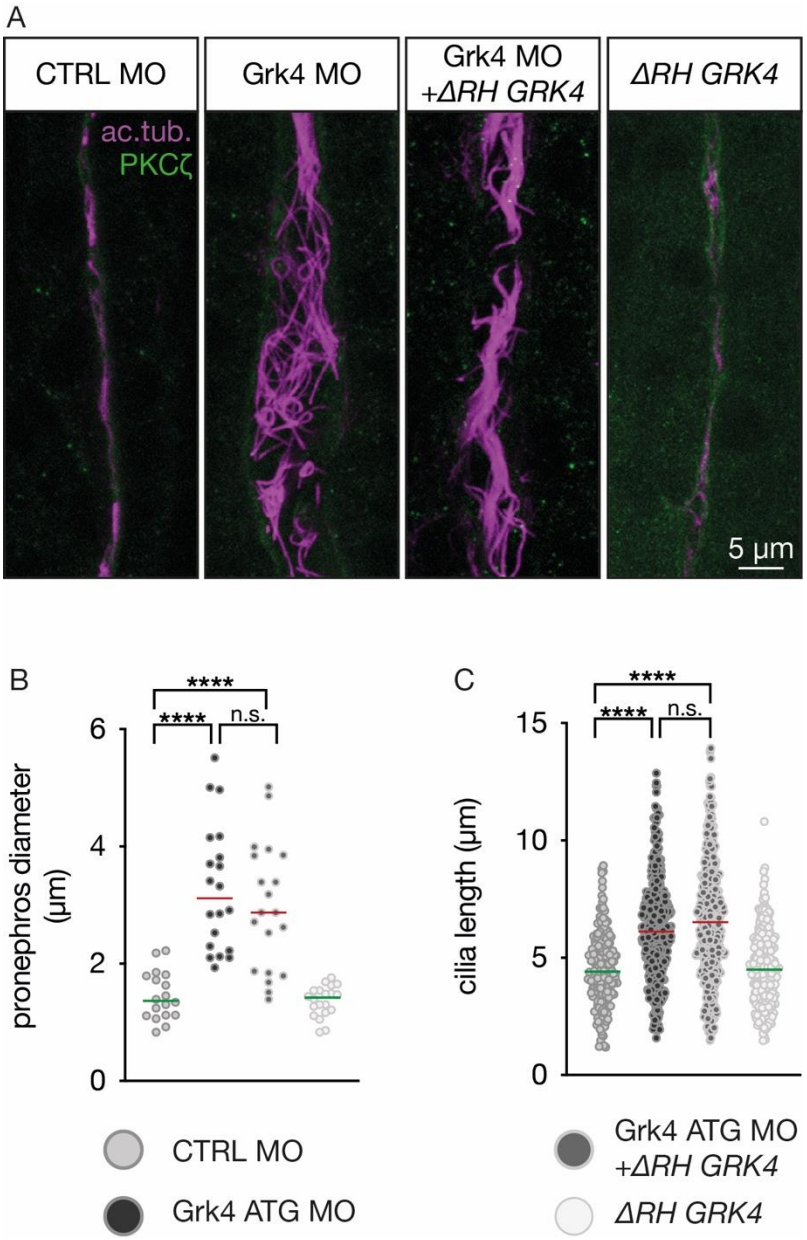

Figure 49: ΔRH GRK4 did not rescue kidney phenotype

A: Representative pictures of the pronephros after CTRL MO, Grk4 ATG MO, Grk4 ATG MO *+ΔRH GRK4* or *ΔRH GRK4* injection. Acetylated tubulin was stained in magenta, PKCζ in green. B: Co-injection of RNA encoding ΔRH GRK4 did not rescue the dilatation of the pronephric duct. Each circle represents one embryo. CTRL MO = 18 embryos, Grk4 ATG MO = 20, Grk4 ATG MO *+ΔRH GRK4* = 20 and *ΔRH GRK4* = 20. Lines indicate medians. One-way ANOVA with Sidak's multiple comparison test. ****: $p < 0.0001$, n.s.: $p = 0.7593$. C: Co-injection with *ΔRH GRK4* did not rescue cilia elongation after Grk4 depletion. Each circle represents one cilium. CTRL MO = 206 cilia, Grk4 ATG MO = 413, Grk4 ATG MO *+ΔRH GRK4* = 446 and *ΔRH GRK4* = 273. Lines indicate medians. Kruskal-Wallis test with Dunn's correction. ****: $p < 0.0001$, n.s.: $p > 0.9999$.

I nucleofected 1BR3 cells with either siCTRL and siGRK4 combined with an ev or with *ΔRH grk4*. GRK4 depletion led to increased cilia length from approximately 3.8 µm to 4.6 µm. Reconstitution with *ΔRH Grk4* failed to rescued cilia elongation (4.6 µm) (Figure 50).

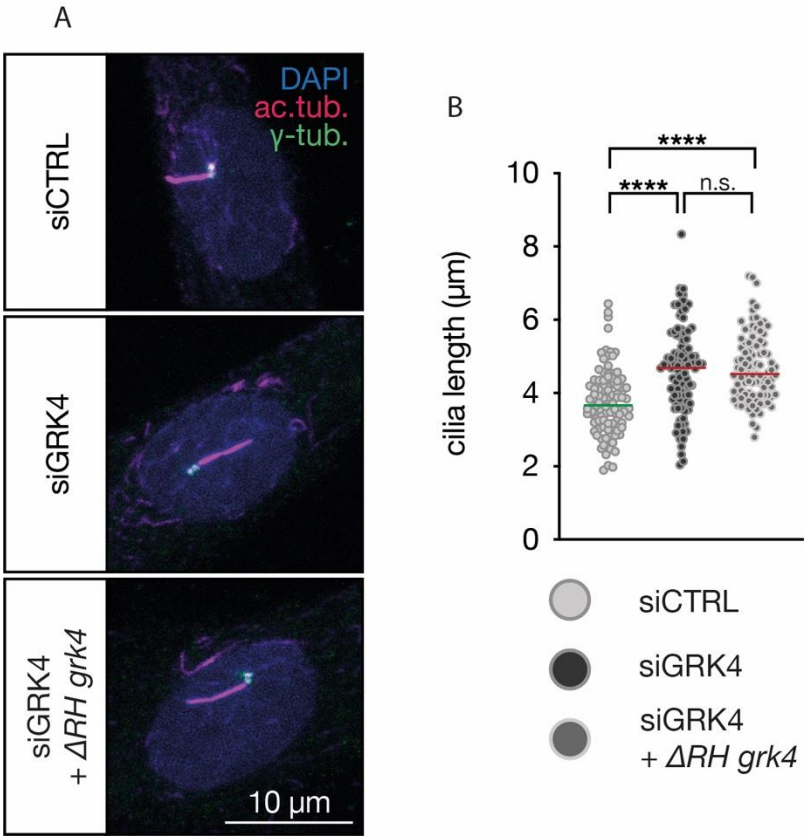

Figure 50: ΔRH Grk4 did not rescue cilia elongation upon GRK4 depletion

A: Representative 2D pictures of confocal z-stacks of human fibroblasts. Acetylated tubulin (cilia) is stained in magenta, γ-tubulin (basal body) is stained in green. B: Depletion of GRK4 led to elongated cilia. Co-nucleofection with ΔRH Grk4 did not prevent increased cilia length. Each circle represents one cilium. N = 3 nucleofections with siCTRL = 99 cilia, siGRK4 = 100 and siGRK4 + *ΔRH grk4* = 97. Lines indicate medians. Kruskal-Wallis test with Dunn's correction. ****: $p < 0.0001$, n.s.: $p > 0.9999$.

Hence, these results demonstrate that the RH domain of GRK4 is necessary for proper kidney development and ciliogenesis (in vivo and in vitro).

5.18 The connection between GRK4 and mTOR

mTOR is a serine/threonine protein kinase, which comes in two protein complexes, namely mTOR complex 1 (mTORC1) and mTORC2. mTOR is known to be involved in many different processes like cell growth, proliferation and metabolism (109). It has been reported that mTOR is also involved in ciliogenesis. Yuan et al. showed that depletion of a complex with inhibitory functions towards mTORC1 led to increased cilia length. Interestingly, treatment with rapamycin, an inhibitor of mTORC1, rescued elongated cilia (110). In 2013,

our lab also published a connection between mTOR and cilia. We found that GRK5, another kinase of the GRK4-6 subfamily, has an inhibitory effect on mTOR signaling. Loss of Grk5 resulted in dysfunctional and elongated cilia. Treatment with rapamycin, which means inhibition of mTOR, rescued some of the observed phenotypes (84). Therefore, we hypothesized that cilium elongation and kidney dysfunction after GRK4 depletion may be potentially driven by elevated mTOR signaling.

We performed rescue experiments with zebrafish embryos. I injected them with either CTRL MO or Grk4 ATG MO. Then, they were treated with 500 nM rapamycin or DMSO from tailbud stage on. At 48 hpf I analyzed the live phenotype according to the most prominent phenotypes: edema formation and otolith defects (Figure 51B and C). Consistent with previous experiments, Grk4 depleted embryos showed a higher percentage of edema formation and otolith defects, compared to control conditions. Treatment with 500 nM rapamycin from tailbud stage on did not prevent these two phenotypes (Figure 51). However, more experiments may be necessary as the variation was larger than usual.

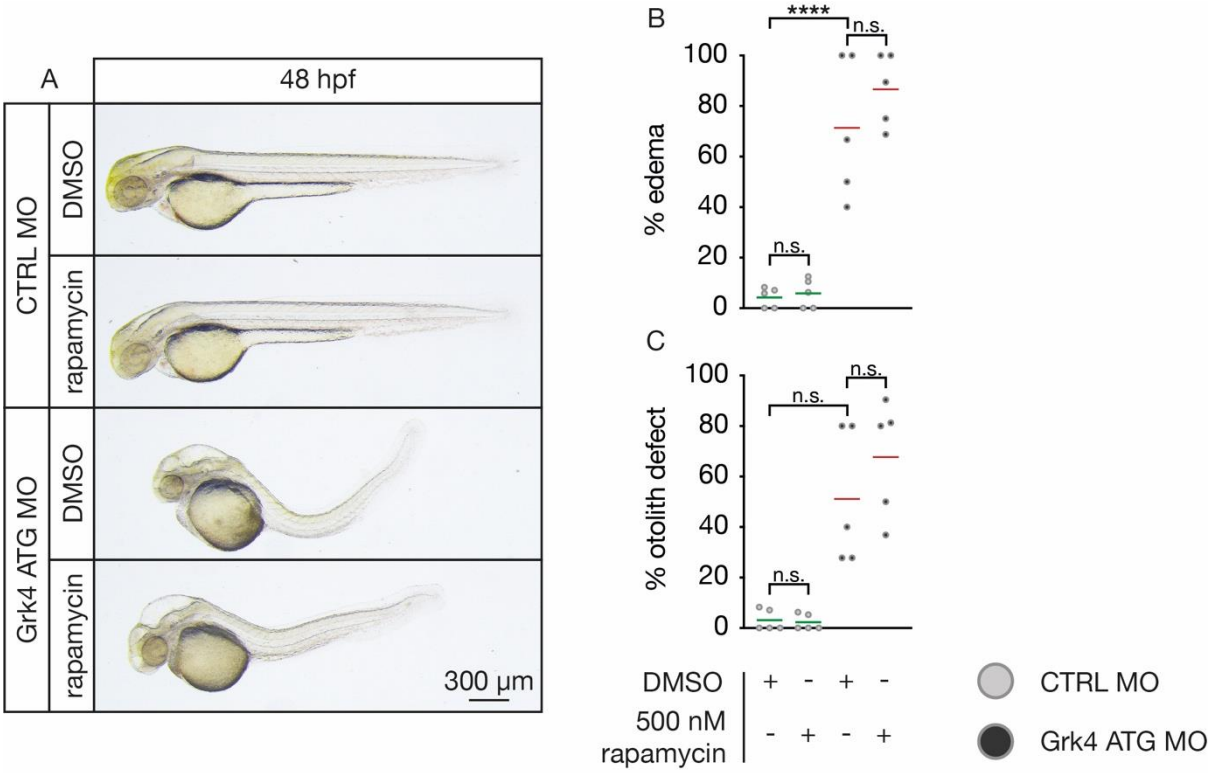

Figure 51: Rapamycin treatment did not rescue edema formation or otolith defects

A: Representative pictures of embryos at 48 hpf. B: Treatment with 500 nM rapamycin did not rescue edema formation. One-way ANOVA with Sidak's multiple comparison test. ****: $p < 0.0001$, n.s.: $p = 0.9982$ (CTRL MO + DMSO vs. CTRL MO + rapamycin) or 0.3880 (Grk4 ATG MO + DMSO VS. GRK4 ATG MO + rapamycin). C: Rapamycin did not prevent otolith defects after Grk4 depletion. Kruskal-Wallis test with

Dunn's correction. n.s.: p > 0.9999 (CTRL MO + DMSO vs. CTRL MO + rapamycin and Grk4 ATG MO + DMSO vs. Grk4 ATG MO + rapamycin), or p = 0.0729 (CTRL MO + DMSO vs. Grk4 ATG MO + DMSO). For B and C: Lines indicate means. Each circle represents one experiment. N = 5 injections with treatment with CTRL MO + DMSO = 75 embryos, CTRL MO + rapamycin = 83, Grk4 ATG MO + DMSO = 86 and Grk4 ATG MO + rapamycin = 87.

We also counted cyst formation of these embryos. Treatment with DMSO after Grk4 ATG MO injection resulted in cyst formation in almost 40 % of the embryos. Interestingly, the treatment with 500 nM rapamycin reduced the percentage of embryos developing cysts. Only 28 % of the embryos showed a glomerulus cyst (Figure 52).

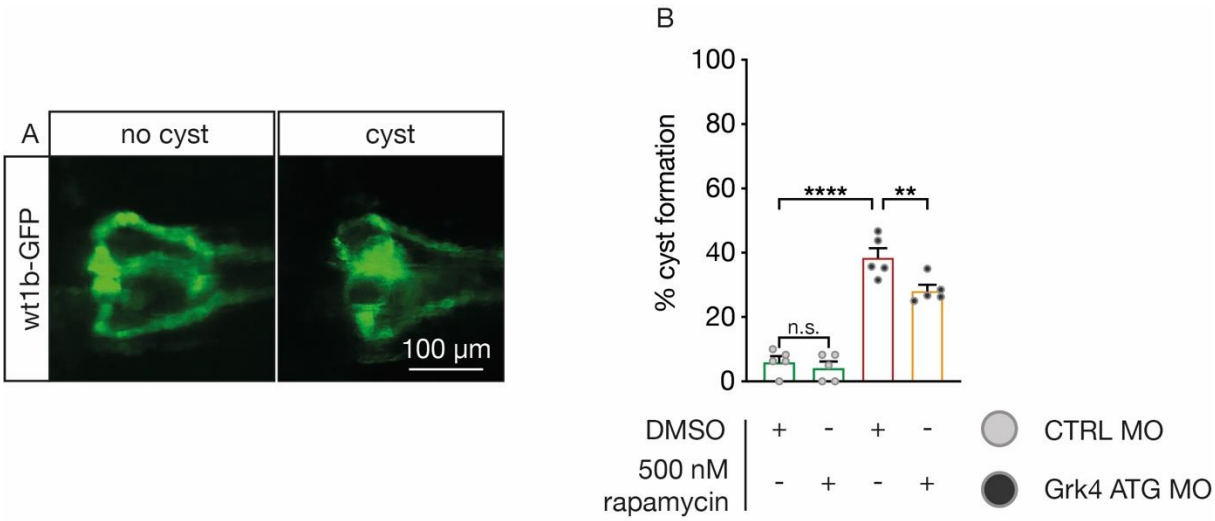

Figure 52: Rapamycin treatment prevented cyst formation upon Grk4 depletion

A: Representative pictures of a normal formed glomerulus (no cyst) and a cystic one after 48 hpf in wt1b-GFP embryos. Dorsal view. B: Treatment with 500 nM rapamycin partially rescued cyst formation. Each circle represents one experiment. N = 5 injections with treatment with CTRL MO + DMSO = 69 embryos, CTRL MO + rapamycin = 78, Grk4 ATG MO + DMSO = 81 and Grk4 ATG MO + rapamycin = 84. Mean with SEM. One-way ANOVA with Sidak's multiple comparison test. ****: p < 0.0001, **: p = 0.0093, n.s.: p = 0.9052.

Last but not least, we analyzed, whether rapamycin is able to rescue the dilation of the pronephric duct and cilia elongation in the developing kidney. Treatment of Grk4 depleted embryos with 500 nM rapamycin significantly rescued the dilatation of the pronephric duct (Figure 53A). CTRL MO injected embryos, treated with DMSO, had a pronephros diameter of 1.3 µm. Treatment of CTRL MO injected embryos with rapamycin even reduced the diameter to 1.09 µm. Grk4 depletion and treatment with DMSO led to the expected dilatation of the developing kidney tubule (2.7 µm). Rapamycin treatment significantly rescued this phenotype (1.9 µm) (Figure 53A). Additionally, CTRL MO injected embryos

had the same cilia length when treated with DMSO or rapamycin (4.03 µm and 4.02 µm). Grk4 depletion increased cilia length to 6.5 µm. Treatment with rapamycin significantly rescued cilia elongation to 4.6 µm (Figure 53B). Taken together, treatment of Grk4 depleted embryos with rapamycin rescued the observed kidney phenotypes, suggesting an inhibitory effect of Grk4 on mTOR.

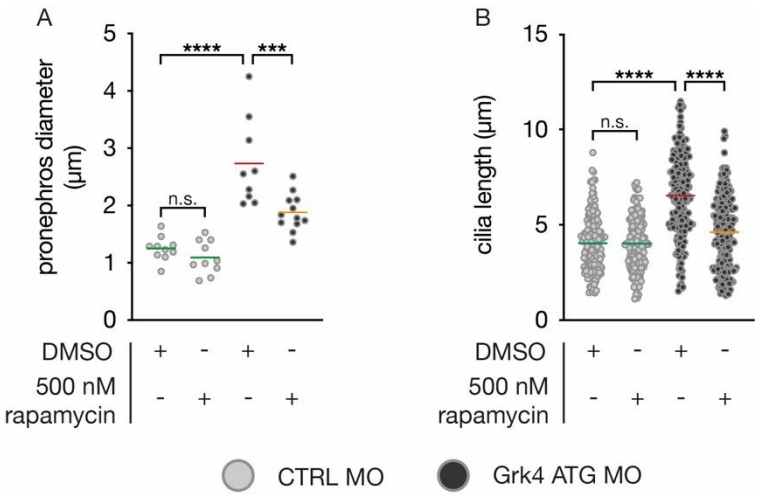

Figure 53: Inhibition of mTOR signaling rescued cilia elongation and dilatation of the pronephric duct

A: Treatment with rapamycin partially rescued the dilatation of the developing kidney. Each circle represents one embryo. CTRL MO + DMSO = 10 embryos, CTRL MO + rapamycin = 10, Grk4 ATG MO + DMSO = 9 and Grk4 ATG MO + rapamycin = 12. Lines indicate means. One-way ANOVA with Sidak's multiple comparison test. ****: $p < 0.0001$, ***: $p = 0.0002$, n.s.: $p = 0.8090$. B: Treatment with rapamycin significantly reduced elongated cilia. Each circle represents one cilium. CTRL MO + DMSO = 165 cilia, CTRL MO + rapamycin = 167, Grk4 ATG MO + DMSO = 215 and Grk4 ATG MO + rapamycin = 234. Lines indicate means. Kruskal-Wallis test with Dunn's correction. ****; $p < 0.0001$, n.s.: $p > 0.9999$.

To further verify this observation, we also used HEK cells for analysis. A further lab member, Oliver Wenzke, did initial experiments with HEK cells. He transfected them with siCTRL, siGRK4 or siGRK4 + *grk4*. Then he measured the cell size. GRK4 depleted cells were bigger than control transfected ones. Reconstitution with zebrafish Grk4 rescued increased cell size in a significant manner (Data not shown). Additionally, he transfected HEK cells with siCTRL and siGRK4 and treated them with rapamycin. GRK4 depleted HEK cells that were treated with 30 nM rapamycin showed a significant reduction in increased cell size (data not shown). He also generated a stable GRK4 knockout (KO) HEK cell line by CRISPR/Cas9 (data not shown), which was used for following experiments.

I treated HEK WT and the GRK4 KO (*GRK4*$^{-/-}$) cells with either 30 nM rapamycin or DMSO as control and measured the cell diameter. *GRK4*$^{-/-}$ cells were bigger than WT cells when treated with DMSO. Interestingly, the increased cell size was reduced by treating *GRK4*$^{-/-}$ cells with 30 nM rapamycin (Figure 54A). I also calculated the protein content of these cells. GRK4 KO cells had a higher protein content than WT cells. Treatment with rapamycin significantly rescued elevated protein levels of KO cells (Figure 54B).

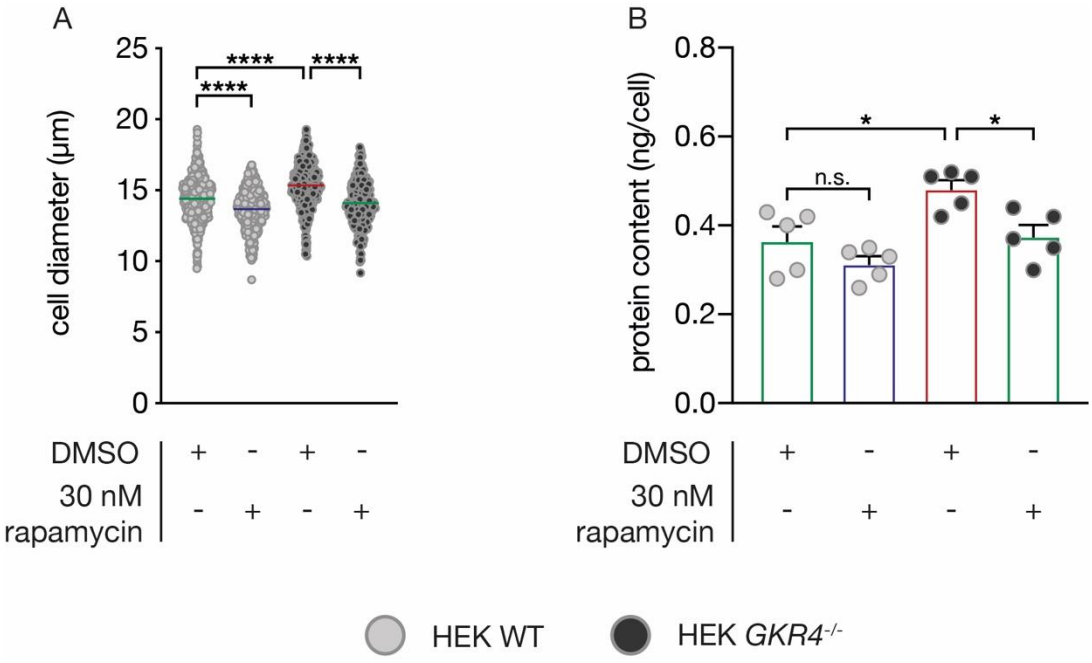

Figure 54: Rapamycin rescued GRK4 KO phenotypes

A: Treatment with rapamycin reduced increased cell size of *GRK4*$^{-/-}$ cells. Each circle represents one cell. HEK WT + DMSO = 518 cells, HEK WT + rapamycin = 465, HEK *GRK4*$^{-/-}$ + DMSO = 483 and HEK *GRK4*$^{-/-}$ + rapamycin = 326. Lines indicate means. Kruskal-Wallis test with Dunn's correction. ****: $p < 0.0001$. B: GRK4 KO cells showed a higher protein content compared to HEK WT cells. Treatment with rapamycin rescued the elevated protein content. Each circle represents one experiment. N = 5 treatments. Mean with SEM. One-way ANOVA with Sidak's multiple comparison test. *: $p = 0.0105$ (HEK WT + DMSO vs. HEK *GRK4*$^{-/-}$ + DMSO) or 0.0195 (HEK *GRK4*$^{-/-}$ + DMSO vs. HEK *GRK4*$^{-/-}$ + rapamycin), n.s.: $p = 0.3747$.

In summary we found that loss of GRK4, through MO injection, siRNA or KO, resulted in increased mTOR signaling, which was rescued by rapamycin treatment.

5.19 GRK4's kinase activity is not necessary for limiting mTOR signaling

Next, I tested whether KiDe GRK4 and kinase hyperactive genetic variants of GRK4 have an impact on elevated mTOR signaling in GRK4 KO cells. I transfected the KO HEK cells with different versions of GRK4: WT, KiDe, R65L or A142V. After transfection I analyzed the cell size and protein content of these cells (Figure 55). Expression of WT GRK4 and GRK4 KiDe significantly reduced increased cell size of HEK GRK4 KO cells. Transfection with one of the two patient variants did not rescue the cell size (Figure 55A). Additionally, WT GRK4 and KiDe GRK4 were able to lower increased protein content of GRK4 KO cells. Both patient variants of GRK4 failed to rescue the protein content (Figure 55B).

Therefore, we concluded that the kinase function of GRK4 may be irrelevant for limiting mTOR signaling.

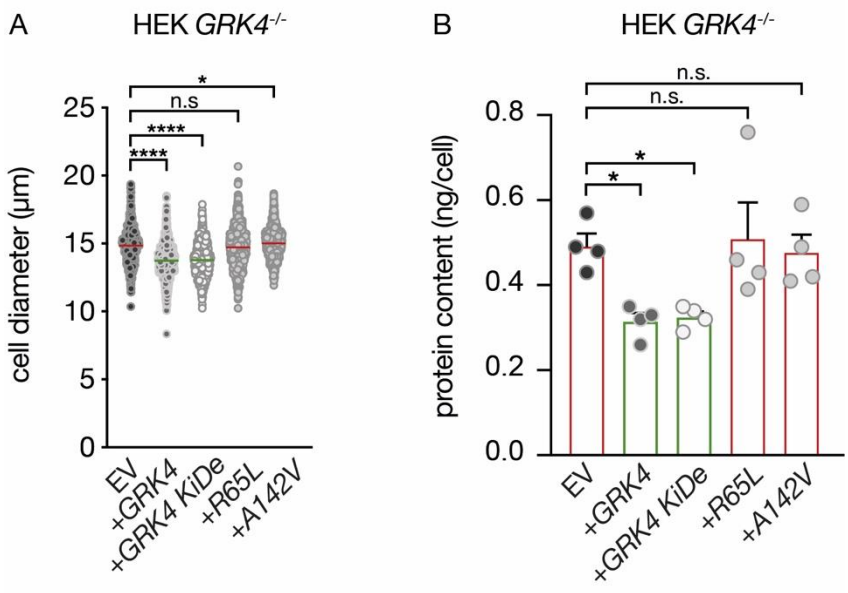

Figure 55: Kinase-independent inhibition of GRK4 on elevated mTOR signaling

A: Expression of WT GRK4 and KiDe GRK4 significantly reduced increased cell diameter of HEK *GRK4*$^{-/-}$. The kinase hyperactive patient variants failed to rescue increased cell size. Each circle represents one cell. EV = 641 cells, *+GRK4* = 820, *+GRK4 KiDe* = 776, *+R65L* = 739 and *+A142V* = 675. Lines indicate means. Kruskal-Wallis test with Dunn's correction. ****: $p < 0.0001$, *: $p = 0.0175$, n.s.: $p = 0.1624$. B: Expression of WT GRK4 and KiDe GRK4 reduced protein content of HEK *GRK4*$^{-/-}$ cells. Both patient variants failed so. Each circle represents one experiment. N = 5 transfections. Mean with SEM. One-way ANOVA with Holm-Sidak's multiple comparison test. *: $p = 0.0398$ (EV vs. *+GRK4*) or 0.0457 (EV vs. *+GRK4 KiDe*), n.s.: $p = 0.9672$.

Taken together I found that loss of GRK4 resulted in embryos with cilia related phenotypes like edema formation or otolith defects. Additionally, these embryos showed glomerulus cyst and a dilation of the pronephric tubule with longer cilia. Rescue experiments with a KiDe version and kinase hyperactive genetic variants of Grk4 showed evidence that the kinase activity of Grk4 may be unimportant for proper kidney and cilia development. Instead, we found that the RH domain of Grk4 plays an important role. Finally, we saw that Grk4 negatively regulates mTOR signaling, independent of its kinase activity. Our findings are not only restricted to zebrafish embryos but are also consistent in human and murine cells.

6 Discussion

6.1 Pathway-specific effects of ADSLD

ADSLD has been described to have a very broad spectrum of clinical phenotypes like growth and mental retardation, psychomotor delay or microcephaly. Up to date it is not fully understood what causes all the different phenotypes. A possible explanation could be the accumulation of toxic intermediates, as a higher concentration of SAICAr is directly connected to a more severe phenotype. Of note, the lack of nucleosides may also be relevant for some phenotypes. This work established an in vivo model to study the mechanism of ADSLD phenotypes. For analyzing the function of Adsl, LOF experiments with the help of two different MOs for Adsl were performed in zebrafish embryos. The depletion of Adsl resulted in typical cilia dysfunction associated phenotypes like edema formation, pinheads or kinked tails. To check for proper cilia function, LR asymmetry was analyzed. A reduced Adsl level impaired heart looping and the liver was misplaced. To further demonstrate that LR asymmetry is affected after Adsl LOF, two important marker genes of the laterality signaling cascade were analyzed. These genes can be directly connected to impaired cilia function for the following reason: the LR axis is specified by the asymmetric induction of *spaw* and *lefty1* in the left lateral plate mesoderm (39,94,96). This induction depends on cilia in a transient tissue, the so-called KV. Cilia in the KV generate a counterclockwise fluid flow by rotating. This flow becomes sensed and is translated into the asymmetric induction of *spaw* on the left side. Therefore, disturbed pattern of *spaw* expression could serve as a readout for impaired ciliogenesis. Indeed, analysis of *spaw* as well as *lefty1*, showed randomized expression. Furthermore, an AB staining showed no differences in the KV size or the number of cilia per KV but cilia were shorter after Adsl depletion. Further experiments should demonstrate that the reduced ciliary length impaired the counterclockwise flow within the KV. One possibility to do that was already published by Wang et al. (111). They injected fluorescent beads which visualized the fluid flow within the KV. In our lab we are not able to directly measure the fluid flow in the KV with fluorescent beads. Therefore, we should analyze the expression of *charon* by WMISH, as it

is the direct target gene of the flow within the KV (30). This will strengthen the hypothesis that the impaired LR asymmetry is based on ciliary malfunctions.

Immunofluorescence staining for Adsl strengthened the observation that Adsl somehow is involved in ciliogenesis. Adsl localized to cilia in the developing kidney of zebrafish (Figure 19). This finding is in agreement with the labs of Travis Stracker and Jens Lüders (87). KD experiments of ADSL in RPE1 cells led to shorter primary cilia and fewer ciliated cells. Adding a siRNA-resistant cDNA of ADSL restored the wild-typic situation in these cells. To investigate the mechanism of ADSL during ciliogenesis they tested two possible explanations: The accumulation of toxic intermediates and the lack of nucleosides. Transfected RPE1 cells with siADSL were exposed to nucleosides and ciliogenesis was analyzed. This was not able to rescue the cilia length or ciliation, suggesting that the lack of nucleosides may not be responsible for defective ciliogenesis. Next, they used MTX to inhibit the DNPS pathway upstream of ADSL. Surprisingly, MTX restored the cilia length and the number of ciliated cells in ADSL deficient cells. To further verify this result they used another drug called MRT00252040, which inhibits the steps 9 and 10 of the DNPS (Figure 7). This led to the same rescue effect like MTX. These experiments showed that the accumulation of the toxic intermediates SAICAr and S-Ado, inhibited by the drugs, may cause defective ciliogenesis. For the proof of principle, they tried in a last experimental setup to mimic the ADSL KD phenotype by adding SAICAr to the cells. Indeed, SAICAr exposure phenocopied the ADSL KD phenotype and disturbed ciliogenesis in those cells (48). I never treated zebrafish embryos with SAICAr. This is an experiment we should focus on in the future to answer the question whether SAICAr treatment also phenocopies the observed phenotypes of Adsl depleted embryos.

Taken together, we can conclude that the effects of ADSL depletion on ciliogenesis may be driven by the accumulation of SAICAr and S-Ado and not due to the lack of nucleosides.

How can the loss of ADSL and the enrichment of the toxic intermediates cause ciliogenesis defects? A possible explanation could be an impact on CP110. The removal of CP110 is necessary for axonemal elongation, as CP110 acts as a suppressor on top of the mother centriole (17,18). Of note, the labs of Travis Stracker and Jens Lüders found that ADSL

depleted cells showed an impaired removal of CP110 after serum starvation. This indicates that ADSL KD led to a higher percentage of cells showing two CP110 foci (one on the daughter centriole and one on the mother centriole). This phenotype could also be rescued by inhibition of the DNPS by MRT00252040. In addition, SAICAr treatment phenocopied the altered CP110 removal after ADSL KD. They also showed that double KD of CP110 and ADSL showed no ciliary phenotype (48). We did not analyze the importance of the removal of Cp110 in zebrafish embryos for proper ciliogenesis. This is an experiment we should focus on in the future. Liu et al. already published in 2021 that the injection of NudCL2 (NudC-like protein 2) MO led to LR asymmetry defects in zebrafish embryos and cilia shortening in the KV. Interestingly, they were able to rescue these phenotypes with a co-injection of the NudCL2 MO and a Cp110 MO (112). We could also try to co-inject the Adsl MO together with a Cp110 MO and analyze LR patterning and ciliogenesis in zebrafish.

Nevertheless, we can conclude that ADSL-associated ciliogenesis defects may occur due to the inhibition of a key step in early ciliogenesis, namely, the removal of CP110. The exact mechanism how ADSL or SAICAr affect CP110 removal still needs to be revealed. Protein interactions studies could give first explanations for these findings. Do ADSL and CP110 directly interact? This question should be addressed with a co-immunoprecipitation.

Several embryos depleted of Adsl developed pinheads including smaller eyes, what is in agreement with the clinical phenotype of ADSLD patients that suffer from microcephaly. There are many processes and signaling cascades that are important for forming the skull and regulating brain size. Defects in genetic or non-genetic factors associated with cell differentiation, progenitor cell proliferation, cell death, cell migration or DNA damage repair could lead to microcephaly (111,113). One differentiates between primary and secondary microcephaly, that can be genetic or acquired. Primary microcephaly is described as congenital microcephaly, as it occurs prior to birth. In contrast, secondary microcephaly develops after birth. The main cause for primary microcephaly (PM) is an imbalance between cell death and progenitor cell production. Patients with secondary microcephaly (SM) are born with a normal head size, that decreases during early

development, due to neurodegeneration and cell death. Reasons for PM can be alterations in neuronal migration or accumulation of toxic metabolites (114). Defects in DNA damage repair pathways also cause PM. In this work, we were able to show that Adsl depleted zebrafish embryos had a smaller pool of neuronal progenitor cells in the developing forebrain. Interestingly, MTX treatment rescued this phenotype, whereas nucleoside treatment failed, meaning that the lower number of Sox2-positive progenitor cells may be caused by toxic intermediates accumulation rather than a consequence of DNA damage. However, it is important to note, that nucleoside treatment rescued enhanced DNA damage after Adsl MO injection in the neural tube of zebrafish embryos. Therefore, we also checked the number of differentiated mature neurons in the neural tube after Adsl KD with an AB staining for Elavl3/4. Inhibition of the accumulation of toxic intermediates by MTX rescued reduced number of Elavl3/4 positive cells after Adsl depletion and restored the number of differentiated neurons. It would be of high interest to analyze the effect on differentiated neurons by rescue experiments with nucleosides. This experiment is important to show that the accumulation of SAICAr is responsible for the loss of neuronal cells, rather than the lack of nucleosides.

A possible explanation for the function of ADSL during brain development could be cilia-mediated SHH signaling. SHH signaling is important for neurodevelopment as its activation is necessary for progenitor proliferation and differentiation (49). I analyzed the expression of two SHH marker genes, namely *PTCH1* and *GLI1*, that are upregulated after SHH activation. Therefore, I made a qPCR of Adsl MO and CTRL MO injected zebrafish embryos. Interestingly *ptch1* and *gli1* were upregulated after loss of Adsl (data not shown), suggesting an activation of Shh. These results do not go in the line with our hypothesis and the literature, as I concluded that the loss of neuronal progenitor and differentiated cells might come from reduced Shh signaling due to malfunctional cilia. It is important to repeat this experiment again to verify the upregulation of *ptch1* and *gli1*.

As already mentioned for the neurodevelopment, the SHH signal pathway also plays a key role in craniofacial development in vertebrates (115). SHH signals are present during the

early stages of craniofacial development. Mice depleted of SHH show multiple craniofacial defects reaching from stomodeum opening defects (116) to hypoplasia of the first pharyngeal arch (117,118) or cyclopia (119). Disturbing Adsl in zebrafish embryos phenocopied the human clinical characteristics and showed less cartilage formation. It is important to analyze whether these defects in cartilage formation also may come from an altered cilia-mediated SHH signaling. As mentioned above, I have to repeat the qPCR experiments of Shh marker genes to verify or reject this hypothesis.

Other common brain developmental disorders associated with cilia are Joubert or Seckel syndrome (44,120). Seckel syndrome is an autosomal recessive disorder causing microcephaly, mental retardation or dwarfism (121), similar to ADSLD. One gene associated with Seckel syndrome is called *ataxia telangiectasia and RAD3-related* (*ATR)*. Mutations in *ATR* lead to DNA damage and replication stress what causes neuroprogenitor cell death (120,122,123). Other genes associated with Seckel syndrome are CEP63 or CENPJ. They are centrosomal proteins. Mutations in one of these genes could lead to cell cycle delay what also may cause loss of progenitors (124–126). Our collaborators found similarities between Seckel syndrome and ADSLD. RPE1 cells depleted for ADSL showed p53 activation and defects in cell cycle progression, but no increased cell death or senescence. Nucleoside treatment was not able to rescue these phenotypes, indicating that the lack of nucleosides may not be responsible for this observation (48). So, the reduced number of neuronal progenitor cells are caused by a different pathway than observed in Seckel syndrome. We hypothesize that the reduction in brain size is due to impaired cell cycle progression and defects in differentiation. Both of them are strictly controlled through cilia (44). As most of the observed phenotypes were rescued by inhibiting the accumulation of the toxic intermediates and were phenocopied by adding SAICAr to the cells, we conclude that SAICAr may be a driver for ADSL depletion phenotypes. We also should try to phenocopy the observed phenotypes after Adsl depletion in zebrafish by SAICAr treatment. Does SAICAr treatment lead to LR asymmetry defects? Does SAICAr shorten

cilia in the KV? Does SAICAr reduce neuronal cell numbers? Does SAICAr contribute to DNA damage? These experiments are important to strengthen our work.

The exact mechanism how SAICAr may affect signaling pathways important for cell proliferation is still unknown and needs to be elucidated in further experiments. Hence, it is important to identify interaction proteins of SAICAr by co-immunoprecipitation for example.

Next, to analyze the human mutations, we performed rescue experiments with two genetic variants of ADSL, namely *R426H* and *V429A*. Both variants are located in the C-terminus region of ADSL. Van Laer et al. performed enzymatic comparisons between human WT ADSL, or how it is also called modern human ADSL, and the genetic variants. In their report they described the *V429A* mutation as an ancestral or Neanderthal version of ADSL, as it was found in the genome of three different Neanderthals and one Denisovan. The *R426H* substitution is located on the same α-helix like the Neanderthal version of ADSL *V429A*. Both residues (aa 426 and 429) are solvent-exposed and away from the active center of ADSL (127). This is surprising as mutations in these residues are associated with ADSLD. During their work they found that modern ADSL and the genetic variants of ADSL have the same enzymology or ligand binding, but differ slightly in thermal stability. However, this difference in thermal stability does not have a great impact on enzymatic activity, as both variants showed almost 80 % activity of the modern human ADSL. They hypothesize that exposure to the solvent of these residues may be more important for causing the clinical phenotypes. Under purine limited conditions, all six enzymes of the DNPS pathway (see red, blue, green and purple dots of Figure 7) can form a so called purinosome. This purinosome increases the substrate channeling and therefore the whole purine biosynthesis (128,129). The mutation *R426H* is already known to negatively affect purinosome assembly (130). As *V429A* is located on the same α-helix like *R426H,* similar effects on purinosome formation would be expected. The authors speculated that this region of ADSL is somehow involved in protein-protein interactions. Defects in this region could also contribute to the clinical phenotypes observed in ADSLD patients. To test this, it is important to make

protein-interaction studies by co-immunoprecipitation of ADSL and the other enzymes of the purinosome. With which of these enzymes does ADSL directly interact? Do the genetic variants *R426H* and *V429A* show less interaction with the enzymes of the purinosome? These are question for further studies.

To strengthen the hypothesis that the lack of nucleosides and the accumulation of the toxic intermediates contribute to different phenotypes of ADSLD, following questions and experiments should be addressed: Can we rescue the reduced number of neuronal cells after Adsl depletion with one the genetic variants? The mutation *R426H* is known to negatively affect the assembly of the purinosome, which is important for purine synthesis. Additionally, we were not able to rescue the neuronal phenotype by treating zebrafish embryos with nucleosides, suggesting that the accumulation of SAICAr and S-Ado may drive this phenotype and not the lack of nucleosides. Therefore, it is interesting to analyze whether the genetic variants of Adsl still catalyze the critical steps of the DNPS when SAICAr and S-Ado accumulate after loss of Adsl. Can they rescue elevated levels of SAICAr after Adsl depletion? These experiments are important to further distinguish between the pathway-specific phenotypes after loss of ADSL.

Taken together, several factors contribute to the etiology of ADSLD. We hypothesize that protein-protein interactions are important for proper development. The complex pathway-specific phenotypes of ADSLD need further research to understand ADSL function in more detail. Nevertheless, the accumulation of SAICAr seems to be a promising target for medical treatment to focus on, as the inhibition of the pathway rescued neurodevelopment-associated phenotypes.

6.2 GRK4 affects ciliogenesis independently of its kinase activity and most likely by interaction with mTOR

The second part of this works deals with the role of GRK4 during kidney development and function. Up to date, GRK4-associated clinical phenotypes like hypertension have only been linked to its kinase activity (83). The conclusion from this work is that GRK4 has a second important function, independently from its kinase activity. For testing this hypothesis, Grk4 LOF experiments by ATG MO injection in zebrafish embryos were performed. Upon Grk4 depletion morphant embryos developed cilia-associated phenotypes like curled tails or the formation of edema (131,132). Co-injections with the different four isoforms of human GRK4 partially rescued these phenotypes, demonstrating their functionality. We also found that loss of Grk4 led to severe kidney phenotypes like cyst formations in the glomerulus, dilatation of the pronephric duct and elongation of kidney cilia. Moreover, we found that morphants had dysfunctional kidneys, as embryos depleted of Grk4 had filtration defects (data not shown). These data are in agreement with the experiments performed with a homozygous Grk4 mutant line (*grk4*$^{mut/mut}$) that showed the same kidney phenotypes like the Grk4 morphants. Additionally, experiments in human fibroblasts and murine cells also showed cilia elongation upon GRK4 KD. These results show that GRK4 is involved in regulating ciliary length control.

A related phenotype was described for the dopamine receptor as its activation is able to induce a massive cilia elongation (107). Nauli et al. treated cells with either dopamine or fenoldopam. Both treatments increased cilia length in porcine kidney proximal tubule cells compared to control treated cells. Interestingly, it has been shown that genetic variants of GRK4 that are associated with hypertension are hyperactive towards dopamine receptor phosphorylation, resulting in increased signaling (83). To reproduce the published data of dopamine dependent cilia elongation, we treated 1BR3 and RPE1 cells with fenoldopam. Surprisingly, we were not able to reproduce already published phenotypes and found no effect on cilia elongation, although DR1 and DR5 are expressed in human fibroblasts (Appendix 1). We did not make Western Blot analysis for DR1 and DR5 in RPE1 cells, but it has already been published by another group (133). For testing fenoldopam in vivo, we

cultured zebrafish embryos in fenoldopam and scored for cilia-associated phenotypes. Like in the cell culture experiments, we were not able to reproduce the findings of Nauli et al. (107). To bring the dopamine function into connection with our Grk4 LOF phenotype, we treated GRK4 depleted cells with SCH 39166, a DR1/5 antagonist. However, treatment with SCH 39166 did not prevent cilia elongation. This leads to the hypothesis, that the observed phenotypes in Grk4 depleted embryos and cells were not attributed to an altered dopamine receptor activity. Worth mentioning is that we did not try to reproduce the data of Nauli et al. in the cells they used, namely porcine kidney proximal tubule cells. Also, we did not try to activate dopamine receptors with dopamine.

In a next step, we wanted to show that the ciliary effect of GRK4 did not depend on its kinase function. Therefore, we performed rescue experiments with a KiDe version of GRK4. Up to date, GRKs are mostly associated with their ability of phosphorylation and thereby desensitization of GPCRs. But more and more research groups find new functions of GRKs, independent of their kinase domain. The working group of Jiménez-Sainz et al. published in 2006 that GRK2 and a kinase-deficient version of GRK2 (GRK2K220R) interact with MEK, a non-receptor protein. They suggest that GRK2 can regulate ERK activity through interaction with MEK independently of its kinase activity, as overexpression of GRK2 and GRK2K220R effectively inhibited chemokine activation of the ERK pathway (134). Second, this observation was confirmed by Liu et al. in 2005, who found that GRK2 directly interacts with AKT (135). In 2004, Johnson et al. discovered that all members of the GRK4 subfamily are able to become transported to the nucleus as they contain a nuclear localization sequence (NLS). This has been shown for GRK5 that binds directly to the DNA in the nucleus, while a truncated form that lacked the NLS failed to do so (136). Another publication from Sorriento et al. in 2008 showed that overexpression of GRK5 led to an increased IκBα concentration. Interestingly, the cytosolic levels of IκBα did not change, but they saw an accumulation of IκBα in the nucleus, which inhibits NFκB activity. Depletion of GRK5 reversed this effect meaning IκBα reduction with an increase of NFκB activity. A KiDe version of GRK5, called GRK5K215R, mimicked the effects of WT GRK5

overexpression on IκBα and NFκB. So, they postulated that GRK5 overexpression leads to an accumulation of IκBα in the nucleus, independently of its kinase activity. They found out that GRK5 directly interacts with IκBα through the RH domain (137).

Summarizing, besides their function in phosphorylating proteins, GRKs have additional functions in protein-interaction.

To verify our hypothesis that fits to the published data of a GRK5 function besides its kinase activity, we tried to rescue our GRK4 LOF phenotype by co-expressing a KiDe version of GRK4. This led to a significantly rescue of edema and cyst formation in zebrafish embryos. Even cilia elongation and the dilatation of the pronephric duct were rescued with the KiDe GRK4 construct. This is in line with our rescue experiments in human fibroblasts and mice organoids, where GRK4 KiDe was able to rescue increased cilia length as effective as the WT version of GRK4. We concluded that our phenotypes observed after depletion of GRK4 may be independent from the kinase activity.

As it was shown that the RH domain of GRK5 is important for protein-protein interactions, we tested the relevance of RH of GRK4. However, the GRK4 construct that lacks the RH domain did not rescue any phenotype in vivo like edema, cyst formation or elongated cilia as well as the dilatation of the pronephric duct. This is consistent with our findings in fibroblast and mice spheroids. Lacking the RH domain failed to rescue cilia elongation in both cell types. This is in agreement with rescue experiments of the human genetic variants of GRK4 that are not only hyperactive towards dopamine receptors, but are also located in the RH domain. Both variants were not able to prevent cilia elongation in the developing kidney of zebrafish embryos. In a future experiment we should confirm the expression of the ΔRH version of GRK4 upon injection in zebrafish embryos as we did it for the genetic variants and the different isoforms.

Nevertheless, these results suggest that protein-protein interactions of GRK4 by its RH domain may be required for proper ciliogenesis and kidney development. In a next step we wanted to analyze if GRK4 interacts with mTOR for two different reasons: First, the loss of GRK5 function leads to cilia elongation like we observed in our Grk4 depleted embryos. Second, it was shown that GRK5 negatively regulates mTOR signaling (84). To test this

hypothesis, we treated MO injected embryos with rapamycin, an inhibitor of mTOR signaling. Interestingly, we were not able to rescue edema and curved tail formation, but rapamycin significantly reduced cyst formation in zebrafish embryos after Grk4 depletion. Additionally, kidney cilia and the dilatation of the pronephric duct were also rescued by treating Grk4 depleted fish with rapamycin. These data strongly indicate that GRK4 negatively regulates mTOR signaling.

This hypothesis could be a possible explanation for our phenotypes observed in Grk4 depleted mice organoids. We observed that the reduced level of Grk4 in mice spheroids did not only lead to elongated cilia, it further leads to increased cell growth and proliferation, which depends on mTOR signaling (109). Next, a GRK4 KO cell line showed that the KO of GRK4 leads to bigger cells with a higher protein content compared to WT cells. This phenotype could be rescued by rapamycin treatment. Of note, WT GRK4 or the KiDe version of GRK4 also rescued increased cell size and protein content, whereas the two patient variants failed. This strengthens the hypothesis that GRK4 acts beside its postulated kinase activity, namely by protein-protein interaction through its RH domain. Moreover, this shows that GRK4 is a negative regulator of mTOR signaling.

To strengthen this hypothesis, we should perform co-immunoprecipitation studies of GRK4 and mTOR. Do they directly interact? Can we precipitate mTOR after loss of GRK4? Can we precipitate mTOR in our KO cells? If not, can we rescue this with the KiDe version of GRK4 or with one of the genetic variants? Another interesting experiment may be the cloning of a version of GRK4 only containing the previously deleted RH domain (see Figure 47). Is this part of GRK4 already sufficient for proper protein-interactions and limiting mTOR signaling? These questions should be addressed in the future.

Furthermore, it is important to know where GRK4 is located in the cell. Recent experiments of our lab showed that overexpressed GRK4 localizes to cilia and microtubules in 1BR3 cells (data not shown). Does endogenous GRK4 also locate to the cilium? Does it locate to the basal body or is it in the cytosol? It is known that the members of the GRK4 subfamily contain a NLS (138). Are we able to detect endogenous GRK4 within the nucleus? I was not able to answer these necessary questions we should focus on in additional experiments.

To sum it up, this work showed that GRK4 is required for ciliogenesis and therefore for proper kidney function in zebrafish embryos. Studies in human and murine cell systems showed that the observations are not restricted to zebrafish. We postulate that GRK4 influences mTOR signaling independently of its kinase activity. The exact mechanism how GRK4 might influence mTOR signaling needs further investigations.

7 References

1. Reiter JF, Leroux MR. Genes and molecular pathways underpinning ciliopathies. Vol. 18, Nature Reviews Molecular Cell Biology. Nature Publishing Group; 2017. p. 533–47.

2. Jain R, Javidan-Nejad C, Alexander-Brett J, Horani A, Cabellon MC, Walter MJ, et al. Sensory functions of motile cilia and implication for bronchiectasis. Front Biosci (Schol Ed). 2012;4:1088–94.

3. Huang S, Hirota Y, Sawamoto K. Various facets of vertebrate cilia: Motility, signaling, and role in adult neurogenesis. Vol. 85, Proceedings of the Japan Academy Series B: Physical and Biological Sciences. 2009. p. 324–36.

4. Spasic M, Jacobs CR. Primary cilia: Cell and molecular mechanosensors directing whole tissue function. Vol. 71, Seminars in Cell and Developmental Biology. Elsevier Ltd; 2017. p. 42–52.

5. Breslow DK, Holland AJ. Mechanism and Regulation of Centriole and Cilium Biogenesis. Vol. 88, Annual Review of Biochemistry. Annual Reviews Inc.; 2019. p. 691–724.

6. Tony Yang TT, Chong WM, Liao JC. STED and STORM superresolution imaging of primary cilia. In: Methods in Molecular Biology. Humana Press Inc.; 2016. p. 169–92.

7. Hirono M. Cartwheel assembly. Vol. 369, Philosophical Transactions of the Royal Society B: Biological Sciences. Royal Society of London; 2014.

8. Uzbekov R, Alieva I. Who are you, subdistal appendages of centriole? Vol. 8, Royal Society Open Science. Royal Society Publishing; 2018.

9. Lovera M, Lüders J. The ciliary impact of nonciliary gene mutations. Vol. 31, Trends in Cell Biology. Elsevier Ltd; 2021. p. 876–87.

10. Wu CT, Chen HY, Tang TK. Myosin-Va is required for preciliary vesicle transportation to the mother centriole during ciliogenesis. Nat Cell Biol. 2018 Feb 1;20(2):175–85.

11. Lu Q, Insinna C, Ott C, Stauffer J, Pintado PA, Rahajeng J, et al. Early steps in primary cilium assembly require EHD1/EHD3-dependent ciliary vesicle formation. Nat Cell Biol. 2015 Mar 2;17(3):228–40.

12. Mukhopadhyay S, Badgandi HB, Hwang SH, Somatilaka B, Shimada IS, Pal K. Trafficking to the primary cilium membrane. Vol. 28, Molecular Biology of the Cell. American Society for Cell Biology; 2017. p. 233–9.

13. Blacque OE, Scheidel N, Kuhns S. Rab GTPases in cilium formation and function. Vol. 9, Small GTPases. Taylor and Francis Inc.; 2018. p. 76–94.

14. Schmidt KN, Kuhns S, Neuner A, Hub B, Zentgraf H, Pereira G. Cep164 mediates vesicular docking to the mother centriole during early steps of ciliogenesis. Journal of Cell Biology. 2012 Dec;199(7):1083–101.

15. Knödler A, Feng S, Zhang J, Zhang X, Das A, Peränen J, et al. Coordination of Rab8 and Rab11 in primary ciliogenesis. Proc Natl Acad Sci U S A. 2010 Apr 6;107(14):6346–51.

16. Insinna C, Lu Q, Teixeira I, Harned A, Semler EM, Stauffer J, et al. Investigation of F-BAR domain PACSIN proteins uncovers membrane tubulation function in cilia assembly and transport. Nat Commun. 2019 Dec 1;10(1).

17. Tsang WY, Dynlacht BD. CP110 and its network of partners coordinately regulate cilia assembly. Vol. 2, Cilia. 2013.

18. Yadav SP, Sharma NK, Liu C, Dong L, Li T, Swaroop A. Centrosomal protein CP110 controls maturation of the mother centriole during cilia biogenesis. Development (Cambridge). 2016 May 1;143(9):1491–501.

19. Kleylein-Sohn J, Westendorf J, le Clech M, Habedanck R, Stierhof YD, Nigg EA. Plk4-Induced Centriole Biogenesis in Human Cells. Dev Cell. 2007 Aug 7;13(2):190–202.

20. Ye X, Zeng H, Ning G, Reiter JF, Liu A. C2cd3 is critical for centriolar distal appendage assembly and ciliary vesicle docking in mammals. Proc Natl Acad Sci U S A. 2014 Feb 11;111(6):2164–9.

21. Chen HY, Kelley RA, Li T, Swaroop A. Primary cilia biogenesis and associated retinal ciliopathies. Vol. 110, Seminars in Cell and Developmental Biology. Elsevier Ltd; 2021. p. 70–88.

22. Shi X, Garcia G, van de Weghe JC, McGorty R, Pazour GJ, Doherty D, et al. Super-resolution microscopy reveals that disruption of ciliary transition-zone architecture causes Joubert syndrome. Nat Cell Biol. 2017 Sep 29;19(10):1178–88.

23. Taschner M, Bhogaraju S, Lorentzen E. Architecture and function of IFT complex proteins in ciliogenesis. Differentiation. 2012 Feb;83(2).

24. Ishikawa H, Marshall WF. Ciliogenesis: Building the cell's antenna. Vol. 12, Nature Reviews Molecular Cell Biology. 2011. p. 222–34.

25. Blacque OE, Reardon MJ, Li C, McCarthy J, Mahjoub MR, Ansley SJ, et al. Loss of C. elegans BBS-7 and BBS-8 protein function results in cilia defects and compromised intraflagellar transport. Genes Dev. 2004 Jul 1;18(13):1630–42.

26. Wilsch-Bräuninger M, Huttner WB. Primary Cilia and Centrosomes in Neocortex Development. Vol. 15, Frontiers in Neuroscience. Frontiers Media S.A.; 2021.

27. Bergmann C, Guay-Woodford LM, Harris PC, Horie S, Peters DJM, Torres VE. Polycystic kidney disease. Vol. 4, Nature Reviews Disease Primers. Nature Publishing Group; 2018.

28. Duong Phu M, Bross S, Burkhalter MD, Philipp M. Limitations and opportunities in the pharmacotherapy of ciliopathies. Vol. 225, Pharmacology and Therapeutics. Elsevier Inc.; 2021.

29. Bay SN, Caspary T. What are those cilia doing in the neural tube? Cilia. 2012 Oct 1;1.

30. Schweickert A, Ott T, Kurz S, Tingler M, Maerker M, Fuhl F, et al. Vertebrate left-right asymmetry: What can nodal cascade gene expression patterns tell us? J Cardiovasc Dev Dis. 2018 Mar 1;5(1).

31. Fakhro KA, Choi M, Ware SM, Belmont JW, Towbin JA, Lifton RP, et al. Rare copy number variations in congenital heart disease patients identify unique genes in left-right patterning. Proc Natl Acad Sci U S A. 2011 Feb 15;108(7):2915–20.

32. Kupffer C. Beobachtungen über die Entwicklung der Knochenfische. Archiv für mikroskopische Anatomie . 1868;4:209–72.

33. Essner JJ, Amack JD, Nyholm MK, Harris EB, Yost HJ. Kupffer's vesicle is a ciliated organ of asymmetry in the zebrafish embryo that initiates left-right development of the brain, heart and gut. Development. 2005 Mar;132(6):1247–60.

34. Ferreira RR, Vermot J. The balancing roles of mechanical forces during left-right patterning and asymmetric morphogenesis. Vol. 144, Mechanisms of Development. Elsevier Ireland Ltd; 2017. p. 71–80.

35. Smith DJ, Montenegro-Johnson TD, Lopes SS. Organized chaos in Kupffer's vesicle: how a heterogeneous structure achieves consistent left-right patterning. Bioarchitecture. 2014;4(3):119–25.

36. Tena TC, Burkhalter MD, Philipp M. Left-right asymmetry in the light of TOR: An update on what we know so far. Biol Cell. 2015;107:306–18.

37. Cooper MS, D'amico LA. A Cluster of Noninvoluting Endocytic Cells at the Margin of the Zebrafish Blastoderm Marks the Site of Embryonic Shield Formation. Vol. 180, DEVELOPMENTAL BIOLOGY. 1996.

38. Okabe N, Xu B, Burdine RD. Fluid dynamics in zebrafish Kupffer's vesicle. Developmental Dynamics. 2008 Dec;237(12):3602–12.

39. Sarah Long*, Nadira Ahmad, Michael Rebagliati†. The zebrafish nodal-related gene southpaw is required for visceral anddiencephalic left-right asymmetry. Development. 2003;130:2303–16.

40. Brent W. Bisgrove, Jeffrey J. Essner, H. Joseph Yost. Regulation of midline development by antagonism of lefty and nodal signaling. Development. 1999;126:3253–62.

41. Chapman AB, Stepniakowski K, Rahbari-Oskoui F. Hypertension in Autosomal Dominant Polycystic Kidney Disease. Vol. 17, Advances in Chronic Kidney Disease. 2010. p. 153–63.

42. K Zerres, G Mücher, L Bachner, G Deschennes, T Eggermannwitz. Autosomal Recessive Polycystic Kidney Disease: The Clinical Experience in North America. Nat Genet. 1994;7:429–32.

43. Zerres K, Mücher G, Bachner L, Deschennes G, Eggermann T, Kääriäinen H, et al. Mapping of the gene for autosomal recessive polycystic kidney disease (ARPKD) to chromosome 6p21-cen. Nat Genet. 1994;7(3):429–32.

44. Andreu-Cervera A, Catala M, Schneider-Maunoury S. Cilia, ciliopathies and hedgehog-related forebrain developmental disorders. Vol. 150, Neurobiology of Disease. Academic Press Inc.; 2021.

45. Bangs F, Anderson K v. Primary cilia and Mammalian Hedgehog signaling. Cold Spring Harb Perspect Biol. 2017 May 1;9(5).

46. Cherry AL, Finta C, Karlström M, Jin Q, Schwend T, Astorga-Wells J, et al. Structural basis of SUFU-GLI interaction in human Hedgehog signalling regulation. Acta Crystallogr D Biol Crystallogr. 2013 Dec;69(12):2563–79.

47. Tschaikner P, Enzler F, Torres-Quesada O, Aanstad P, Stefan E. Hedgehog and Gpr161: Regulating cAMP Signaling in the Primary Cilium. Cells. 2020;9(1):118.

48. Dutto I, Gerhards J, Herrera A, Souckova O, Škopová V, Smak JA, et al. Pathway-specific effects of ADSL deficiency on neurodevelopment. Elife. 2022 Feb 1;11.

49. Han YG, Alvarez-Buylla A. Role of primary cilia in brain development and cancer. Vol. 20, Current Opinion in Neurobiology. 2010. p. 58–67.

50. Stottmann RW, Tran P v., Turbe-Doan A, Beier DR. Ttc21b is required to restrict sonic hedgehog activity in the developing mouse forebrain. Dev Biol. 2009 Nov 1;335(1):166–78.

51. Baudoin JP, Viou L, Launay PS, Luccardini C, Espeso Gil S, Kiyasova V, et al. Tangentially Migrating Neurons Assemble a Primary Cilium that Promotes Their Reorientation to the Cortical Plate. Neuron. 2012 Dec 20;76(6):1108–22.

52. Guo J, Otis JM, Suciu SK, Catalano C, Xing L, Constable S, et al. Primary Cilia Signaling Promotes Axonal Tract Development and Is Disrupted in Joubert Syndrome-Related Disorders Models. Dev Cell. 2019 Dec 16;51(6):759-774.e5.

53. Pareek V, Pedley AM, Benkovic SJ. Human de novo purine biosynthesis. Vol. 56, Critical Reviews in Biochemistry and Molecular Biology. Taylor and Francis Ltd.; 2021. p. 1–16.

54. Jaeken J, van den Berghe G. An infantile autistic syndrome characterised by the presence of succinylpurines in body fluids. Lancet. 1984;324:1058–61.

55. van den Bergh F, Vincent MF, van den Berghe G. Residual Adenylosuccinase Activities in Fibroblasts of Adenylosuccinase-Deficient Children: Parallel Deficiency with Adenylosuccinate and Succinyl-AICAR in Profoundly Retarded Patients and Non-parallel Deficiency in a Mildly Retarded Girl. Vol. 16, J. Inher. Metab. Dis. 1993.

56. Daignan-Fornier B, Pinson B. Yeast to study human purine metabolism diseases. Vol. 8, Cells. MDPI; 2019.

57. Chen P, Wang D, Chen H, Zhou Z, He X. The nonessentiality of essential genes in yeast provides therapeutic insights into a human disease. Genome Res. 2016 Oct 1;26(10):1355–62.

58. Katritch V, Cherezov V, Stevens RC. Structure-Function of the G-protein-Coupled Receptor Superfamily. Annu Rev Pharmacol Toxicol. 2013;53:531–56.

59. Venkatakrishnan AJ, Deupi X, Lebon G, Tate CG, Schertler GF, Madan Babu M. Molecular signatures of G-protein-coupled receptors. Vol. 494, Nature. 2013. p. 185–94.

60. Chaudhary PK, Kim S. The grks reactome: Role in cell biology and pathology. Vol. 22, International Journal of Molecular Sciences. MDPI; 2021.

61. Hilger D, Masureel M, Kobilka BK. Structure and dynamics of GPCR signaling complexes. Nat Struct Mol Biol. 2018 Jan 1;25(1):4–12.

62. Pierce KL, Premont RT, Lefkowitz RJ. Seven-transmembrane receptors. Vol. 3, Nature Reviews Molecular Cell Biology. 2002. p. 639–50.

63. Hurowitz EH, Melnyk JM, Chen YJ, Kouros-Mehr H, Simon MI, Shizuya H. Genomic Characterization of the Human Heterotrimeric G Protein a, (3, and 7 Subunit Genes. Vol. 7, DNA RESEARCH. 2000.

64. Krupnick JG, Benovic JL. THE ROLE OF RECEPTOR KINASES AND ARRESTINS IN G PROTEIN-COUPLED RECEPTOR REGULATION AGONIST-SPECIFIC DESENSITIZATION OF G PROTEIN-COUPLED RECEPTORS. Annu Rev Pharmacol Toxicol. 1998;38:289–319.

65. Lefkowitz RJ, Shenoy SK. Transduction of Receptor Signals by b-Arrestins. Science (1979). 2005;308(5721):512–7.

66. Kohout TA, Lefkowitz RJ. Regulation of G Protein-Coupled Receptor Kinases and Arrestins During Receptor Desensitization. Mol Pharmacol. 2003;63(1):9–18.

67. Harris RC, Zhang MZ. Dopamine, the kidney, and hypertension. Curr Hypertens Rep. 2012 Apr;14(2):138–43.

68. Sallese M, Mariggiò S, Collodel G, Moretti E, Piomboni P, Baccetti B, et al. G protein-coupled receptor kinase GRK4. Molecular analysis of the four isoforms and ultrastructural localization in spermatozoa and germinal cells. J Biol Chem. 1997;272(15):10188–95.

69. Virlon B, Firsov D, Cheval L, Reiter E, Troispoux C, Guillou F, et al. Rat G Protein-Coupled Receptor Kinase GRK4: Identification, Functional Expression, and Differential Tissue Distribution of Two Splice Variants. Endocrinology. 1998;139(6):2784–95.

70. DeWire SM, Ahn S, Lefkowitz RJ, Shenoy SK. β-Arrestins and cell signaling. Vol. 69, Annual Review of Physiology. 2007. p. 483–510.

71. Premont RT, Gainetdinov RR. Physiological roles of G protein-coupled receptor kinases and arrestins. Vol. 69, Annual Review of Physiology. 2007. p. 511–34.

72. Gurevich E v., Gurevich V v. Arrestins: Ubiquitous regulators of cellular signaling pathways. Vol. 7, Genome Biology. 2006.

73. Sorkin A, von Zastrow M. Endocytosis and signalling: Intertwining molecular networks. Vol. 10, Nature Reviews Molecular Cell Biology. 2009. p. 609–22.

74. Sparks MA, Crowley SD, Gurley SB, Mirotsou M, Coffman TM. Classical renin-angiotensin system in kidney physiology. Compr Physiol. 2014;4(3):1201–28.

75. Wu C, Lu H, Cassis LA, Daugherty A. Molecular and Pathophysiological Features of Angiotensinogen: A Mini Review. N Am J Med Sci (Boston). 2011;4(4):183–90.

76. Iwai M, Horiuchi M. Devil and angel in the renin-angiotensin system: ACE-angiotensin II-AT1 receptor axis vs. ACE2-angiotensin-(1-7)-Mas receptor axis. Vol. 32, Hypertension Research. 2009. p. 533–6.

77. Carneiro De Morais CP, Polidoro JZ, Ralph DL, Pessoa TD, Oliveira-Souza M, Barauna VG, et al. Proximal tubule NHE3 activity is inhibited by beta-arrestin-biased angiotensin II type 1 receptor signaling. Am J Physiol Cell Physiol. 2015;309:541–50.

78. Li XC, Hopfer U, Zhuo JL. AT 1 receptor-mediated uptake of angiotensin II and NHE-3 expression in proximal tubule cells through a microtubule-dependent endocytic pathway. Am J Physiol Renal Physiol. 2009;297:1342–52.

79. Siddiqui AH, Hussain T. Impaired angiotensin II AT1 receptor function and enhanced Na, K-ATPase affinity for sodium in proximal tubule of streptozotocin-treated diabetic rats. Clin Exp Hypertens. 2007 Sep;29(7):435–44.

80. Zeng C, Sanada H, Watanabe H, Eisner GM, Felder RA, Jose PA, et al. Functional genomics of the dopaminergic system in hypertension. Physiol Genomics. 2004;19:233–46.

81. Olivares-Hernández A, Figuero-Pérez L, Cruz-Hernandez JJ, Sarmiento RG, Usategui-Martin R, Miramontes-González JP. Dopamine receptors and the kidney: An overview of health-and pharmacological-targeted implications. Vol. 11, Biomolecules. MDPI AG; 2021. p. 1–16.

82. Felder RA, Sanada H, Xu J, Yu PY, Wang Z, Watanabe H, et al. G protein-coupled receptor kinase 4 gene variants in human essential hypertension. Proc Natl Acad Sci U S A. 2002;99(6):3872–7.

83. Yang J, Villar VAM, Jones JE, Jose PA, Zeng C. G protein-coupled receptor kinase 4 role in hypertension. Hypertension. 2015 Jun 1;65(6):1148–55.

84. Burkhalter MD, Fralish GB, Premont RT, Caron MG, Philipp M. Grk5l controls heart development by limiting mTOR signaling during symmetry breaking. Cell Rep. 2013 Aug 29;4(4):625–32.

85. Bollig F, Perner B, Besenbeck B, Köthe S, Ebert C, Taudien S, et al. A highly conserved retinoic acid responsive element controls wt1a expression in the zebrafish pronephros. Development. 2009 Sep 1;136(17):2883–92.

86. Perner B, Englert C, Bollig F. The Wilms tumor genes wt1a and wt1b control different steps during formation of the zebrafish pronephros. Dev Biol. 2007 Sep 1;309(1):87–96.

87. Dutto I, Gerhards J, Herrera A, Souckova O, Škopová V, Smak JA, et al. Pathway-specific effects of ADSL deficiency on neurodevelopment. Elife. 2022 Feb 8;11.

88. Felder RA, Sanada H, Xu J, Yu PY, Wang Z, Watanabe H, et al. G protein-coupled receptor kinase 4 gene variants in human essential hypertension. Proc Natl Acad Sci U S A. 2002;99(6):3872–7.

89. Song Z, Zhang X, Jia S, Yelick PC, Zhao C. Zebrafish as a Model for Human Ciliopathies. Vol. 43, Journal of Genetics and Genomics. Institute of Genetics and Developmental Biology; 2016. p. 107–20.

90. Chambers BE, Gerlach GF, Clark EG, Chen KH, Levesque AE, Leshchiner I, et al. Tfap2a is a novel gatekeeper of nephron differentiation during kidney development. Development (Cambridge). 2019 Jul 1;146(13).

91. Jaffe M. Kimberly, Thiberge Y. Stephan, Bisher E. Margaret, Burdine D. Rebecca. Imaging Cilia in Zebrafish. Methods Cell Biol. 2010;97:415–35.

92. Hanahan D. Studies on Transformation of Escherichia coli with Plasmids. Vol. 166, J. Mol. Biol. 1983.

93. Bertani G. Lysogeny at Mid-Twentieth Century: P1, P2, and Other Experimental Systems. Vol. 186, Journal of Bacteriology. 2004. p. 595–600.

94. Lin CY, Tsai MY, Liu YH, Lu YF, Chen YC, Lai YR, et al. Klf8 regulates left-right asymmetric patterning through modulation of Kupffer's vesicle morphogenesis and spaw expression. J Biomed Sci. 2017 Jul 17;24(1).

95. Long S, Ahmad N, Rebagliati M. The zebrafish nodal-related gene southpaw is required for visceral and diencephalic left-right asymmetry. Vol. 130, Development. 2003. p. 2303–16.

96. Schier AF. Nodal Signaling in Vertebrate Development. Annu Rev Cell Dev Biol. 2003;19:589–621.

97. Gou Y, Vemaraju S, Sweet EM, Kwon HJ, Riley BB. sox2 and sox3 Play unique roles in development of hair cells and neurons in the zebrafish inner ear. Dev Biol. 2018 Mar 1;435(1):73–83.

98. Gong J, Hu S, Huang Z, Hu Y, Wang X, Zhao J, et al. The Requirement of Sox2 for the Spinal Cord Motor Neuron Development of Zebrafish. Front Mol Neurosci. 2020 Mar 27;13.

99. Chen HL, Yuh CH, Wu KK. Nestin is essential for zebrafish brain and eye development through control of progenitor cell apoptosis. PLoS One. 2010 Feb 19;5(2).

100. Zhou ZW, Tapias A, Bruhn C, Gruber R, Sukchev M, Wang ZQ. DNA damage response in microcephaly development of MCPH1 mouse model. DNA Repair (Amst). 2013 Aug;12(8):645–55.

101. Mah LJ, El-Osta A, Karagiannis TC. γh2AX: A sensitive molecular marker of DNA damage and repair. Vol. 24, Leukemia. Nature Publishing Group; 2010. p. 679–86.

102. Raterman ST, Metz JR, Wagener FADTG, von den Hoff JW. Zebrafish Models of Craniofacial Malformations: Interactions of Environmental Factors. Vol. 8, Frontiers in Cell and Developmental Biology. Frontiers Media S.A.; 2020.

103. Marie S, Cuppens H, Heuterspreute M, Jaspers M, Zambrano Tola E, Gu XX, et al. Mutation Analysis in Adenylosuccinate Lyase Deficiency: Eight Novel Mutations in the Re-evaluated Full ADSL Coding Sequence. Vol. 13, HUMAN MUTATION. 1999.

104. van Laer B, Kapp U, Soler-Lopez M, Moczulska K, Pääbo S, Leonard G, et al. Molecular comparison of Neanderthal and Modern Human adenylosuccinate lyase. Sci Rep. 2018 Dec 1;8(1).

105. De M, Lazari FM, Liu X, Nakamura K, Benovic JL, Ascoli M. Role of G Protein-Coupled Receptor Kinases on the Agonist-Induced Phosphorylation and Internalization of the Follitropin Receptor. Vol. 13, Molecular Endocrinology. 1999.

106. Sallese M, Salvatore L, Sala G, Storto M, Launey T, Nicoletti F, et al. The G-protein-coupled receptor kinase GRK4 mediates homologous desensitization of metabotropic glutamate receptor 1. FASEB J. 2000;14(15):2569–80.

107. Upadhyay VS, Muntean BS, Kathem SH, Hwang JJ, AbouAlaiwi WA, Nauli SM, et al. Roles of dopamine receptor on chemosensory and mechanosensory primary cilia in renal epithelial cells. Front Physiol. 2014;5.

108. Allen SJ, Parthasarathy G, Darke PL, Diehl RE, Ford RE, Hall DL, et al. Structure and function of the hypertension variant A486V of G protein-coupled receptor kinase 4. Journal of Biological Chemistry. 2015 Aug 14;290(33):20360–73.

109. Saxton RA, Sabatini DM. mTOR Signaling in Growth, Metabolism, and Disease. Vol. 168, Cell. Cell Press; 2017. p. 960–76.

110. Yuan S, Li J, Diener DR, Choma MA, Rosenbaum JL, Sun Z. Target-of-rapamycin complex 1 (Torc1) signaling modulates cilia size and function through protein synthesis regulation. Proc Natl Acad Sci U S A. 2012 Feb 7;109(6):2021–6.

111. Wang G, Yost HJ, Amack JD. Analysis of gene function and visualization of cilia-generated fluid flow in Kupffer's vesicle. Journal of Visualized Experiments. 2013;(73).

112. Liu M, Zhang W, Li M, Feng J, Kuang W, Chen X, et al. NudCL2 is an autophagy receptor that mediates selective autophagic degradation of CP110 at mother centrioles to promote ciliogenesis. Cell Res. 2021 Nov 1;31(11):1199–211.

113. Passemard S, Kaindl AM, Verloes A. Chapter 13 - Microcephaly. Handb Clin Neurol. 2013;111:129–41.

114. Becerra-Solano LE, Mateos-Sánchez L, López-Muñoz E. Microcephaly, an etiopathogenic vision. Vol. 62, Pediatrics and Neonatology. Elsevier (Singapore) Pte Ltd; 2021. p. 354–60.

115. Xavier GM, Seppala M, Barrell W, Birjandi AA, Geoghegan F, Cobourne MT. Hedgehog receptor function during craniofacial development. Vol. 415, Developmental Biology. Academic Press Inc.; 2016. p. 198–215.

116. Tabler JM, Bolger TG, Wallingford J, Liu KJ. Hedgehog activity controls opening of the primary mouth. Dev Biol. 2014 Dec 1;396(1):1–7.

117. Yamagishi C, Yamagishi H, Maeda J, Tsuchihashi T, Ivey K, Hu T, et al. Sonic hedgehog is essential for first pharyngeal arch development. Pediatr Res. 2006 Mar;59(3):349–54.

118. Smoak IW, Byrd NA, Abu-Issa R, Goddeeris MM, Anderson R, Morris J, et al. Sonic hedgehog is required for cardiac outflow tract and neural crest cell development. Dev Biol. 2005 Jul 15;283(2):357–72.

119. Chiang C, Litingtung Y, Lee E, Youngt KE, Cordent JL, Westphal H, et al. Cyclopia and defective axial patterning in mice lacking Sonic hedgehog gene function. Nature. 1996;383:407–13.

120. Stiff T, Tena TC, O'Driscoll M, Jeggo PA, Philipp M. ATR promotes cilia signalling: Links to developmental impacts. Hum Mol Genet. 2016 Apr 15;25(8):1574–87.

121. Shanske A, Caride DG, Menasse-Palmer L, Bogdanow A, Marion RW. Central Nervous System Anomalies in Seckel Syndrome: Report of a New Family and Review of the Literature. Vol. 70, J. Med. Genet. 1997.

122. Murga M, Bunting S, Montãa MF, Soria R, Mulero F, Cãamero M, et al. A mouse model of ATR-Seckel shows embryonic replicative stress and accelerated aging. Nat Genet. 2009 Aug;41(8):891–8.

123. O'Driscoll M, Ruiz-Perez VL, Woods CG, Jeggo PA, Goodship JA. A splicing mutation affecting expression of ataxia-telangiectasia and Rad3-related protein (ATR) results in Seckel syndrome. Nat Genet. 2003 Apr 1;33(4):497–501.

124. McIntyre RE, Lakshminarasimhan Chavali P, Ismail O, Carragher DM, Sanchez-Andrade G, Forment J v., et al. Disruption of Mouse Cenpj, a Regulator of Centriole Biogenesis, Phenocopies Seckel Syndrome. PLoS Genet. 2012;8(11).

125. Al-Dosari MS, Shaheen R, Colak D, Alkuraya FS. Novel CENPJ mutation causes Seckel syndrome. J Med Genet. 2010 Jun;47(6):411–4.

126. Marjanović M, Sánchez-Huertas C, Terré B, Gómez R, Scheel JF, Pacheco S, et al. CEP63 deficiency promotes p53-dependent microcephaly and reveals a role for the centrosome in meiotic recombination. Nat Commun. 2015 Jul 9;6.

127. van Laer B, Kapp U, Soler-Lopez M, Moczulska K, Pääbo S, Leonard G, et al. Molecular comparison of Neanderthal and Modern Human adenylosuccinate lyase. Sci Rep. 2018 Dec 1;8(1).

128. Songon An, Ravindra Kumar, Erin D. Sheets, Stephen J. Benkovic. Reversible Compartmentalization of de Novo Purine Biosynthetic Complexes in Living Cells. Science (1979). 2008 Apr 5;320(5872):103–6.

129. French JB, Fang Y, Benkovic SJ. The purinosome, a multi-protein complex involved in the de novo biosynthesis of purines in humans. Chemical Communications. 2013 Apr 23;49(40):4444–52.

130. Baresova V, Skopova V, Sikora J, Patterson D, Sovova J, Zikanova M, et al. Mutations of ATIC and ADSL affect purinosome assembly in cultured skin fibroblasts from patients with AICA-ribosiduria and ADSL deficiency. Hum Mol Genet. 2012 Apr;21(7):1534–43.

131. Sun Z, Amsterdam A, Pazour GJ, Cole DG, Miller MS, Hopkins N. A genetic screen in zebrafish indentifies cilia genes as a principal cause of cystic kidney. Development. 2004 Aug;131(16):4085–93.

132. Zaghloul NA, Katsanis N. Zebrafish Assays of Ciliopathies. In: Methods in Cell Biology. Academic Press Inc.; 2011. p. 257–72.

133. Baba K, Debruyne JP, Tosini G. Dopamine 2 Receptor Activation Entrains Circadian Clocks in Mouse Retinal Pigment Epithelium. Sci Rep. 2017 Dec 1;7(1).

134. Jiménez-Sainz MC, Murga C, Kavelaars A, Jurado-Pueyo M, Krakstad BF, Heijnen CJ, et al. G protein-coupled receptor kinase 2 negatively regulates chemokine signaling at a level downstream from G protein subunits. Mol Biol Cell. 2006 Jan;17(1):25–31.

135. Liu S, Premont RT, Kontos CD, Zhu S, Rockey DC. A crucial role for GRK2 in regulation of endothelial cell nitric oxide synthase function in portal hypertension. Nat Med. 2005 Sep;11(9):952–8.

136. Johnson LR, Scott MGH, Pitcher JA. G Protein-Coupled Receptor Kinase 5 Contains a DNA-Binding Nuclear Localization Sequence. Mol Cell Biol. 2004 Dec;24(23):10169–79.

137. Sorriento D, Ciccarelli M, Santulli G, Campanile A, Altobelli GG, Cimini V, et al. The G-protein-coupled receptor kinase 5 inhibits NFB transcriptional activity by inducing nuclear accumulation of IB. Proc Natl Acad Sci U S A. 2008;105(46):17818–23.

138. Johnson LR, Robinson JD, Lester KN, Pitcher JA. Distinct Structural Features of G Protein-Coupled Receptor Kinase 5 (GRK5) Regulate Its Nuclear Localization and DNA-Binding Ability. PLoS One. 2013 May 2;8(5).

8 Appendix

8.1 Dopamine receptors in 1BR3 cells

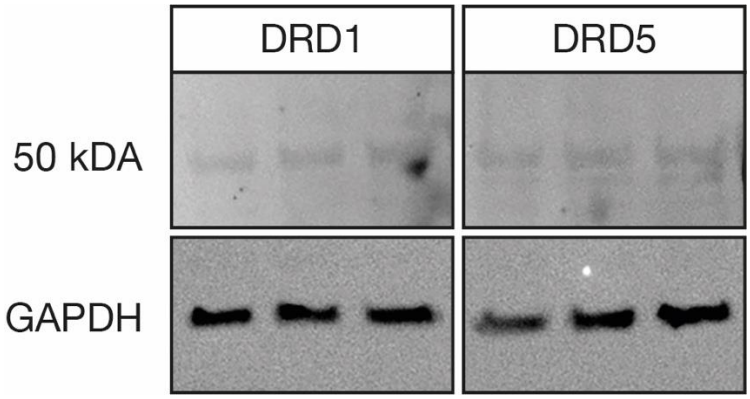

Appendix 1: Western blot of 1BR3 cells showed dopamine receptors

Western blot of 1BR3 cells verified that both, Dopamine D1 receptor (DRD1) and Dopamine D5 receptor (DRD5) were expressed in human fibroblasts.

9 Acknowledgments

My first thanks goes to my supervisor Prof. Dr. Melanie Philipp who always supported me during the last years. I have learned so much from you. Thanks for helping me becoming the researcher I am right now.

Second I want to thank my TAC members Prof. Dr. Ludger Schöls and Dr. Jens Lüders for sharing their expertise with me.

I also want to thank the Graduate Training Center of Neuroscience (International Max Planck Research School).

Next, I want to thank the whole Phillip lab and our animal care takers. Especially Max Duong Phu, who was my longest lab partner. We really had great discussions in our small office. I will miss this. I also want to thank you, Martin, for being such a nice and precious colleague. I think the lab will miss our awesome singing performances.

I also want to thank the members of our old institute in Ulm. A special thanks goes to you Cori. Thanks for always listening and helping me. Thanks for every coffee break we had. Thanks for being a friend for life.

My biggest thanks goes to my family and my partner Steven. Mum, dad and Sari, you always supported me in any possible way without ever demanding anything. You gave me so much strength. Thanks for being the best family one could imagine. Next I want to thank you Steven for like everything. It is impossible to list all the things you did to help me. You were always there for me during the good and the bad times and we know I had both of them. To all of you: Thanks for your unconditional love and support.

Last but not least I want to thank my good friends Missi and Melli for critical reading of my thesis.